NASA
UACRL F910461-12

FIRST ANNUAL PROGRESS REPORT

ANALYTICAL STUDY OF CATALYTIC REACTORS FOR HYDRAZINE DECOMPOSITION

by

ARTHUR S. KESTEN

prepared for

NATIONAL AERONAUTICS AND SPACE ADMINISTRATION

May, 1967

CONTRACT NAS 7-458

United Aircraft Research Laboratories
UNITED AIRCRAFT CORPORATION
EAST HARTFORD, CONNECTICUT

Copy #55

NASA
UACRL F910461-12

FIRST ANNUAL PROGRESS REPORT

ANALYTICAL STUDY OF CATALYTIC REACTORS FOR HYDRAZINE DECOMPOSITION

by

Arthur S. Kesten

prepared for

NATIONAL AERONAUTICS AND SPACE ADMINISTRATION

May, 1967

CONTRACT NAS 7-458

RESEARCH LABORATORIES
United Aircraft Corporation
East Hartford, Connecticut

Analytical Study of Catalytic Reactors for Hydrazine Decomposition

First Annual Progress Report

April 15, 1966 - April 14, 1967

Contract No. NAS 7-458

TABLE OF CONTENTS

ABSTRACT

An analytical study of catalyzed hydrazine decomposition reaction chambers was performed in order to establish procedures capable of predicting the steady-state and transient behavior of the system. The study included the development of computer programs to calculate the temperature and reactant concentration distribution as functions of time and axial position in typical reaction chamber configurations. The computer programs evolved are based upon models of the reactor system which consider both thermal and catalytic decomposition of reactants, along with simultaneous heat and mass transfer between the free-gas phase and the gas within the pores of the catalyst pellets. Results obtained using these computer programs are in excellent agreement with data available from small scale engine firings using Shell 405 catalyst thus permitting not only correlation of the test data but also indirect determination of hydrazine and ammonia decomposition kinetics on 405 catalyst.

FOREWORD

This work was performed by United Aircraft Research Laboratories for the National Aeronautics and Space Administration under Contract NAS 7-458 initiated April 15, 1966.

Included among those who cooperated in performance of the work under Contract NAS 7-458 were Dr. A. S. Kesten, Program Manager, Dr. W. G. Burwell, Chief, Kinetics and Thermal Sciences Section, Mr. D. B. Smith, and Mrs. E. Smith of UARL.

This work was conducted under program management of the NASA Chief, Liquid Propulsion Experimental Engineering Systems, NASA Headquarters, Washington, D. C., and the Technical Manager was Mr. T. W. Price, Jet Propulsion Laboratory, Pasadena, California

Report F910461-12

Analytical Study of Catalytic Reactors for Hydrazine Decomposition

First Annual Progress Report

April 15, 1966 - April 14, 1967

Contract No. NAS 7-458

SUMMARY

The Research Laboratories of United Aircraft Corporation under Contract NAS 7-458 with the National Aeronautics and Space Administration are performing an analytical study of catalytic reactors for hydrazine decomposition. This first annual technical report summarizes work performed under this continuing contract from April 15, 1966 to April 14, 1967. Work during this period has included the development of computer programs which are used to calculate the temperature and concentrations of hydrazine and ammonia as functions of time and axial position in typical reaction chamber configurations. The computer programs are based upon steady-state and transient models of the reactor system which consider both thermal and catalytic decomposition of reactants, along with simultaneous heat and mass transfer between the free-gas phase and the gas within the pores of the catalyst pellets. The steady-state model contains a detailed mathematical description of the processes of heat and mass transfer in the pores of the catalyst pellets, while the transient model uses over-all coefficients to evaluate the effects of heat and mass diffusion on reaction rates in the porous catalyst particles. These coefficients are defined in terms of the physical properties and operating parameters of the reactor system.

The computer programs representing the steady-state and transient models of the reactor system have been used to calculate temperature and reactant concentration distributions for various initial bed temperatures, feed temperatures, chamber pressures, mass flow rates, injector locations, and catalyst size distributions. The results have been compared, wherever possible, to available measurements of temperature profiles and exhaust concentrations made during firings of typical hydrazine engine reaction chambers employing Shell 405 catalyst. Excellent agreement between theoretical and experimental results is indicated.

This agreement has permitted verification of kinetics information for use in both the steady-state and transient programs. In particular, estimates have been permitted of the rate laws and associated rate constants governing the heterogeneous, vapor-phase decomposition of hydrazine and ammonia on the Shell 405 catalyst.

INTRODUCTION

Effective design of distributed-feed catalyzed monopropellant hydrazine rocket engines and gas generators requires accurate procedures for predicting the effects of the design parameters of the reactor system on the steady-state and transient performance of the system. Prior to the present undertaking, this general capability did not exist, although simplified methods had been developed for predicting the steady-state performance of idealized catalytic reactors (Refs. 1 and 2). These simplified methods do not adequately describe the combined processes of heat transfer, diffusion, and chemical reaction and are restricted to consideration of a single decomposition reaction at any axial location within the reaction chamber. To overcome these deficiencies, a more comprehensive theoretical analysis was deemed necessary. Preliminary investigations at United Aircraft Research Laboratories demonstrated the feasibility of such an analysis and, further, indicated that both transient and steady-state performance characteristics could be predicted.

Based upon the above investigations, a comprehensive analytical program was formulated with the objectives of (a) developing computer programs for predicting the temperature and concentration distributions in monopropellant hydrazine catalytic reactors, and (b) performing calculations using these computer programs to demonstrate the effects of various system parameters on the performance of the reactor and, ultimately, to establish guidelines for reactor design. During the first year of the contract period attention has been focused on describing the steady-state and transient behavior of a reactor system in which complete radial mixing in the free-gas (or liquid) phase was assumed. Currently, the steady-state program is being extended to include radial as well as axial variations in temperature and concentrations. This portion of the program, scheduled for completion in April of 1968, will permit an analysis of various injection schemes which exhibit radial nonuniformities. Effort during the first annual reporting period is described in detail in succeeding sections of this report.

DISCUSSION

The analysis of a hydrazine engine reaction system carried out to date pertains to a reaction chamber of arbitrary cross section packed with catalyst particles into which liquid hydrazine is injected at arbitrarily selected axial locations. At these locations, hydrazine injection is taken as uniform across the cross section of the chamber. Catalyst particles are represented as "equivalent" spheres with a diameter taken as a function of the particle size and shape. Both thermal and catalytic vapor phase decomposition of hydrazine and ammonia are considered in developing equations describing the concentration distributions of these reactants. Diffusion of reactants from the free-gas phase to the outside surface of the catalyst pellets is taken into account. Since the catalyst material is impregnated on the interior and exterior surfaces of porous particles, the diffusion of reactants into the porous structure must also be considered. In addition, the conduction of heat within the porous particles must be taken into account since the decomposition reactions are accompanied by the evolution or absorption of heat.

A treatment of the transport processes described above constitutes a general model of the reaction chamber. The analysis of the steady-state performance of a reactor based on this model can be carried out in a straight-forward manner. However, the analysis of the transient behavior of the system using this general model is quite complicated since both the reactant concentrations and the rate constants for decomposition, which are exponentially dependent on temperature, will be functions not only of time, but also of position within the catalyst particles.

To circumvent these complications, the transient behavior of the system can be analyzed by employing a second model which takes heat and mass diffusion within the catalyst particles into account by considering their effects on the rates of the catalytic reactions through the "utilization factor." This factor, which is defined as the ratio of actual reaction rate to that which would be produced by the catalyst particle if negligible temperature and concentration gradients existed within the particle, can be calculated as a function of temperature and reactant concentration at the outside surface of a catalyst particle at steady-state. If it is assumed that, even under transient conditions, utilization factors are functions only of surface temperatures and concentrations, the analysis of the transient behavior of the reactor system becomes tractable. Using this method then, the temperature and reactant concentrations can be described as functions of time and position in the reaction chamber.

Included in succeeding sections of this report are detailed descriptions of (a) the development of the computer programs representing the steady-state and transient models of the reactor system, (b) the establishment of kinetics information pertinent to Shell 405 catalyst particles (Refs. 3, 4, 5, and 6) for use in both of these programs, and (c) the use of these programs to calculate temperature and reactant concentration distributions for various reactor operating conditions.

Steady-State Model

In developing the present steady-state model, the temperature and reactant concentrations in the interstitial phase (i.e., the free-fluid phase as distinguished from the gas phase within the porous particles) are assumed to vary only with axial distance along the bed. In the entrance region of the reaction chamber, where the temperature is low enough to permit the existence of liquid hydrazine, vaporization of liquid is assumed to occur as a result of decomposition of vapor hydrazine within the pores of the catalyst particles. That is, catalytic reaction is assumed to be fast enough to keep liquid hydrazine from wetting the pores of the particles; the hydrazine concentration at the surface of the catalyst particles at any axial location in the entrance region is then computed from the vapor pressure of liquid hydrazine in the interstitial phase at the same axial location. Neglecting axial diffusion of heat or mass, the change in enthalpy of the interstitial phase in the region where liquid hydrazine is present (i.e., where $h_i < h_i^V$) is related to the concentration gradient at the surface of the porous catalyst particles by

$$G \frac{dh_i}{dz} + H^{N_2H_4} D_p A_p \left(\frac{dc_p^{N_2H_4}}{dx} \right)_s + F(h_i - h_F) = 0 \qquad \text{for } h_i \le h_i^V \quad (1)$$

The variation of mass flow rate, G, with axial distance is easily computed from the rate of feed of liquid hydrazine from the distributed injectors into the system. In the region where liquid hydrazine exists at temperatures below the vaporization temperature, the temperature may be obtained from

$$T_i = T_F + \frac{h_i - h_F}{C_f} \qquad \text{for } h_i < h_i^L \quad (2)$$

In the two-phase region, where $T_i = T_{vap}$, the weight-fraction of vapor may be computed from

$$\text{WEIGHT - FRACTION VAPOR} = \frac{h_i - h_i^L}{h_i^V - h_i^L} \qquad \text{for } h_i^L \le h_i \le h_i^V \quad (3)$$

At the axial position at which the enthalpy of the interstitial phase is just equal to the enthalpy of vapor hydrazine at the boiling point ($h_i = h_i^V$), the fraction of hydrazine injected upstream of that point which has been decomposed is easily calculated from an overall heat balance. The associated amounts of ammonia, nitrogen, and hydrazine formed from decomposition of hydrazine can then be calculated taking the decomposition reaction as

$$2N_2H_4 \longrightarrow 2NH_3 + N_2 + H_2$$

It should be noted that this is the overall reaction scheme determined experimentally for both homogeneous decomposition of hydrazine (Refs. 7, 8, 9) and low pressure heterogeneous decomposition of hydrazine on platinum surfaces (Ref. 10).*

In the remainder of the reaction chamber, where $h_i > h_i^V$, heat is being supplied to the system by homogeneous as well as heterogeneous decomposition of hydrazine. In addition, at sufficiently high temperature, heat is removed from the system by the endothermic decomposition of ammonia. For $h_i > h_i^V$ then, the change in enthalpy with axial distance is related to the concentration gradients at the surface of the porous catalyst particles by

$$G\frac{dh_i}{dz} + H^{N_2H_4} r_{hom}\,\gamma + A_p\left[H D_p\left(\frac{dc_p}{dx}\right)_s\right]^{N_2H_4} + A_p\left[H D_p\left(\frac{dc_p}{dx}\right)_s\right]^{NH_3} + F(h_i - h_F) = 0 \qquad (4)$$

The changes in reactant weight fractions in the interstitial phase with axial distance are related to the concentration gradients at the surface of the porous catalyst particles by

$$\frac{dw_i^{N_2H_4}}{dz} = \frac{1}{G}\left\{F - r_{hom}\delta - A_p\left[D_p\left(\frac{dc_p}{dx}\right)_s\right]^{N_2H_4}\right\} - \frac{F c_i^{N_2H_4}}{G\rho_i} \qquad (5)$$

$$\frac{dw_i^{NH_3}}{dz} = \frac{1}{G}\left\{r_{hom}\delta\,\frac{M^{NH_3}}{M^{N_2H_4}} + A_p\left[D_p\left(\frac{dc_p}{dx}\right)_s\right]^{N_2H_4}\frac{M^{NH_3}}{M^{N_2H_4}} - A_p\left[D_p\left(\frac{dc_p}{dx}\right)_s\right]^{NH_3}\right\} - \frac{F c_i^{NH_3}}{G\rho_i} \qquad (6)$$

*It is more commonly assumed, without benefit of experimental evidence, that the decomposition reaction is $3\,N_2H_4 \longrightarrow 4\,NH_3 + N_2$, followed by dissociation of one of the four ammonia molecules to nitrogen and hydrogen. This two-step process leads to the same overall reaction cited above but assumes that a minimum of 25 percent of the ammonia produced by hydrazine decomposition also decomposes. The fractional ammonia dissociation, f, calculated assuming the validity of the two-step process is related to the fractional ammonia dissociation calculated in the present report by

$$(f)_{\text{two-step process}} = \frac{3\,(f)_{\text{present report}} + 1}{4}$$

$$\frac{dw_i^{N_2}}{dz} = \frac{1}{G}\left\{\frac{1}{2} r_{hom}\delta \frac{M^{N_2}}{M^{N_2H_4}} + \frac{A_p}{2}\left[D_p\left(\frac{dc_p}{dx}\right)_s\right]^{N_2H_4}\frac{M^{N_2}}{M^{N_2H_4}} + \frac{A_p}{2}\left[D_p\left(\frac{dc_p}{dx}\right)_s\right]^{NH_3}\frac{M^{N_2}}{M^{NH_3}}\right\} - \frac{Fc_i^{N_2}}{G\rho_i} \tag{7}$$

$$\frac{dw_i^{H_2}}{dz} = \frac{1}{G}\left\{\frac{1}{2} r_{hom}\delta \frac{M^{H_2}}{M^{N_2H_4}} + \frac{A_p}{2}\left[D_p\left(\frac{dc_p}{dx}\right)_s\right]^{N_2H_4}\frac{M^{H_2}}{M^{N_2H_4}} + \frac{3A_p}{2}\left[D_p\left(\frac{dc_p}{dx}\right)_s\right]^{NH_3}\frac{M^{H_2}}{M^{NH_3}}\right\} - \frac{Fc_i^{H_2}}{G\rho_i} \tag{8}$$

The changes in reactant concentrations with axial distance are then given by

$$\frac{dc_i^J}{dz} = \rho_i \frac{dw_i^J}{dz} + \frac{c_i^J}{\rho_i}\frac{d\rho_i}{dz} \tag{9}$$

where

$$\frac{1}{\rho_i}\frac{d\rho_i}{dz} = \frac{1}{\bar{M}}\frac{d\bar{M}}{dz} - \frac{1}{T_i}\frac{dT_i}{dz} \tag{10}$$

and

$$\frac{1}{\bar{M}}\frac{d\bar{M}}{dz} = -\frac{1}{\sum_J \frac{w_i^J}{M^J}}\sum_J \frac{1}{M^J}\frac{dw_i^J}{dz} \tag{11}$$

The temperature of the interstitial phase in this region is related to the enthalpy by

$$h_i - h_i^V = \int_{T_{vap}}^{T_i} C_f \, dT_i \tag{12}$$

where C_f is the specific heat of the gas mixture and is a function of temperature as well as the concentration of the constituents of the mixture.

The reactant concentration profile in the porous particles at any axial location must satisfy the diffusion equation for mass transport as well as an analogous equation for heat conduction. Neglecting the effect of the translational motion

of the gas stream on diffusion within the porous particles and assuming constant diffusion coefficients, D_p, and thermal conductivities, K_p, these equations may be written as

$$D_p \nabla^2 c_p - r_{het} = 0 \tag{13}$$

$$K_p \nabla^2 T_p - H r_{het} = 0 \tag{14}$$

Using Eqs. (13) and (14), Prater (Ref. 11) has pointed out that temperature and concentration are related quite simply by

$$T_p - (T_p)_s = - \frac{H D_p}{K_p} \left[(c_p)_s - c_p \right] \tag{15}$$

The use of this relationship enables the reaction rate, r_{het}, to be written as a function of concentration alone instead of concentration and temperature. Equation (13) can then be solved for the concentration at any point in the porous particle in terms of the concentration at the surface of the particle, $(c_p)_s$. The solution is derived in Appendix A as an implicit integral equation given by

$$c_p(x) = (c_p)_s - \left[\frac{1}{x} - \frac{1}{a} \right] \int_0^x \xi^2 \frac{r_{het}(c_p)}{D_p} \, d\xi - \int_x^a \left[\frac{1}{\xi} - \frac{1}{a} \right] \xi^2 \frac{r_{het}(c_p)}{D_p} \, d\xi \tag{16}$$

The rate of chemical reaction on the catalyst surfaces, $r_{het}(c_p)$, is given, in general, by (Ref. 12)

$$r_{het}(c_p) = k_o (c_p)_s^{1-n} (c_p)^n \exp \left\{ \gamma\beta \left(1 - c_p/(c_p)_s \right) / \left[1 + \beta \left(1 - c_p/(c_p)_s \right) \right] \right\} \tag{17}$$

where the parameters, k_o, n, γ, and β are defined in the list of symbols.

If the reactant concentration at the surface of the particle, $(c_p)_s$, is equal to the concentration in the interstitial phase, c_i, Eqs. (16) and (17) can be solved simultaneously with the equations describing the changes in enthalpy and reactant concentrations in the interstitial phase with axial distance to yield the

steady-state temperature and concentration profiles in the reaction chamber. In the liquid region of the chamber, for example, it is assumed that liquid hydrazine wets the outside surface of the catalyst particles so that $(c_p)_s^{N_2H_4} = c_i^{N_2H_4}$ where $c_i^{N_2H_4}$ is the vapor concentration in equilibrium with liquid hydrazine at temperature T_i. In the vapor region of the reactor it can be shown that $(c_p)_s^{NH_3} \sim c_i^{NH_3}$ at the temperatures existing in the chamber since the rate of transport of material from the bulk fluid to the outside surface of the catalyst particles is much greater than the rate of dissociation of ammonia within the particles. However, in the case of hydrazine decomposition in the vapor region the rate of catalytic decomposition is so high that $(c_p)_s^{N_2H_4} \ll c_i^{N_2H_4}$ and the reaction rate is governed by the rate of mass transfer from the bulk vapor to the outside surface of the catalyst particles. This rate is given approximately by $(k_c c_i)^{N_2H_4}$ where the mass transfer coefficient, $k_c^{N_2H_4}$, may be estimated from (Ref. 13)

$$k_c^{N_2H_4} = \frac{0.61\,G}{\rho_i}\left(\frac{\mu}{\rho_i D_i^{N_2H_4}}\right)^{-0.667}\left(\frac{G}{A_p\,\mu}\right)^{-0.41} \qquad (18)$$

For hydrazine decomposition in the vapor region, then, the terms $\left[D_p\,(\partial c_p/\partial x)_s\right]^{N_2H_4}$ in Eqs. (4), (5), (6), (7) and (8) can be replaced by $(k_c\,c_i)^{N_2H_4}$.

In the liquid-vapor region the situation is somewhat more complicated since it is difficult to predict whether liquid or a combination of liquid and vapor wets the outside surface of the catalyst particles. Both of these options are presently in the computer program representing the steady-state model. In the case in which both the liquid and vapor are taken to wet the particle surface, it is assumed that, at a given axial location, the fraction of the surface covered by vapor is equal to the weight-fraction of vapor present. Decomposition rates, computed assuming pure liquid surface coverage and then pure vapor coverage, are weighted accordingly. Fortuitously, for the system considered here, the liquid-vapor region is so narrow that the choice of either of these options has negligible effect on the resulting temperature distributions. This point is discussed further in the section covering the results of steady-state calculations.

Finite difference methods have been used to program for digital computation the ordinary differential equations describing the changes in enthalpy and reactant concentrations in the interstitial phase. No iteration is necessary to solve these equations numerically when the incremental axial distances are sufficiently small. The size of a succeeding increment is calculated at each axial position as a function of the rates of change of temperature and fractional ammonia dissociation with axial distance. However, Eq. (16), which must be solved simultaneously with the differential equations, is an implicit integral equation which requires an iterative procedure for solution. Hand calculations have indicated that convergence to a solution for $c_p(x)$ is difficult to achieve unless the initial estimate of the concentration distribution is fairly accurate. Methods have been developed for generating this estimate and an iterative procedure has been devised which effects

rapid convergence over a fairly wide range of conditions. This procedure is presently used as a subroutine in the main program representing the steady-state model. Sample calculations have been made to illustrate the use of this subroutine for computing concentration profiles in the porous catalyst particles, the associated temperature profiles, and the concentration gradients at the particle surface. The subroutine was run for values of the reaction rate constant, k_0, between 2.0 sec^{-1} and 2.0 x 10^6 sec^{-1}, and for $\beta = 0.171$, $\gamma = 18.3$, $D_p = 0.84 \times 10^{-5}$ ft^2/sec, $a = 0.005$ ft, $n = 1$, and $(c_p)_s = 0.357$ lb/ft^3. The values chosen for β, γ, D_p, n, and $(c_p)_s$ are reasonable for the decomposition of hydrazine within Shell 405 catalyst pellets. The resulting concentration profiles are plotted for each reaction rate constant in Fig. 1 and the associated temperature profiles are shown in Fig. 2. The concentration gradient at the particle surface is plotted as a function of the reaction rate constant in Fig. 3.

Transient Model

In developing the transient model, the temperature and the concentrations of reactants in the interstitial phase are assumed to vary only with time and axial distance along the bed. In this system film coefficients are used to describe heat and mass transfer between the interstitial phase and the outside surface of the catalyst pellets. The reactant concentrations, c_p, and the temperature, T_p, are taken as uniform within the interior of the porous particles. Heat and mass diffusion within the particles are taken into account by considering their effects on the utilization factor previously defined. That is, reaction rates computed on the basis of uniform c_p and T_p are multiplied by a utilization factor determined by analogy with the steady-state system. In addition, it is assumed that liquid velocities are sufficiently low relative to other rate processes so that, for all practical purposes, steady-state in the liquid and liquid-vapor regions is achieved as soon as the liquid reaches a given axial location in the reactor.

The transient model is concerned then with the vapor region only, where velocities are about three orders of magnitude greater than in the liquid region. Here it is reasonable to assume that gas velocities are so great that the time lag from the entrance to the vapor region to any position z for the fluid is negligible compared with other transient effects. With this assumption the rates of change of temperature and reactant weight fractions with axial distance in the interstitial phase are given by

$$\frac{\partial T_i}{\partial z} = -\frac{H^{N_2H_4}}{G\bar{C}_F} r_{hom}\delta - \frac{A_p}{G\bar{C}_F}\left[h_c\,(T_i - T_p)\right] - \frac{F}{G\bar{C}_F}\left[(h_i^v - h_F) + \bar{C}_F\,(T_i - T_{vap})\right] \qquad (19)$$

$$\frac{\partial w_i^{N_2H_4}}{\partial z} = \frac{1}{G}\left\{F - r_{hom}\,\delta - A_p k_c^{N_2H_4}\left(c_i^{N_2H_4} - c_p^{N_2H_4}\right)\right\} - \frac{Fc_i^{N_2H_4}}{G\rho_i} \qquad (20)$$

$$\frac{\partial w_i^{NH_3}}{\partial z} = \frac{1}{G}\left\{r_{hom}\,\delta\,\frac{M^{NH_3}}{M^{N_2H_4}} - A_p k_c^{NH_3}\left(c_i^{NH_3} - c_p^{NH_3}\right)\right\} - \frac{Fc_i^{NH_3}}{G\rho_i} \qquad (21)$$

$$\frac{\partial w_i^{N_2}}{\partial z} = \frac{1}{G}\left\{r_{hom}\,\delta\,\frac{M^{N_2}}{2M^{N_2H_4}} - A_p\,k_c^{N_2}\left(c_i^{N_2} - c_p^{N_2}\right)\right\} - \frac{Fc_i^{N_2}}{G\rho_i} \qquad (22)$$

$$\frac{\partial w_i^{H_2}}{\partial z} = \frac{1}{G}\left\{r_{hom}\,\delta\,\frac{M^{H_2}}{2M^{N_2H_4}} - A_p\,k_c^{H_2}\left(c_i^{H_2} - c_p^{H_2}\right)\right\} - \frac{Fc_i^{H_2}}{G\rho_i} \qquad (23)$$

The changes in reactant concentrations with axial distance can then be obtained using the above equations together with Eqs. (9), (10), and (11). At a given axial location the rates of change of temperature and reactant concentrations in the catalyst particles with time are given by

$$\frac{dT_p}{dt} = -\frac{1}{\rho_s C_s}\left[(H\,r_{het})^{N_2H_4} + (H r_{het})^{NH_3}\right] + \frac{3h_c}{a\rho_s C_s}\left(T_i - T_p\right) \qquad (24)$$

$$\frac{dc_p^{N_2H_4}}{dt} = -\frac{1}{\alpha_p} r_{het}^{N_2H_4} + \frac{3k_c^{N_2H_4}}{\alpha_p\, a}\left(c_i^{N_2H_4} - c_p^{N_2H_4}\right) \qquad (25)$$

$$\frac{dc_p^{NH_3}}{dt} = \frac{1}{\alpha_p}\left[r_{het}^{N_2H_4}\,\frac{M^{NH_3}}{M^{N_2H_4}} - r_{het}^{NH_3}\right] + \frac{3\,k_c^{NH_3}}{\alpha_p\, a}\left(c_i^{NH_3} - c_p^{NH_3}\right) \qquad (26)$$

$$\frac{dc_p^{N_2}}{dt} = \frac{1}{\alpha_p}\left[r_{het}^{N_2H_4}\frac{M^{N_2}}{2M^{N_2H_4}} + r_{het}^{NH_3}\frac{M^{N_2}}{2M^{NH_3}}\right] + \frac{3k_c^{N_2}}{\alpha_p a}\left(c_i^{N_2} - c_p^{N_2}\right) \quad (27)$$

$$\frac{dc_p^{H_2}}{dt} = \frac{1}{\alpha_p}\left[r_{het}^{N_2H_4}\frac{M^{H_2}}{2M^{N_2H_4}} + r_{het}^{NH_3}\frac{3M^{H_2}}{2M^{NH_3}}\right] + \frac{3k_c^{H_2}}{\alpha_p a}\left(c_i^{H_2} - c_p^{H_2}\right) \quad (28)$$

Recalling that the reaction of hydrazine on the catalyst surfaces is extremely fast, so that the reaction rate is controlled by the rate of transport of hydrazine to the catalyst surfaces, Eq. (25) can be used to define $r_{het}^{N_2H_4}$ by noting that $(dc_p^{N_2H_4}/dt)$ and $c_p^{N_2H_4}$ are both approximately equal to zero. The reaction rate is then given by

$$r_{het}^{N_2H_4} = \frac{3k_c^{N_2H_4}}{a} c_i^{N_2H_4} \quad (29)$$

The reaction rate of ammonia on the catalyst surfaces, $r_{het}^{NH_3}$, is computed by multiplying the rate of reaction calculated on the basis of uniform T_p and c_p (see section on Kinetics Information) by the utilization factor determined by analogy with the steady-state system. Under steady-state conditions the concentration gradient at the particle surface, $(dc_p^{NH_3}/dx)$, can be used to define this utilization factor which, for a first-order reaction, is given by:

$$\text{UTILIZATION FACTOR} = \left[3D_p(dc_p/dx)\right]_s \Big/ \left[a\,(c_p)_s k_o\right] \quad (30)$$

The subroutine in the steady-state program which calculates concentration distributions in the catalyst particles has been used to compute the concentration gradients at the particle surface and the corresponding utilization factors for about 100 different reactor operating conditions covering the range of interest of each of the parameters in this program. The results were then plotted as a function of a dimensionless diffusion parameter, $a\sqrt{k_o/D_p}$. All of the results fell within the limits of the dashed curves shown in Fig. 4. The mean results are shown as the solid curve in this figure.

Heat and mass transfer coefficients may be estimated from (Ref. 13).

$$k_c^J = \left(\frac{0.61\,G}{\rho_i}\right)\left(\frac{\mu}{\rho_i D_i^J}\right)^{-0.667}\left(\frac{G}{A_p\mu}\right)^{-0.41} \quad (31)$$

$$h_c = 0.74 \left(\frac{G}{A_p \mu}\right)^{-0.41} (\bar{C}_F G) \tag{32}$$

The ordinary and partial differential equations representing the transient model of the reactor system (Eqs. (19) through (28) along with Eqs. (9) through (11)) must be solved simultaneously for the variation of temperatures and reactant concentrations with time and axial position in the reactor. The partial differential equations representing the changes in interstitial temperature and reactant concentrations with axial distance can be treated as ordinary differential equations by integrating them at constant time. This can be accomplished, together with integrating Eqs. (24) through (28) at fixed axial positions, by establishing a network containing fixed time intervals and intervals of axial distance. Ideally, then, reactant concentrations and temperatures in the interstitial phase and in the catalyst particles could be computed at the ith time and jth axial distance from

$$(T_p)_{i,j} = (T_p)_{i-1,j} + \left(\frac{dT_p}{dt}\right)_{i-1,j} \Delta t \tag{33}$$

$$(c_p)^J_{i,j} = (c_p)^J_{i-1,j} + \left(\frac{dc_p}{dt}\right)^J_{i-1,j} \Delta t \tag{34}$$

$$(T_i)_{i,j} = (T_i)_{i,j-1} + \left(\frac{\partial T_i}{\partial z}\right)_{i,j-1} \Delta z \tag{35}$$

$$(c_i)^J_{i,j} = (c_i)^J_{i,j-1} + \left(\frac{\partial c_i}{\partial z}\right)^J_{i,j-1} \Delta z \tag{36}$$

This procedure is satisfactory as long as the intervals of time and axial distance are chosen to be sufficiently small so that the differential quantities are approximately constant in each interval. In the system considered here this restriction leads to rather long computing times. The restriction can be relaxed somewhat by rearranging each of the differential equations in the form

$$\frac{dg}{ds} = \alpha - \beta g \tag{37}$$

where it is required now that only the quantities α and β remain approximately constant while integrating the equation from s_{k-1} to s_k (corresponding to Δt or Δz). Equation (37) can be integrated to obtain

$$g_k = g_{k-1} e^{-\beta(s_k - s_{k-1})} + \frac{\alpha}{\beta}\left[1 - e^{-\beta(s_k - s_{k-1})}\right] \qquad (38)$$

where g_k is the value of g at s_k , and g_{k-1} is the value of g at s_{k-1} . An alternative form of Eq. (38) is

$$g_k = g_{k-1} + \left(\frac{dg}{ds}\right)_{k-1}\left[\frac{1 - e^{-\beta(s_k - s_{k-1})}}{\beta}\right] \qquad (39)$$

It can be seen that, for small values of ($s_k - s_{k-1}$), Eq. (39) reduces to the same form as Eqs. (33) through (36). It is convenient to use equations of the form of Eq. (38) in place of Eqs. (33) and (34) to compute particle concentrations and temperatures, and to use equations of the form of Eq. (39) in place of Eqs. (35) and (36) to compute interstitial concentrations and temperatures.

Kinetics Information

A number of investigators have reported rate expressions for the kinetics of homogeneous, vapor-phase decomposition of hydrazine (Refs. 7, 8, and 9). The rate expression chosen for use in this work was that of Ref. 7 because the results were obtained in a reactor similar to the one of interest here. The equation reported is

$$r_{hom}^{N_2H_4} = 2.14 \times 10^{10}\ c_i^{N_2H_4}\ e^{-33{,}000/T_i} \qquad lb/ft^3 - sec \qquad (40)$$

where $c_i^{N_2H_4}$ is in lb/ft^3 and T_i is in deg R.

Similar information relating to the catalytic decomposition of hydrazine is not available. However, a rate expression of the same form as Eq. (40) was chosen to represent the kinetics of the heterogeneous decomposition. Qualitative evidence from rocket firings at various feed temperatures indicates a rather low activation energy. A value of 2500 x 1.986 Btu/lb-mole was chosen rather arbitrarily and a preexponential factor in the Arrhenius type rate law was computed by using engine test data to make a rough estimate of the reaction rate at a typical feed temperature. These approximations have led to the following expression for reaction rate:

$$r_{het}^{N_2H_4} = 10^{10}\ c_p^{N_2H_4}\ e^{-2500/T_p} \qquad lb/ft^3 - sec \qquad (41)$$

where $c_p^{N_2H_4}$ is in lb/ft^3 and T_p is in deg R.

Melton (Ref. 14) and Logan and Kemball (Ref. 15) have conducted low pressure experiments on the vapor-phase decomposition of ammonia on platinum catalysts. They report a reaction rate expression of the form:

$$r_{het}^{NH_3} = \alpha^{NH_3} \frac{C_P^{NH_3}}{\left[C_P^{H_2}\right]^n} e^{-50,000/T_p} \qquad lb/ft^3 - sec \qquad (42)$$

where T_p is in deg R and n is given as 1.0 by Melton and as 1.6 by Logan and Kemball. Melton states however that ". . . The inhibitive action of hydrogen is probably a little greater than that corresponding to the first power of hydrogen. . ." A similar dependence on hydrogen concentration at higher pressures was questionable particularly if hydrogen was physically absorbed on the platinum catalyst. Increasing hydrogen concentration beyond a certain point might then have much less effect on impeding the reaction rate. It was decided to perform computer calculations using the steady-state program assuming no dependence of $r_{het}^{NH_3}$ on the hydrogen concentration and then see if the value of α^{NH_3} which best fits the experimental data decreases as the pressure increases. Such behavior would indicate that the dependence on hydrogen concentration did indeed extend to higher pressures. This behavior was in fact observed. It was assumed, of course, that the order of the ammonia dissociation reaction with respect to hydrogen is the same on the Shell 405 catalyst as it is on platinum. Although this assumption remains untested, subsequent calculations using the steady-state program exhibit the best agreement with the available engine test data when $r_{het}^{NH_3}$ is given by

$$r_{het} = 0.3 \times 10^{11} \frac{C_p^{NH_3}}{(C_p^{H_2})^{1.6}} e^{-50,000/T_p} \qquad lb/ft^3 - sec \qquad (43)$$

where the concentrations are expressed in lb/ft^3.

It should be emphasized that the value of 0.3×10^{11} for α^{NH_3} was obtained by comparing experimental data with temperature and concentration profiles calculated using the computer program representing the steady-state model. It is implicitly assumed in this model that the temperature at the surface of the catalyst pellet is equal to the interstitial temperature at the same axial location. This assumption has little effect on the calculated rates of the diffusion-controlled hydrazine decomposition and it is fairly accurate in regions of the reaction chamber where only ammonia is decomposing. However, in regions where both hydrazine and ammonia are decomposing simultaneously, the catalyst particle surface temperatures may be higher than the interstitial temperatures. If this were taken into account in the steady-state model the value of α^{NH_3} exhibiting closest agreement with experimental data would be somewhat larger than 0.3×10^{11}. In the simpler format of the transient model the differences between the particle surface and interstitial temperatures are accounted for and the rates of heat transfer corresponding to these temperature differences are expressed in terms of a heat transfer coefficient.

Theoretically then, the transient model, when extrapolated to steady-state and compared with experimental data, should yield a more accurate value of α^{NH_3}. The value obtained using the extrapolated transient results is 1×10^{11}. However, heat transfer coefficients used in this model are estimated using correlations developed for nonreacting systems. In regions where significant chemical reaction takes place, such as the zones in which both hydrazine and ammonia are decomposing, actual heat transfer rates are considerably higher than those calculated in the transient model. This would lead to a value of α^{NH_3} less than 1×10^{11}. The actual value of α^{NH_3} is probably between the one estimated using the steady-state program (0.3×10^{11}) and the one estimated using the transient program (1×10^{11}).

Results of Calculations

Calculations were made with the computer programs representing the steady-state and transient models of the reactor system to evaluate the effects on temperature and reactant concentration distributions of such parameters as initial bed temperature, feed temperature, chamber pressure, mass flow rate, axial injection profile, and catalyst size distribution. The sensitivity of the calculated results to variations in the rate constants associated with the catalytic decomposition reactions was also determined. The results have been compared, wherever possible, to available measurements of temperature profiles and exhaust concentrations made during firings of typical hydrazine engine reaction chambers.

Steady-State Results

A series of calculations was made using the steady-state program for cases for which experimental information is available (Ref. 2) in order to examine the effectiveness of the steady-state model and to establish the rate constants associated with the catalytic decomposition reactions. The results of these calculations are shown in Figs. 5 through 19. For each of these cases the catalyst bed packing was taken to consist of 25-30 mesh catalyst particles for the first 0.2 in. and 1/8 in. x 1/8 in. cylindrical pellets for the remainder of the bed. This configuration is referred to in the figures as the "standard bed configuration." Except where the rate constants α^{NH_3} and $\alpha^{N_2H_4}$ were varied, the rates of the catalytic decomposition reactors were given by Eqs. (41) and (43). Equation (43) was simplified somewhat by noting that, since hydrogen diffusion is quite rapid, $c_p^{H_2} \sim c_i^{H_2}$. The reactor operating conditions of chamber pressure and mass flow rate were varied, as was the feed temperature, T_F; although, in each of these cases, T_F was between approximately 510 and 530 deg R.

Temperature distributions are plotted in Fig. 5 for a case in which the reactor operating conditions were taken as $G = 3.12$ lb/ft^2- sec and $P = 479.5$ psia. Temperature profiles are plotted for $\alpha^{NH_3} = 0.3 \times 10^{10}$, 0.3×10^{11}, and 0.3×10^{12} (lb/ft^3)$^{0.6}$ (sec)$^{-1}$. An enlarged view of the temperature profile in the liquid-vapor region is shown to illustrate the effects of pure liquid as opposed to a combination of liquid and vapor wetting the outside surface of the catalyst particles. Also shown in Fig. 5 are temperature measurements obtained by Rocket Research

Corporation (Ref. 2) during the course of engine firings under the same operating conditions. Comparison of the calculated results with the experimental data indicates better correspondence of results with $\alpha^{NH_3} = 0.3 \times 10^{11}$ $(lb/ft^3)^{0.6}$ $(sec)^{-1}$. The calculated mole-fraction profiles associated with this rate constant, together with experimental values of mole-fractions, are shown in Fig. 6. The corresponding fractional ammonia dissociation profile is shown in Fig. 7. The results of similar calculations made for G = 2.43 lb/ft^2-sec and P = 1042 psia are shown in Figs. 8 through 10; those made for G = 6.29 lb/ft^2-sec and P = 974 psia are shown in Figs. 11 through 13; those made for G = 1.52 lb/ft^2-sec and P = 217.9 psia are shown in Figs. 14 through 16, and those made for G = 1.51 lb/ft^2-sec and P = 111.4 psia are shown in Figs. 17 through 19.

In each of the above calculations the rate constant for the catalytic decomposition of hydrazine was taken as 10^{10} sec^{-1}. Since catalytic decomposition of hydrazine is diffusion-controlled in the vapor region, varying this rate constant would only affect the width of the liquid and liquid-vapor regions. These regions are extremely narrow for the cases examined above because of the large surface area of the small catalyst particles in these regions and because of the high vapor pressure of liquid hydrazine at the feed temperatures considered.

The effects of various reactor operating conditions on steady-state temperature profiles are illustrated more specifically in Figs. 20 through 23. A reference case was chosen in which the operating conditions were G = 3.0 lb/ft^2-sec, P = 100 psia, and T_F = 530 R, and the catalyst bed configuration was the "standard bed configuration." Chamber pressure, mass flow rate, catalyst bed configuration and axial injection profile were then varied in turn and the resulting temperature distributions were plotted. In Fig. 20 temperature distributions are plotted for chamber pressures of 100, 500, and 1000 psia with all other conditions taken as those of the reference case. Increasing pressure causes the peak temperature to rise and shift slightly toward the inlet of the reactor. This is due to the inhibiting action of hydrazine on the rate of ammonia dissociation. Temperature profiles are shown in Fig. 21 for mass flow rates of 1.5, 3.0, and 6.0 lb/ft^2-sec. Increasing flow rate causes the peak temperature to rise and shift slightly away from the reactor inlet. The effect of changing the catalyst bed configuration on the temperature distribution is shown in Fig. 22. Temperature profiles are plotted for beds packed with all 25-30 mesh particles, all 1/8 in. x 1/8 in. cylindrical pellets, and the standard non-uniform particle size distribution. It is apparent that the larger particles slow down the rates of the catalytic decomposition reactions. The effects of distributed injectors on temperature profiles are illustrated in Fig. 23. Temperature distributions are plotted for the reference case, for the case in which 2/3 of the hydrazine is injected at the inlet and the remaining 1/3 is injected uniformly over the first 1/2 in. of the reactor, and for the case in which 1/3 of the hydrazine is injected at the inlet and the remaining 2/3 is injected uniformly over the first 1/2 in. of the reactor. In these cases the bed was taken to be packed with all 25-30 mesh particles.

Steady-state temperature and reactant concentration distributions can also be obtained using the transient program by running the calculations out to long (essentially infinite) times. A comparison of the steady-state axial temperature profiles computed from the steady-state and transient programs is shown in Fig. 24 for reactor operating conditions of $G = 3.12$ lb/ft^2- sec, P(feed pressure) = 479.5 psia, and $T_F = 509$ deg R and for the standard bed configuration. The rate constant for the catalytic decomposition of ammonia, α^{NH_3}, was taken as 10^{11} (lb/ft^3)$^{0.6}$ (sec)$^{-1}$ (see section on Kinetics Information). A comparison of the associated axial profiles of mole-fraction of ammonia computed from the steady-state and transient models is shown in Fig. 25.

Transient Results

A series of calculations was made using the transient program for the same cases cited previously in order to examine the effectiveness of the transient model of the reactor system. The results of these calculations are shown in Figs. 26 through 44. In each of these cases the catalyst bed configuration was taken as the standard configuration, the feed temperature varied slightly between approximately 510 and 530 deg R, and the initial bed temperature was taken equal to the feed temperature. Temperature distributions are plotted for various times up to steady-state in Fig. 26 for a case in which the reactor operating conditions were taken as $G = 3.12$ lb/ft^2- sec and P(feed pressure) = 479.5 psia. The vaporization time noted in Fig. 26 is defined as the time required, under steady-state conditions, for liquid hydrazine to flow from the reactor inlet to the interface between the liquid-vapor and vapor regions. Temperatures are cross-plotted as a function of time at three axial positions in Fig. 27. Also shown in Fig. 27 are temperature measurements obtained by Rocket Research Corporation (Ref. 16) during the course of engine firings under the same operating conditions. The calculated mole-fraction profiles corresponding to the temperature profiles shown in Fig. 26 are illustrated in Figs. 28, 29, 30 and 31 for hydrazine, ammonia, nitrogen, and hydrogen, respectively. The chamber exit pressure for this case was calculated as a function of time and plotted in Fig. 32. It is interesting to note that the chamber exit pressure rises sharply, initially, as hydrazine and the products of hydrazine decomposition in the upstream end of the reaction chamber flow through the reactor, drops as hydrazine decomposes on the catalyst surfaces further downstream in the reactor and as the products of hydrazine decomposition diffuse into the catalyst particles, and rises again once the concentrations of the products of hydrazine decomposition equilibrate between the vapor phase and the catalyst particles in the downstream end of the reactor. The results of similar calculations made for $G = 2.43$ lb/ft^2-sec and P (feed pressure) = 1040 psia are shown, except for the concentration profiles, in Figs. 33 through 35; those made for $G = 6.29$ lb/ft^2-sec and $P = 974$ psia are shown in Figs. 36 through 38; those made for $G = 1.52$ lb/ft^2-sec and $P = 217.9$ psia are shown in Figs. 39 through 41, and those made for $G = 1.51$ lb/ft^2-sec and $P = 111.4$ psia are shown in Figs. 42 through 44.

The effects of various reactor operating conditions on the variation of gas temperature at the chamber exit with time can be better illustrated by comparing, with a reference case, the results of calculations made in turn for various chamber pressures, mass flow rates, catalyst bed configurations, axial injection profiles, and initial bed temperatures. A reference case was chosen in which the operating conditions were taken as G = 3.0 lb/ft^2- sec, P (feed pressure) = 100 psia, T_F = 530 deg R and T_p (initial) = 530 deg R, and the catalyst bed configuration was taken as the "standard bed configuration." The bed length was taken as 0.25 ft. In Fig. 45 exit gas temperatures are plotted as a function of time for feed pressures of 100 and 1000 psia with all other conditions taken as those of the reference case. Very little effect of pressure on transient response is noted. The marked effect of mass flow rate on transient response time is shown in Fig. 46 where exit gas temperatures are plotted versus time for mass flow rates of 1.5, 3.0, and 6.0 lb/ft^2- sec. The effect of changing the catalyst bed configuration on the temperature variation with time is illustrated in Fig. 47. Exit gas temperatures are plotted as a function of time for beds packed with all 25-30 mesh particles, all 1/8 in. x 1/8 in. cylindrical pellets, and the standard non-uniform particle size distribution. The effects of distributed injectors on temperature profiles is shown in Fig. 48. Exit gas temperatures are plotted as functions of time for a constant mass flow rate and for the case in which 1/3 of the hydrazine is injected at the inlet and the remaining 2/3 is injected uniformly over the first 1/2 in. of the reactor. In these cases the bed was taken to be packed with all 25-30 mesh particles and the initial bed temperature was taken as 1200 deg R in order to insure vaporization of the cold hydrazine injected downstream of the inlet. Finally, the effects of varying the initial bed temperatures are illustrated in Fig. 49. Exit gas temperatures are plotted versus time in Fig. 49 for initial bed temperatures of 530, 1200, and 1500 deg R.

REFERENCES

1. Grant, A. F., Jr.: Basic Factors Involved in the Design and Operation of Catalytic Monopropellant-Hydrazine Reaction Chambers. Jet Propulsion Laboratory Report No. 20-77, December 31, 1954.

2. Rocket Research Corporation: Development of Design and Scaling Criteria for Monopropellant Hydrazine Reactors Employing Shell 405 Spontaneous Catalyst. RRC-66-R-76, January, 1967.

3. Armstrong, W. E., D. S. LaFrance, and H. H. Voge: Development of Catalysts for Monopropellant Decomposition of Hydrazine (U). Part I, Experimental Studies (Confidential). Part II, Engineering Calculations (Confidential). Shell Development Company Report S-13864, 1962.

4. Armstrong, W. E., R. D. Hawthorn, D. S. LaFrance, C. Z. Morgan, L. B. Ryland, and H. H. Voge: Development of Catalysts for Monopropellant Decomposition of Hydrazine (U). Shell Development Company Report S-13889, 1963. (Confidential)

5. Armstrong, W. E., C. Z. Morgan, L. B. Ryland, and H. H. Voge: Development of Catalysts for Monopropellant Decomposition of Hydrazine (U). Shell Development Company Report S-13917, 1964 (Confidential)

6. Armstrong, W. E., C. Z. Morgan, L. B. Ryland, and H. H. Voge: Development of Catalysts for Monopropellant Decomposition of Hydrazine (U). Shell Development Company Report S-13947, 1964 (Confidential)

7. Eberstein, I. J., and I. Glassman: The Gas-Phase Decomposition of Hydrazine and Its Methyl Derivations. Tenth Symposium (International) on Combustion, Pittsburgh, The Combustion Institute, 1965, pp. 365-374.

8. McHale, E. T., B. E. Knox, and H. B. Palmer: Determination of the Decomposition Kinetics of Hydrazine Using a Single-Pulse Shock Tube. Tenth Symposium (International) on Combustion, The Combustion Institute, Pittsburgh, 1965, pp. 341-351.

9. Michel, K. W., and H. GG. Wagner: The Pyrolysis and Oxidation of Hydrazine Behind Shock Waves. Tenth Symposium (International) on Combustion, The Combustion Institute, Pittsburgh, 1965, pp. 353-364.

10. Askey, P. J.: The Thermal Decomposition of Hydrazine. J. Am. Chem. Soc., Vol. 52, 1930, pp. 970-974.

11. Prater, D. C.: The Temperature Produced by Heat of Reaction in the Interior of Porous Particles. Chemical Engineering Science, Vol. 8, 1958, pp. 284-286.

12. Weisz, P. B., and J. S. Hicks: The Behavior of Porous Catalyst Particles in View of Internal Heat and Mass Diffusion Effects. Chemical Engineering Science, Vol. 17, 1962, pp. 265-275.

13. Bird, R. B., W. E. Stewart, and E. N. Lightfoot: Transport Phenomena. John Wiley & Sons, Inc., New York, 1960.

14. Melton, C. E., and P. H. Emmett: Transient Species Observed in the Catalyzed Decomposition of Ammonia. J. of Physical Chemistry, 68, 1964, pp. 3318-3324.

15. Logan, S. R., and C. Kemball: The Catalytic Decomposition of Ammonia on Evaporated Metal Films. Transactions of the Faraday Society, 56, 1960, pp. 144-153.

16. Unpublished Data. Rocket Research Corp.

17. Irving, J., and N. Mullineux: Mathematics in Physics and Engineering. Academic Press, Inc., New York, 1959, p. 731.

LIST OF SYMBOLS

a	Radius of spherical particle, ft
A_p	Total external surface of catalyst particle per unit volume of bed, ft^{-1}
c_i	Reactant concentration in interstitial fluid, lb/ft^3
c_p	Reactant concentration in gas phase within the porous particle, lb/ft^3
c_p^*	Equals $c_p - (c_p)_s$, lb/ft^3
C_f	Specific heat of fluid in the interstitial phase, Btu/lb - deg R
$\bar{C}_f$	Average specific heat of fluid in the interstitial phase, Btu/lb - deg R
C_s	Specific heat of catalyst particle, Btu/lb - deg R
D_i	Diffusion coefficient of reactant gas in the interstitial fluid, ft^2/sec
D_p	Diffusion coefficient of reactant gas in the porous particle, ft^2/sec
F	Rate of feed of hydrazine from distributed injectors into the system, lb/ft3- sec
g	Dependent variable in Eq. (37)
G	Mass flow rate, lb/ft^2- sec
h	Enthalpy, Btu/lb
h_c	Heat transfer coefficient, Btu/ft^2- sec - deg R
H	Heat of reaction (negative for exothermic reaction), Btu/lb
k_c	Mass transfer coefficient, ft/sec
k_o	Reaction rate constant, equals $\alpha e^{-\gamma}$, sec^{-1}
K_p	Thermal conductivity of the porous catalyst particle, Btu/ft-sec-deg R
M	Molecular weight, lb/lb mole
$\bar{M}$	Average molecular weight, lb/lb mole
n	Order of decomposition reaction
P	Chamber pressure, psia

LIST OF SYMBOLS (cont'd)

Q	Activation energy, Btu/lb mole
r_{het}	Rate of (heterogeneous) chemical reaction on the catalyst surfaces, lb/ft^3 - sec
r_{hom}	Rate of (homogeneous) chemical reaction in the interstitial phase, lb/ft^3 - sec
s	Independent variable in Eq. (37)
R	Gas constant, equals 10.73 psia - ft^3/lb mole - deg R
t	Time, sec
t^*	Actual time minus time required, under steady-state conditions, for liquid hydrazine to flow from the reactor inlet to the interface between the liquid-vapor and vapor regions, sec
T	Temperature, deg R
u	Mathematical function (defined in Appendix I)
v	Mathematical function (defined in Appendix I)
w_i	Weight fraction of reactant in interstitial phase
x	Radial distance from the center of the spherical catalyst particle, ft
z	Axial distance, ft
α	Preexponential factor in rate equation, or Constant in Eq. (37)
α_p	Intraparticle void fraction
β	Equals $\frac{-(c_p)_s \, H \, D_p}{K_p \, (T_p)_s}$, or Constant in Eq. (37)
γ	Equals $Q / R(T_p)_s$
δ	Interparticle void fraction
μ	Viscosity of interstitial fluid, lb/ft - sec
ρ_i	Density of interstitial fluid, lb/ft^3
ρ_s	Bulk density of catalyst particle, lb/ft^3

LIST OF SYMBOLS (cont'd)

ϕ	Mathematical function (defined in Appendix I)

Subscripts

F	Refers to feed
i	Refers to interstitial phase, or
	Time index in transient model
j	Axial distance index in transient model
k	Index in Eqs. (38) and (39)
P	Refers to gas within the porous catalyst particle
S	Refers to surface of catalyst particle

Superscripts

J	Refers to chemical species
L	Refers to liquid at vaporization temperature
V	Refers to vapor at vaporization temperature

APPENDIX I

DERIVATION OF INTEGRAL EQUATIONS REPRESENTING THE CONCENTRATION PROFILES OF REACTANTS WITHIN THE CATALYST PARTICLES

In this section equations are developed to describe the steady-state concentration profiles of hydrazine vapor and of ammonia within the catalyst particles. The reactant concentration profiles in the porous particles at any axial location can be found as solutions to:

$$D_p \nabla^2 c_p - r_{het}(c_p) = 0 \qquad \text{(I-1)}$$

If the catalyst particles are taken to be "equivalent" spheres of radii a, and if concentration c_p^* is defined such that $c_p^* = c_p - (c_p)_s$, Eq. (I-1) can be written as

$$D_p \left[\frac{1}{x^2} \frac{d}{dx} \left(x^2 \frac{dc_p^*}{dx} \right) \right] - r_{het} = 0 \qquad \text{(I-2)}$$

where x is the radial distance from the center of a sphere. The boundary conditions associated with Eq. (I-2) are

$$c_p^* = 0 \quad \text{AT} \quad x = a, \qquad \frac{dc_p^*}{dx} = 0 \quad \text{AT} \quad x = 0 \qquad \text{(I-3)}$$

Equation (I-2) can be rearranged to get

$$\frac{d}{dx} \left(x^2 \frac{dc_p^*}{dx} \right) = \frac{r_{het} x^2}{D_p} = \phi(x, c_p^*) \qquad \text{(I-4)}$$

The solution to Eq. (I-4) is most easily obtained by converting it into a Fredholm integral equation (see Ref. 17) of the form

$$c_p^*(x) = \frac{1}{x^2 \left[u(x) v'(x) - u'(x) v(x) \right]} \int_0^a G(x, \xi) \, \phi(\xi, c_p^*) \, d\xi \qquad \text{(I-5)}$$

where $u(x)$ is a solution of

$$\frac{d}{dx}\left(x^2 \frac{du}{dx}\right) = 0 \tag{I-6}$$

subject to the condition that

$$\left[u \frac{dc_p^*}{dx} - \frac{du}{dx} c_p^*\right]_{x=0} = 0 \tag{I-7}$$

and $v(x)$ is a solution of

$$\frac{d}{dx}\left(x^2 \frac{dv}{dx}\right) = 0 \tag{I-8}$$

subject to the condition that

$$\left[v \frac{dc_p^*}{dx} - \frac{dv}{dx} c_p^*\right]_{x=a} = 0 \tag{I-9}$$

The Green's function, $G(x,\xi)$ is given by

$$G(x,\xi) = \begin{cases} u(\xi)\, v(x) & \text{FOR} \quad 0 \le \xi \le x \\ u(x)\, v(\xi) & \text{FOR} \quad x \le \xi \le a \end{cases} \tag{I-10}$$

The function $u(x)$ can be determined by first integrating Eq. (I-6) to get

$$u = -\frac{A_1}{x} + B_1 \tag{I-11}$$

Applying Eq. (I-7) together with the first of boundary conditions (I-3) to Eq. (I-11), it is found that $A = 0$ and

$$u = B_1 \tag{I-12}$$

The function $v(x)$ can be determined in a similar manner by first integrating Eq. (I-8) to get

$$v = -\frac{A_2}{x} + B_2 \qquad \text{(I-13)}$$

and then applying Eq. (I-9) and the second of boundary conditions (I-3) to Eq. (I-13) to get

$$v = A_2\left[\frac{1}{a} - \frac{1}{x}\right] \qquad \text{(I-14)}$$

Equations (I-10), (I-12), and (I-14) can now be combined to get

$$G(x,\xi) = \begin{cases} A_2 B_1\left[\frac{1}{a} - \frac{1}{x}\right] & \text{FOR} \quad 0 \le \xi \le x \\ A_2 B_1\left[\frac{1}{a} - \frac{1}{\xi}\right] & \text{FOR} \quad x \le \xi \le a \end{cases} \qquad \text{(I-15)}$$

In addition,

$$x^2\left[u(x)\,v'(x) - u'(x)\,v(x)\right] = A_2 B_1 \qquad \text{(I-16)}$$

Equations (I-15) and (I-16) can now be substituted into Eq. (I-5) to get

$$c_p^*(x) = \left[\frac{1}{a} - \frac{1}{x}\right]\int_0^x \phi(\xi, c_p^*)\,d\xi + \int_x^a \left[\frac{1}{a} - \frac{1}{\xi}\right]\phi(\xi, c_p^*)\,d\xi \qquad \text{(I-17)}$$

or

$$c_p(x) = (c_p)_s - \left[\frac{1}{x} - \frac{1}{a}\right]\int_0^x \xi^2 \frac{r_{het}(c_p)}{D_p}\,d\xi - \int_x^a \left[\frac{1}{\xi} - \frac{1}{a}\right]\xi^2 \frac{r_{het}(c_p)}{D_p}\,d\xi \qquad \text{(I-18)}$$

Equation (I-18) is an implicit integral equation which can be solved numerically to determine the concentration at any point in a porous particle in terms of $(c_p)_s$, the concentration at the surface of the particle. The gradients of c_p, evaluated at the particle surfaces at given axial locations, can then be obtained from the slopes of curves of c_p versus x at $x = a$.

FIG. 1

EFFECT OF REACTION RATE CONSTANT
ON CONCENTRATION PROFILE WITHIN CATALYST PARTICLE

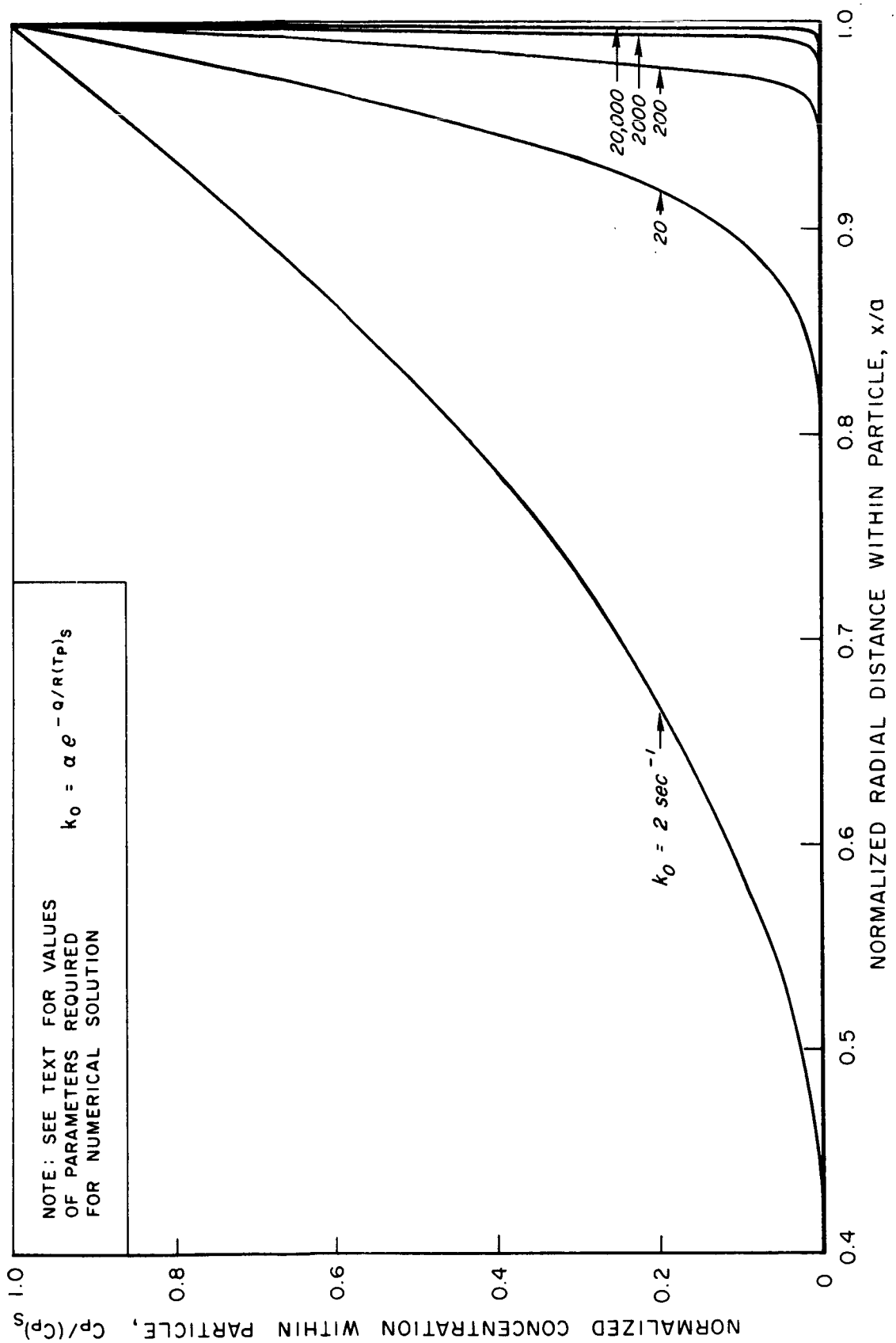

FIG. 2

EFFECT OF REACTION RATE CONSTANT
ON TEMPERATURE PROFILE WITHIN CATALYST PARTICLE

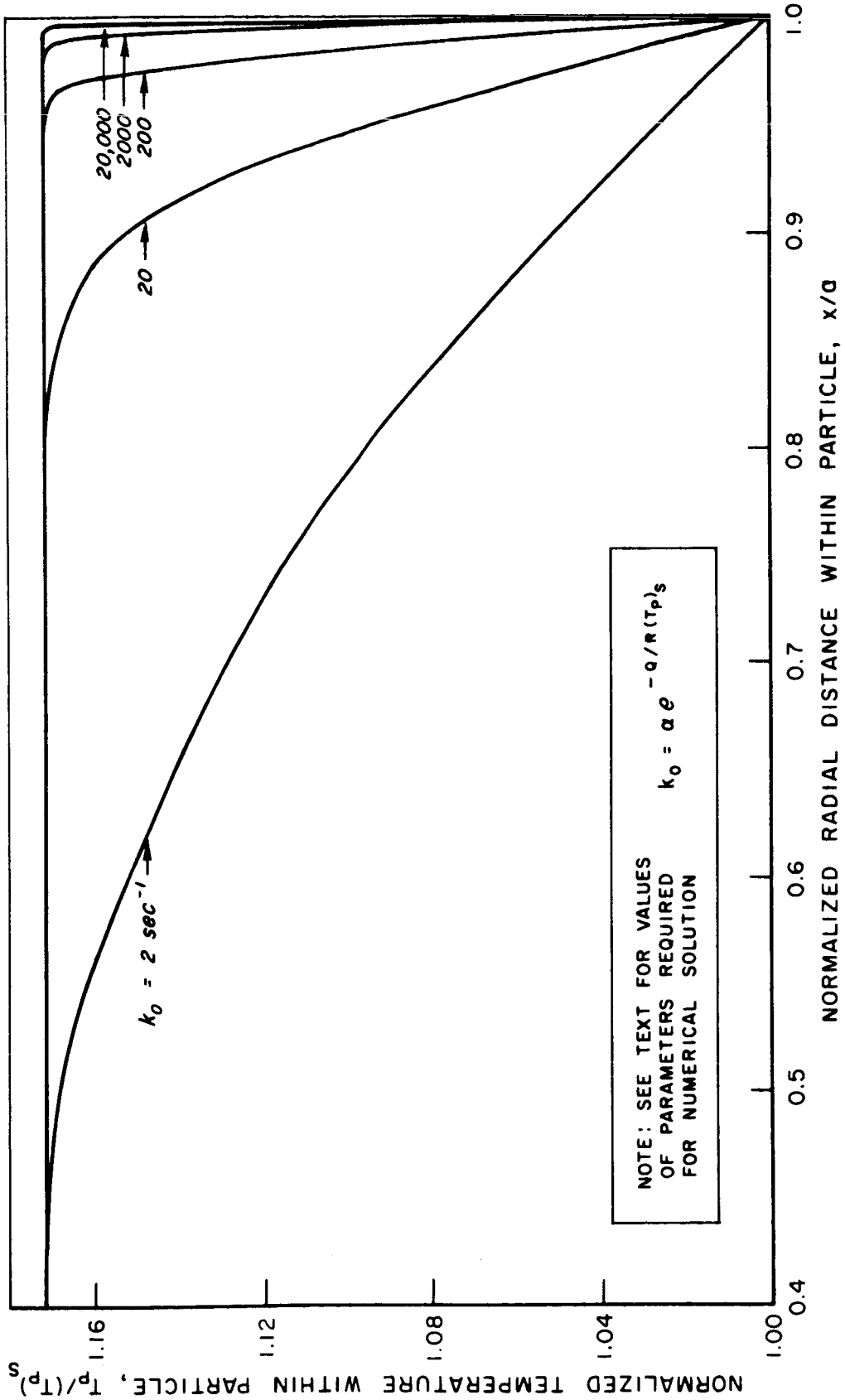

FIG. 3

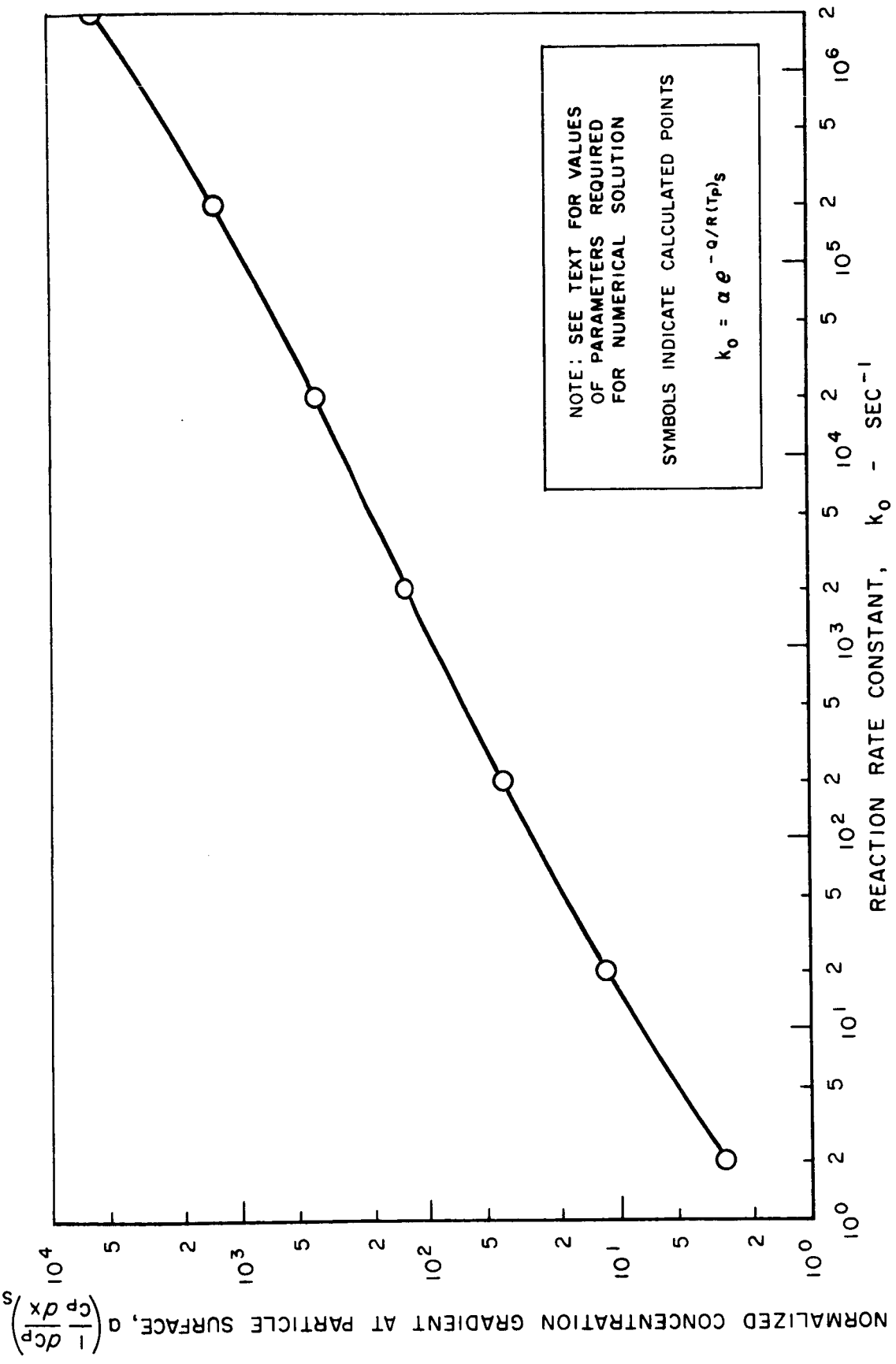
VARIATION OF CONCENTRATION GRADIENT AT PARTICLE SURFACE WITH REACTION RATE CONSTANT
NOTE: SEE TEXT FOR VALUES OF PARAMETERS REQUIRED FOR NUMERICAL SOLUTION
SYMBOLS INDICATE CALCULATED POINTS
$k_o = \alpha e^{-Q/R(T_p)_s}$
NORMALIZED CONCENTRATION GRADIENT AT PARTICLE SURFACE, $\alpha \left(\frac{1}{C_p}\frac{dC_p}{dx}\right)_s$
REACTION RATE CONSTANT, k_o - SEC^{-1}
10^0 2 5 10^1 2 5 10^2 2 5 10^3 2 5 10^4 2 5 10^5 2 5 10^6 2
10^0 2 5 10^1 2 5 10^2 2 5 10^3 2 5 10^4

FIG. 4

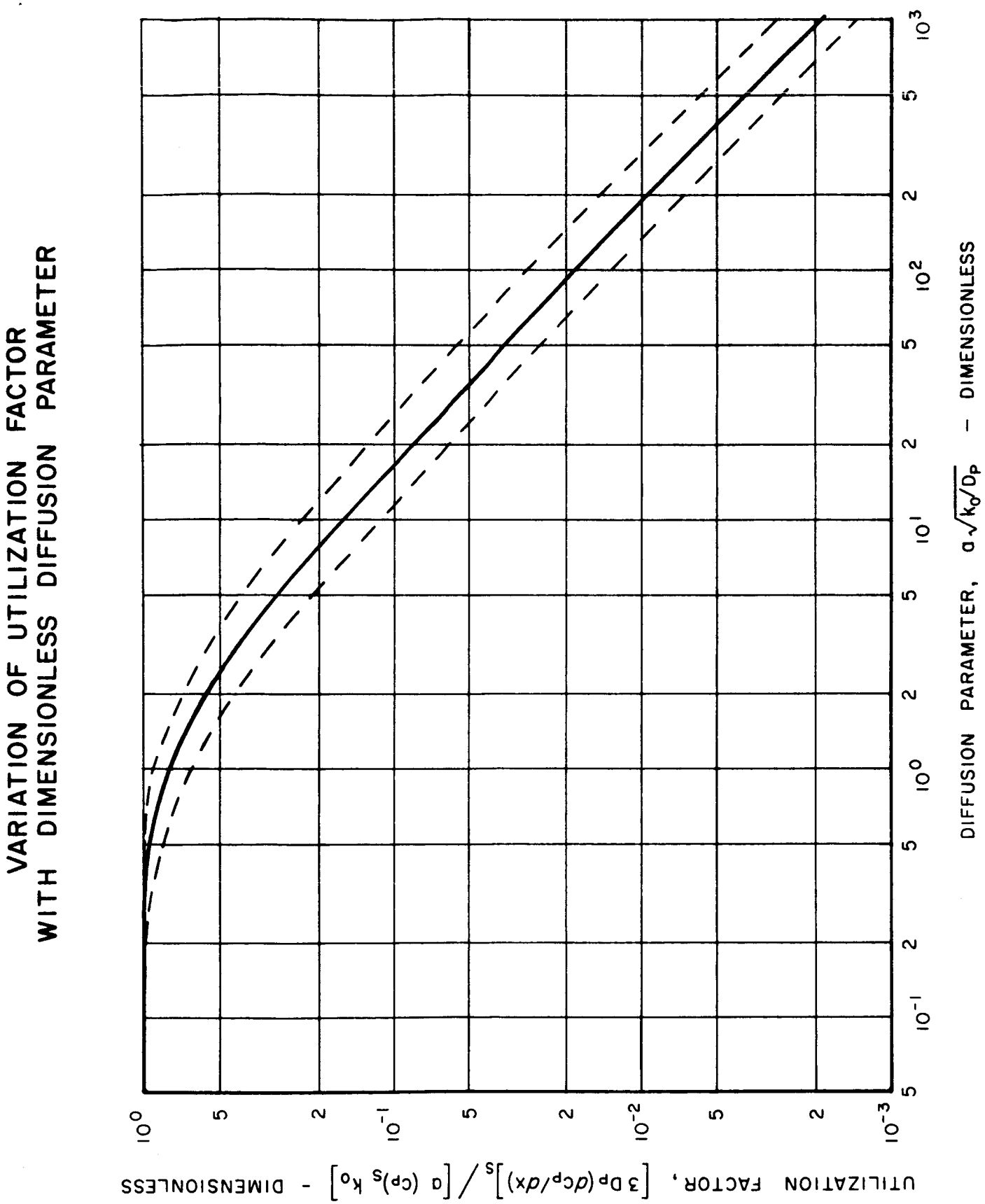
VARIATION OF UTILIZATION FACTOR
WITH DIMENSIONLESS DIFFUSION PARAMETER
UTILIZATION FACTOR, $[3 D_P (dc_P/dx)]_S / [a (cp)_S k_o]$ - DIMENSIONLESS
DIFFUSION PARAMETER, $a\sqrt{k_o/D_P}$ - DIMENSIONLESS
10^0
5
2
10^{-1}
5
2
10^{-2}
5
2
10^{-3}
5
2
10^{-1}
5
2
10^0
5
2
10^1
5
2
10^2
5
2
10^3

FIG. 5

STEADY-STATE AXIAL TEMPERATURE PROFILES FOR VARIOUS RATE CONSTANTS FOR THE CATALYTIC DECOMPOSITION OF AMMONIA

P = 479.5 PSIA
G = 3.12 LB/FT^2 - SEC
STANDARD BED CONFIGURATION (SEE TEXT)

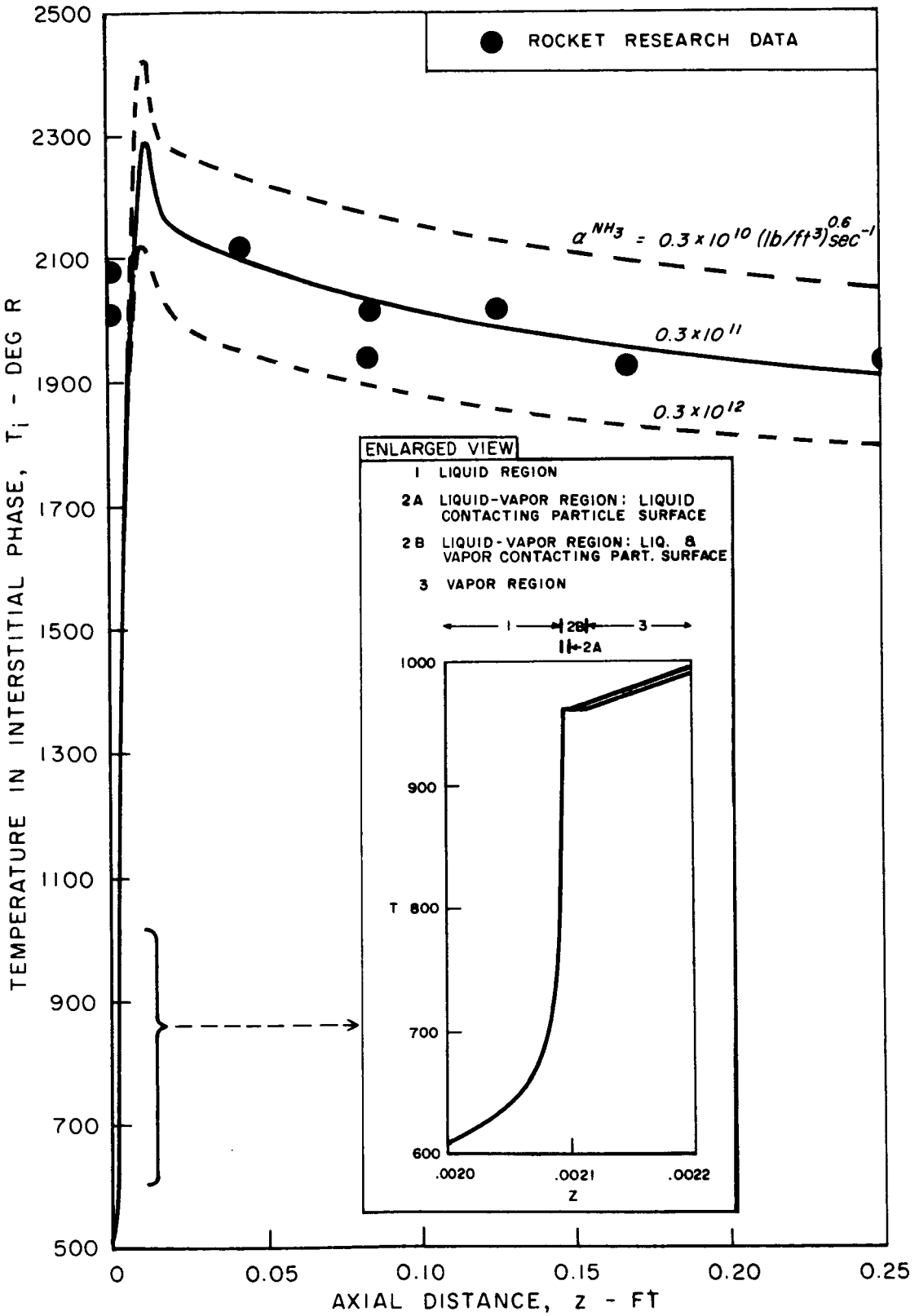

FIG. 6

STEADY-STATE AXIAL PROFILES OF MOLE-FRACTIONS OF REACTANTS

P = 479.5 PSIA
G = 3.12 LB/FT^2-SEC
STANDARD BED CONFIGURATION (SEE TEXT)

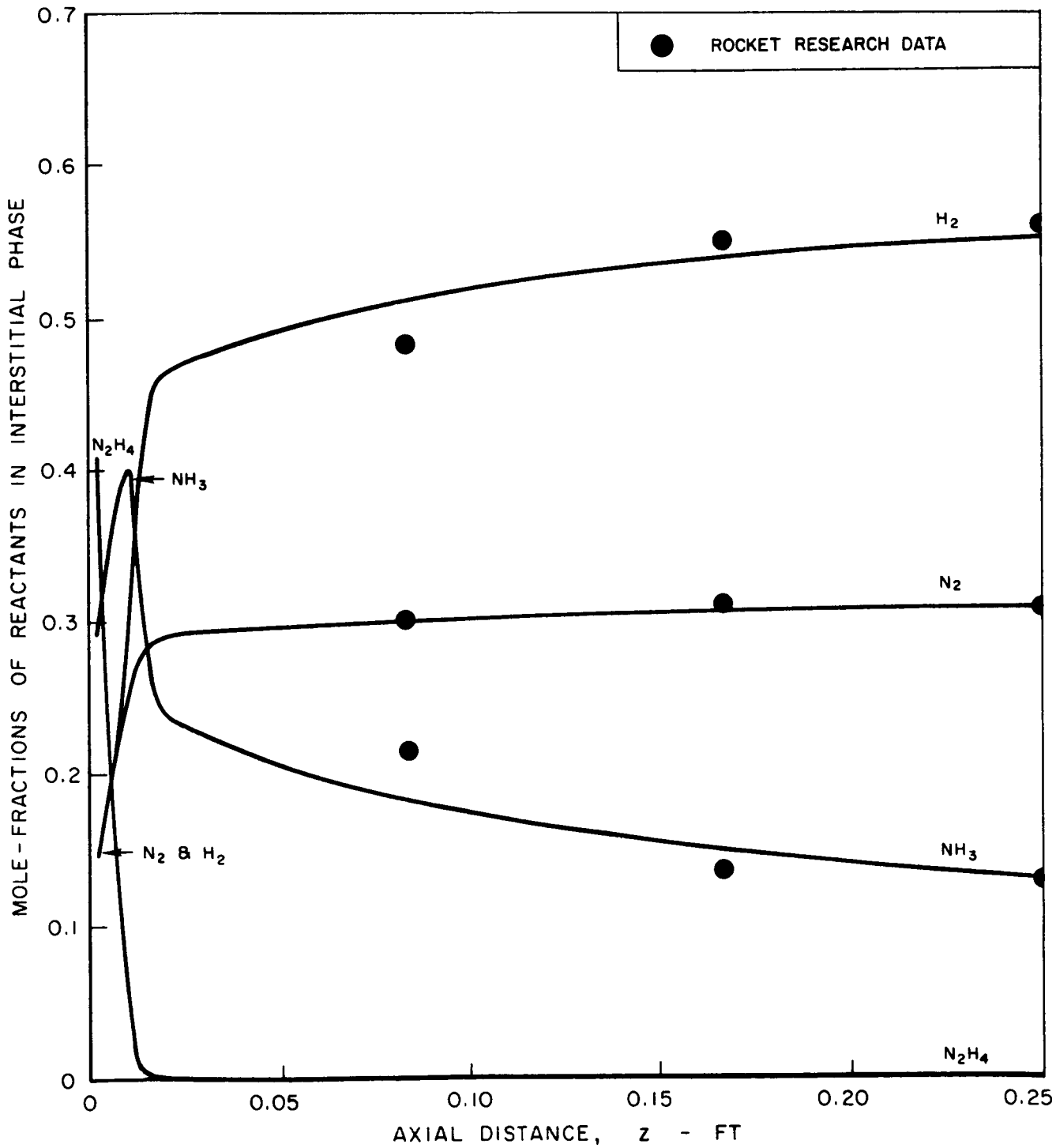

FIG. 7

STEADY-STATE AXIAL PROFILE OF FRACTIONAL AMMONIA DISSOCIATION

P = 479.5 PSIA
G = 3.12 LB/FT^2 - SEC
STANDARD BED CONFIGURATION (SEE TEXT)

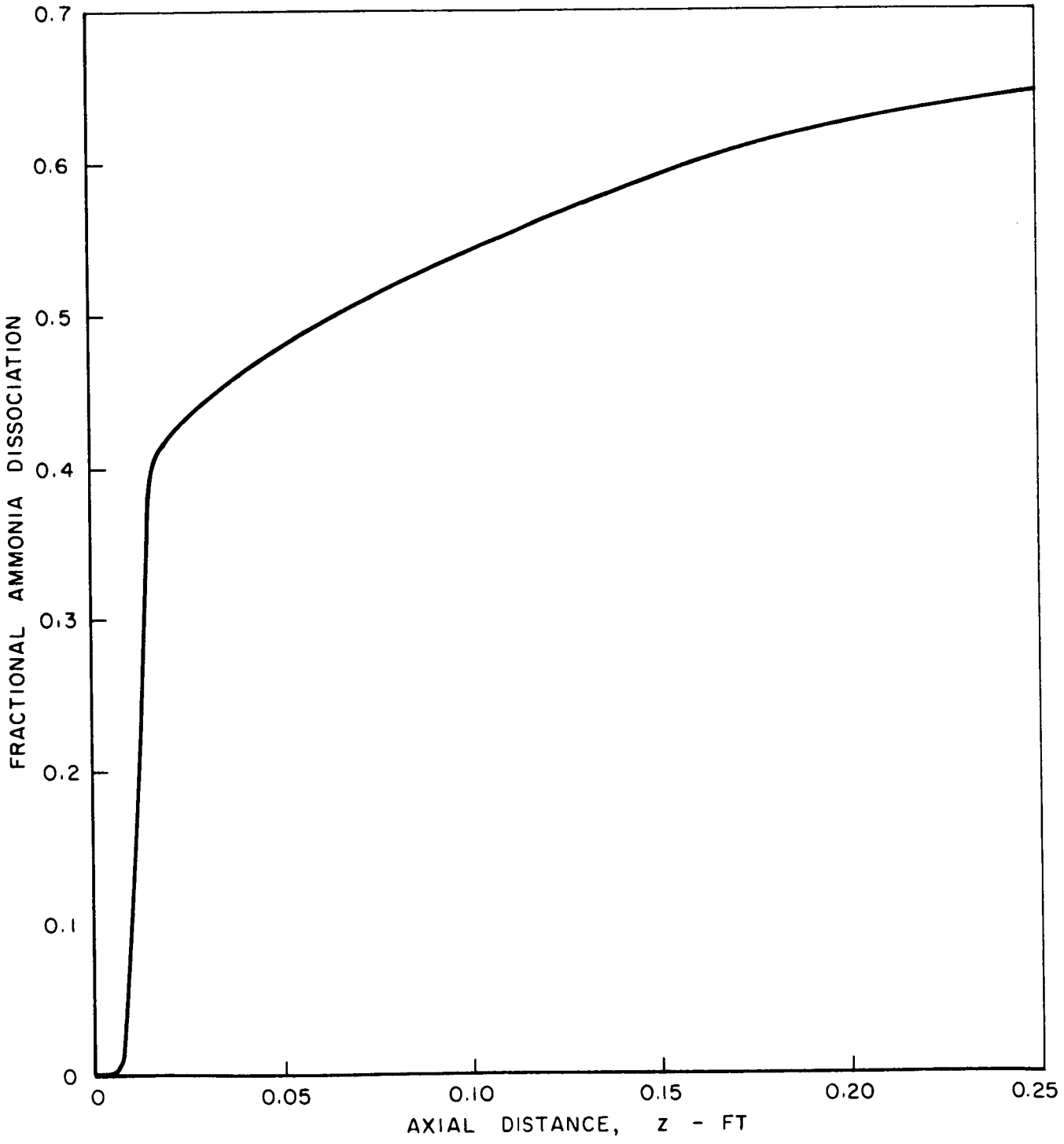

FIG. 8

STEADY-STATE AXIAL TEMPERATURE PROFILE

P = 1042 PSIA
G = 2.43 LB/FT^2 - SEC
STANDARD BED CONFIGURATION (SEE TEXT)

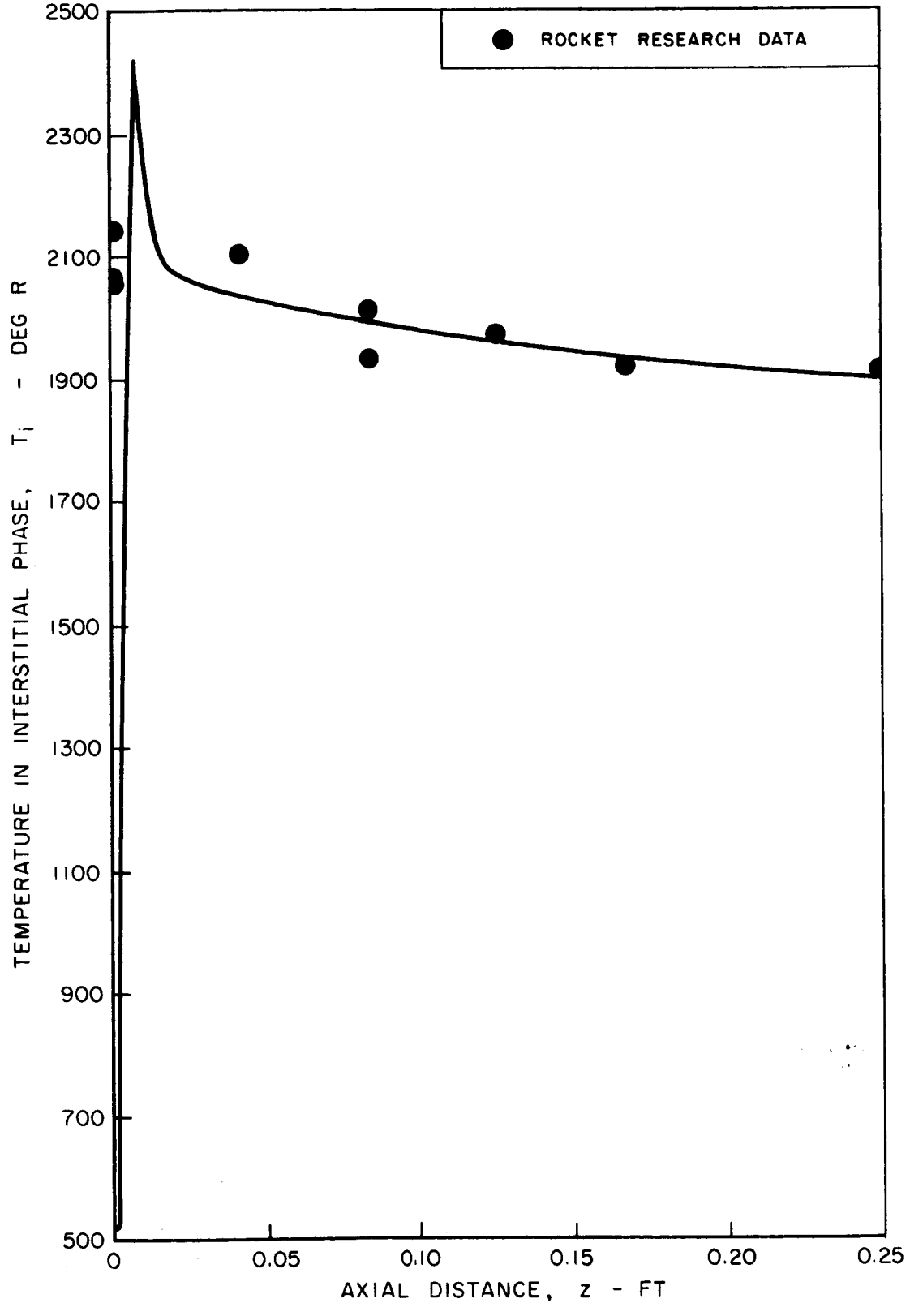

STEADY-STATE AXIAL PROFILES OF MOLE-FRACTIONS OF REACTANTS

P = 1042 PSIA
G = 2.43 LB/FT^2 - SEC
STANDARD BED CONFIGURATION (SEE TEXT)

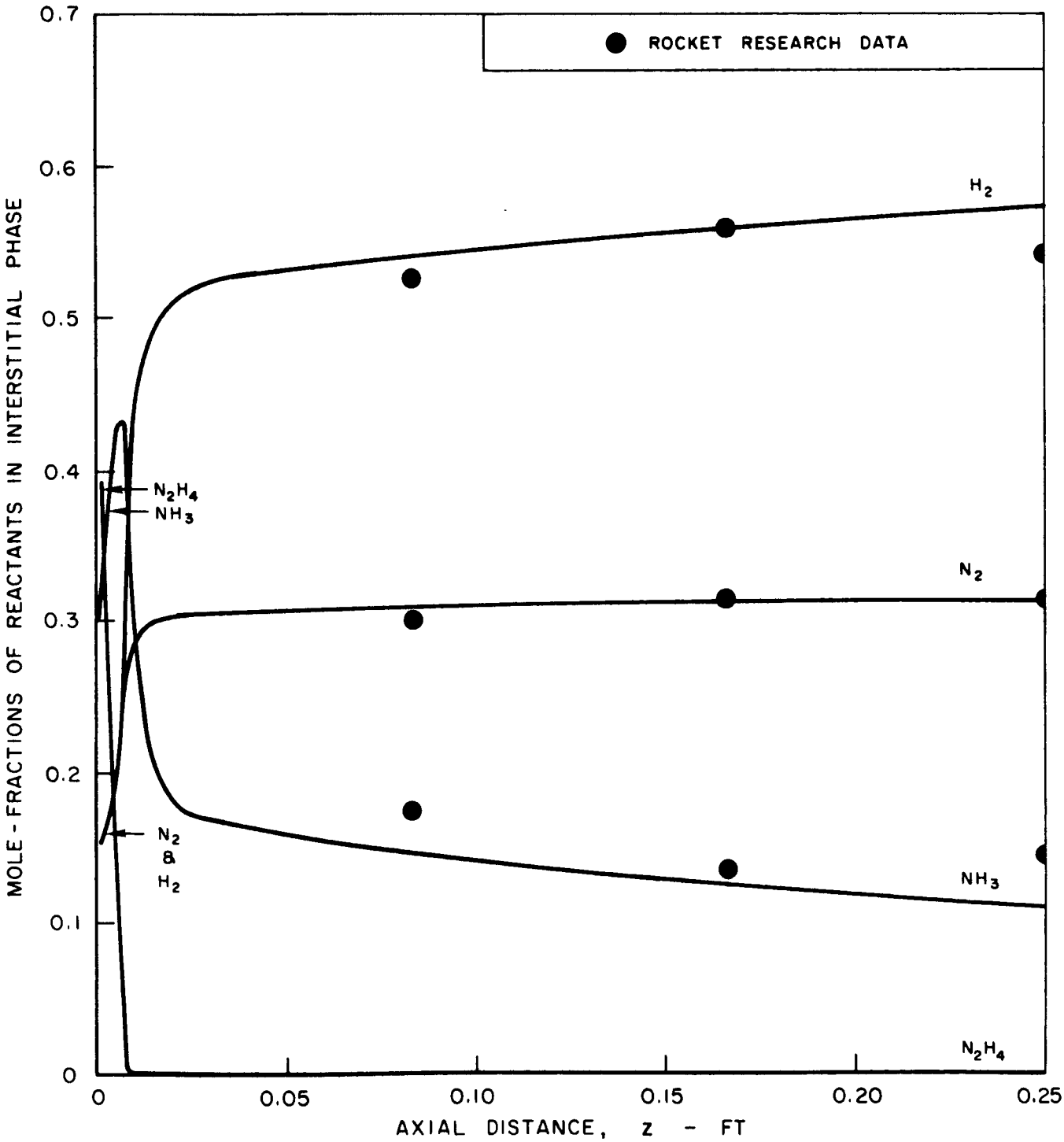

FIG. 10

STEADY-STATE AXIAL PROFILE OF FRACTIONAL AMMONIA DISSOCIATION

P = 1042 PSIA
G = 2.43 LB/FT^2 - SEC
STANDARD BED CONFIGURATION (SEE TEXT)

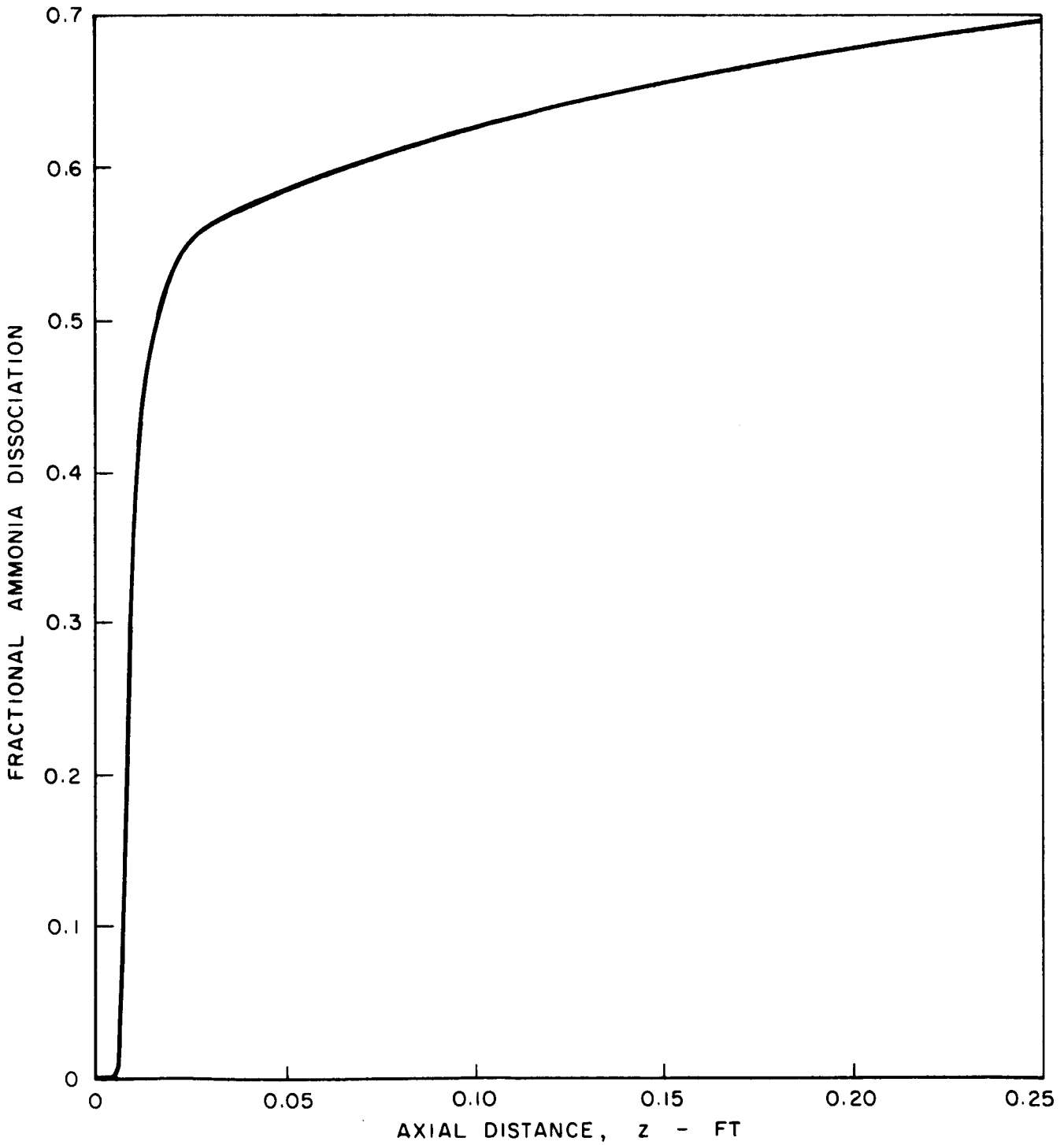

FIG. 11

STEADY-STATE AXIAL TEMPERATURE PROFILE

P = 974 PSIA
G = 6.29 LB/FT^2 - SEC
STANDARD BED CONFIGURATION (SEE TEXT)

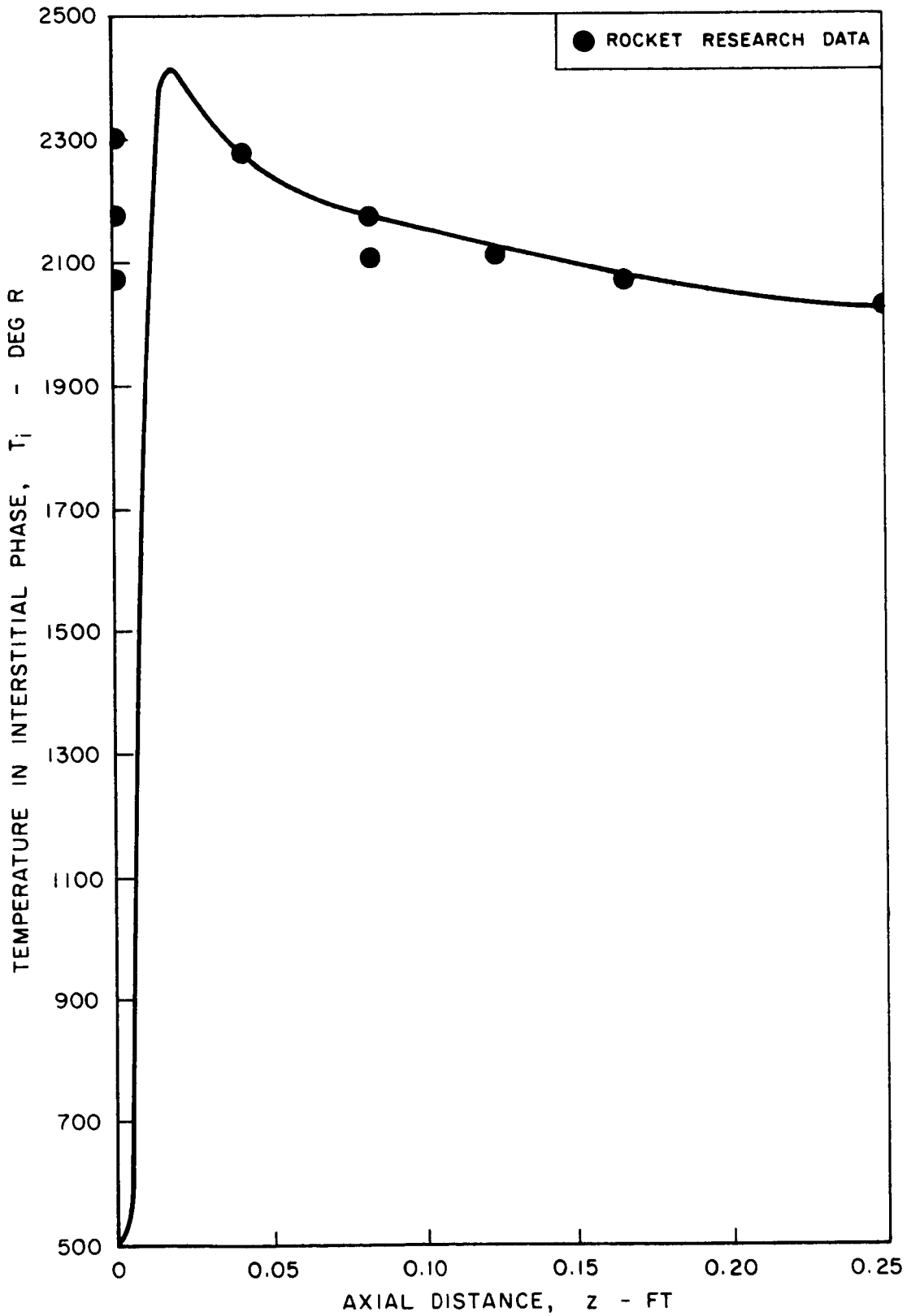

FIG. 12

STEADY-STATE AXIAL PROFILES OF MOLE-FRACTIONS OF REACTANTS

P = 974 PSIA
G = 6.29 LB/FT^2- SEC
STANDARD BED CONFIGURATION (SEE TEXT)

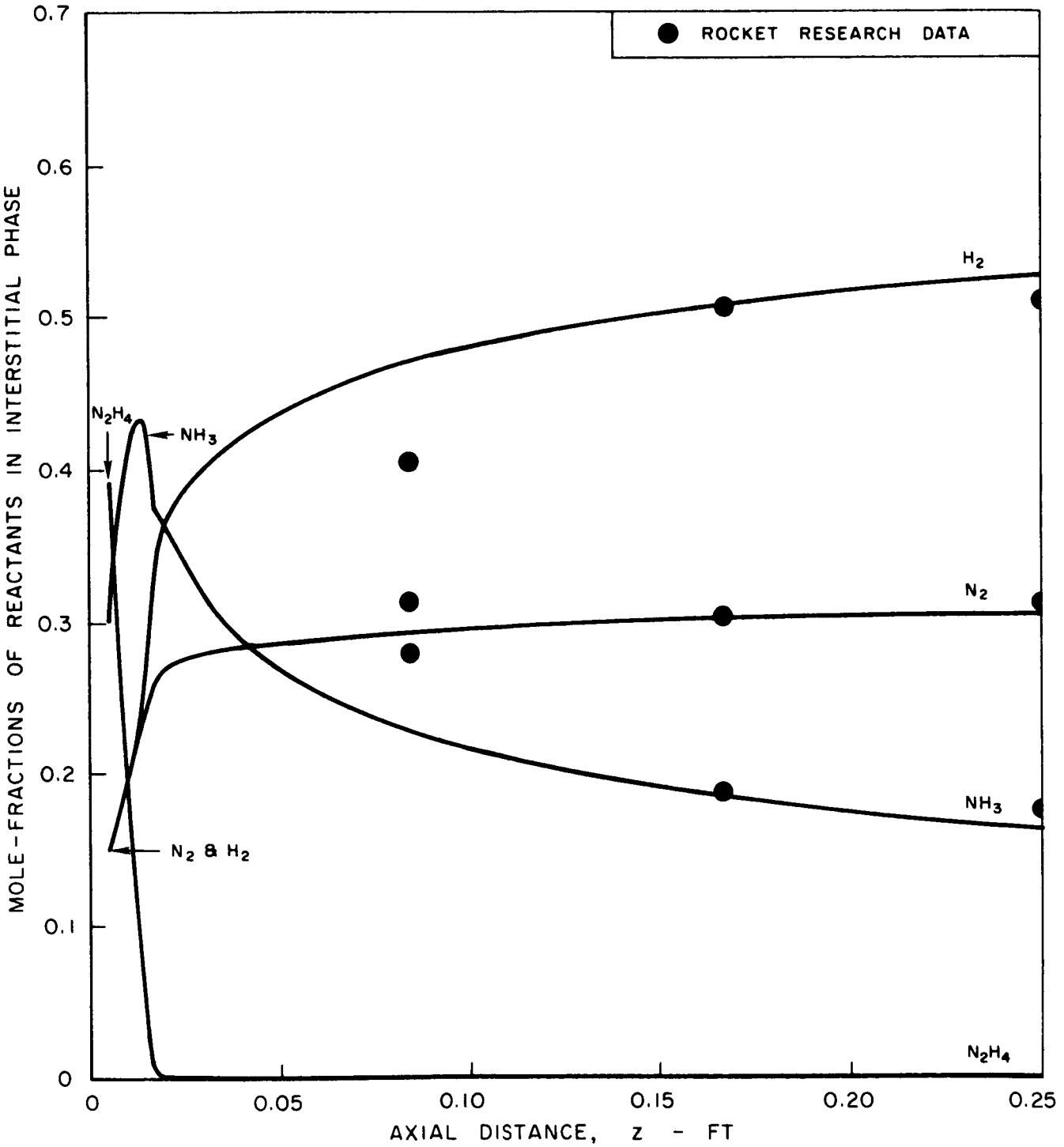

FIG. 13

STEADY-STATE AXIAL PROFILE OF FRACTIONAL AMMONIA DISSOCIATION

P = 974 PSIA
G = 6.29 LB/FT^2-SEC
STANDARD BED CONFIGURATION (SEE TEXT)

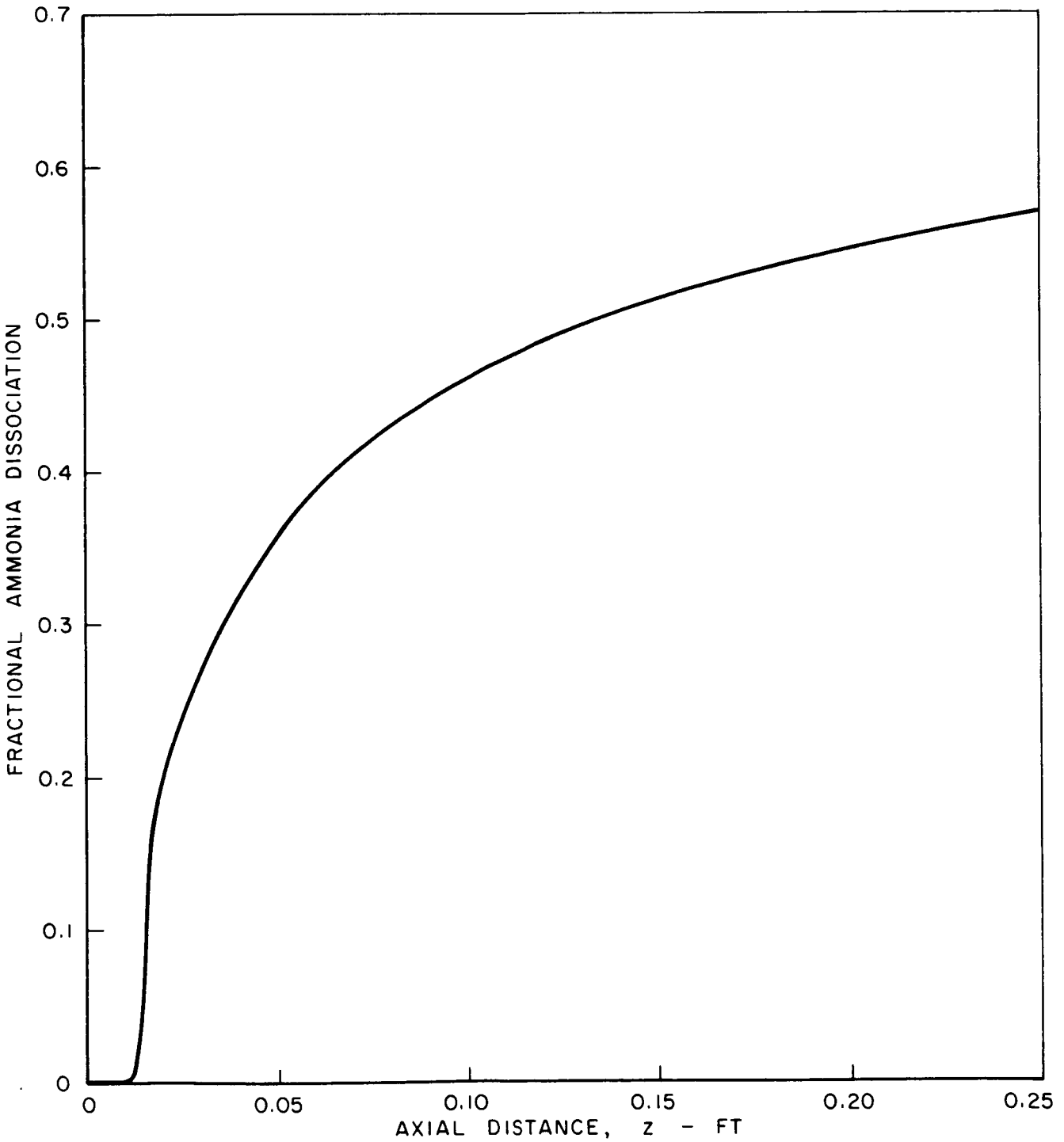

FIG. 14

STEADY-STATE AXIAL TEMPERATURE PROFILE

P = 217.9 PSIA
G = 1.52 LB/FT^2 - SEC
STANDARD BED CONFIGURATION (SEE TEXT)

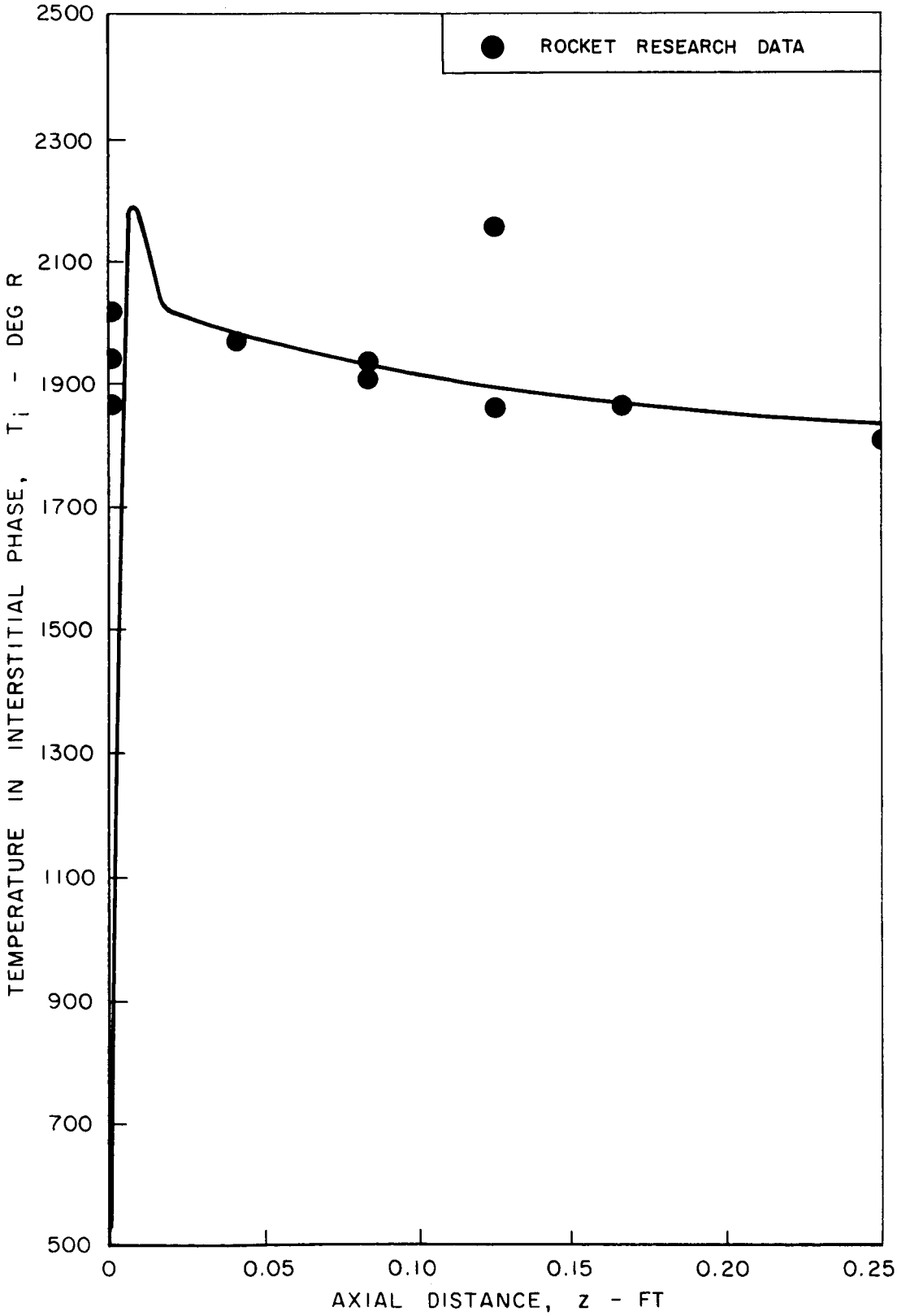

STEADY-STATE AXIAL PROFILES OF MOLE-FRACTIONS OF REACTANTS

P = 217.9 PSIA
G = 1.52 LB/FT^2 - SEC
STANDARD BED CONFIGURATION (SEE TEXT)

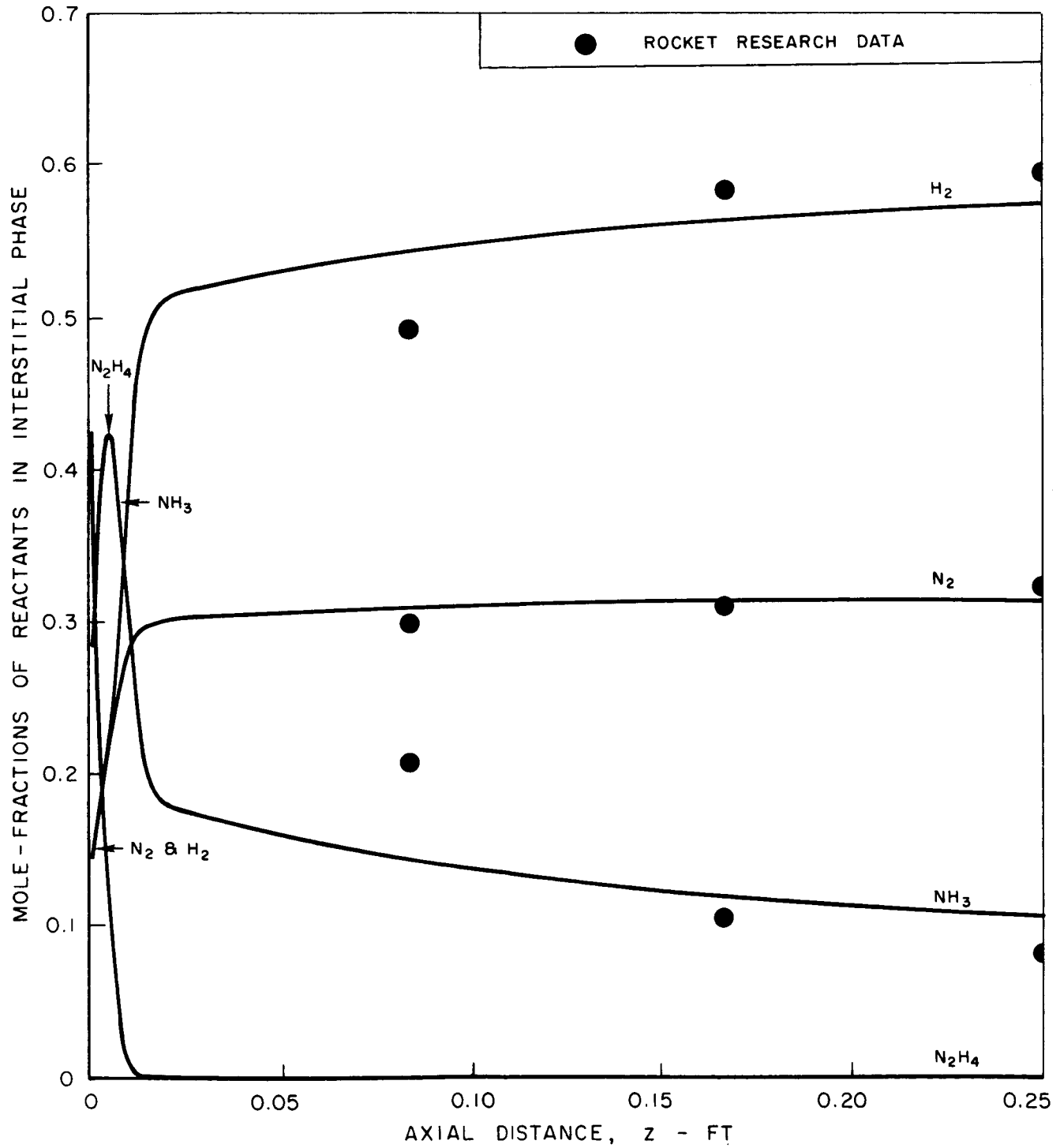

FIG. 16

STEADY-STATE AXIAL PROFILE OF FRACTIONAL AMMONIA DISSOCIATION

P = 217.9 PSIA
G = 1.52 LB/FT^2 - SEC
STANDARD BED CONFIGURATION (SEE TEXT)

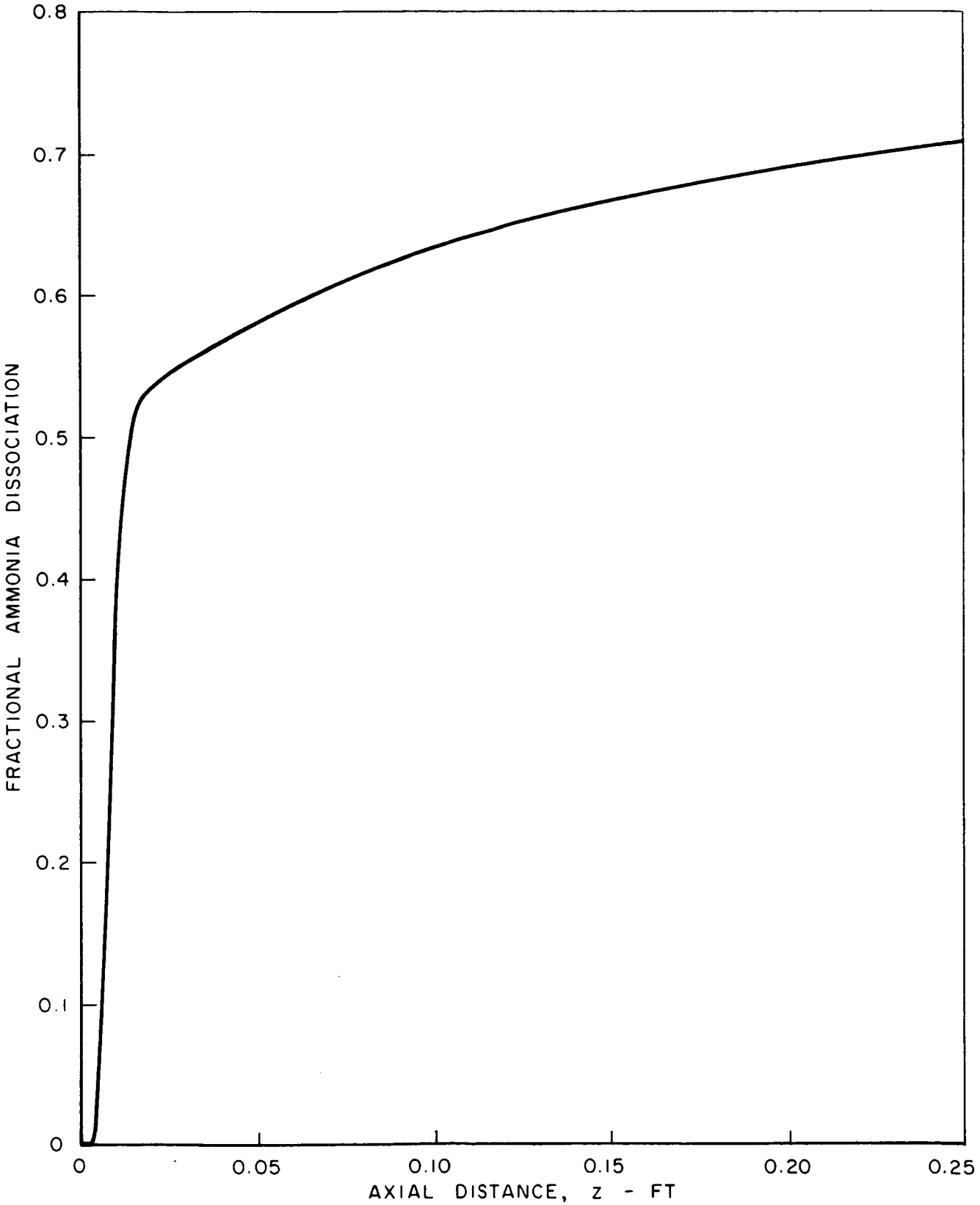

FIG. 17

STEADY-STATE AXIAL TEMPERATURE PROFILE

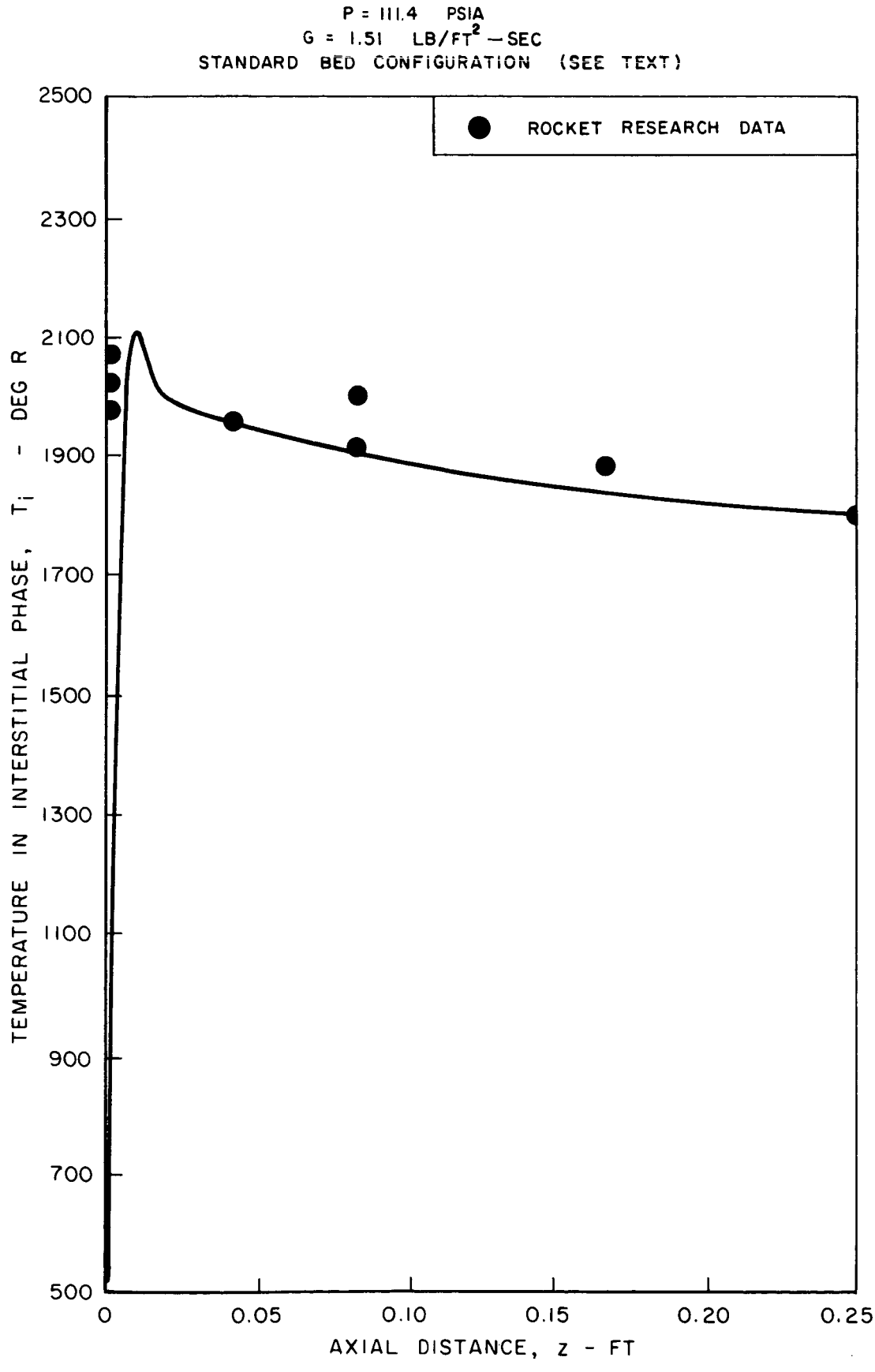

FIG. 18

STEADY-STATE AXIAL PROFILES OF MOLE-FRACTIONS OF REACTANTS

P = 111.4 PSIA
G = 1.51 LB/FT^2 - SEC
STANDARD BED CONFIGURATION (SEE TEXT)

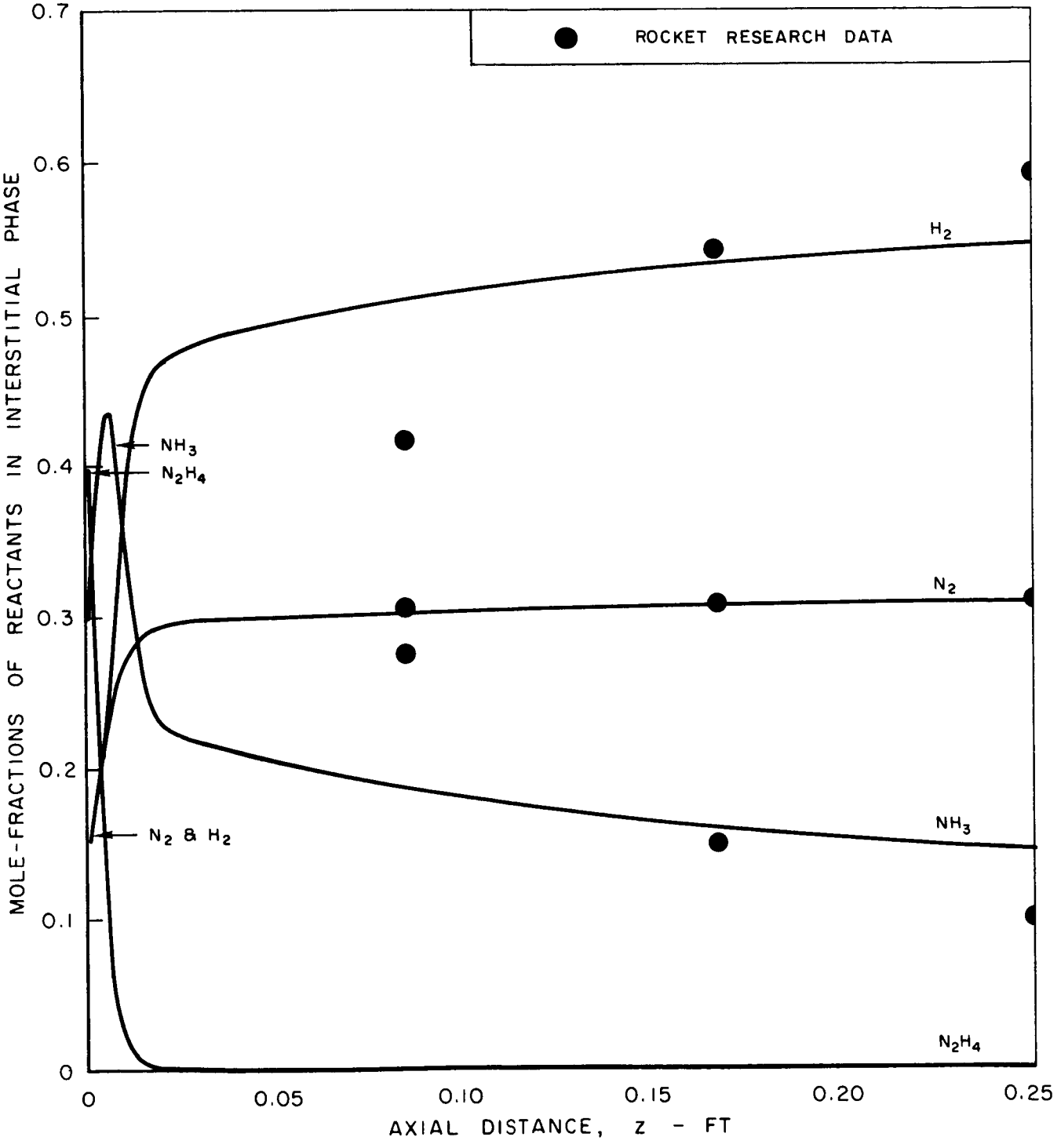

FIG. 19

STEADY-STATE AXIAL PROFILE OF FRACTIONAL AMMONIA DISSOCIATION

P = 111.4 PSIA
G = 1.51 LB/FT^2 - SEC
STANDARD BED CONFIGURATION (SEE TEXT)

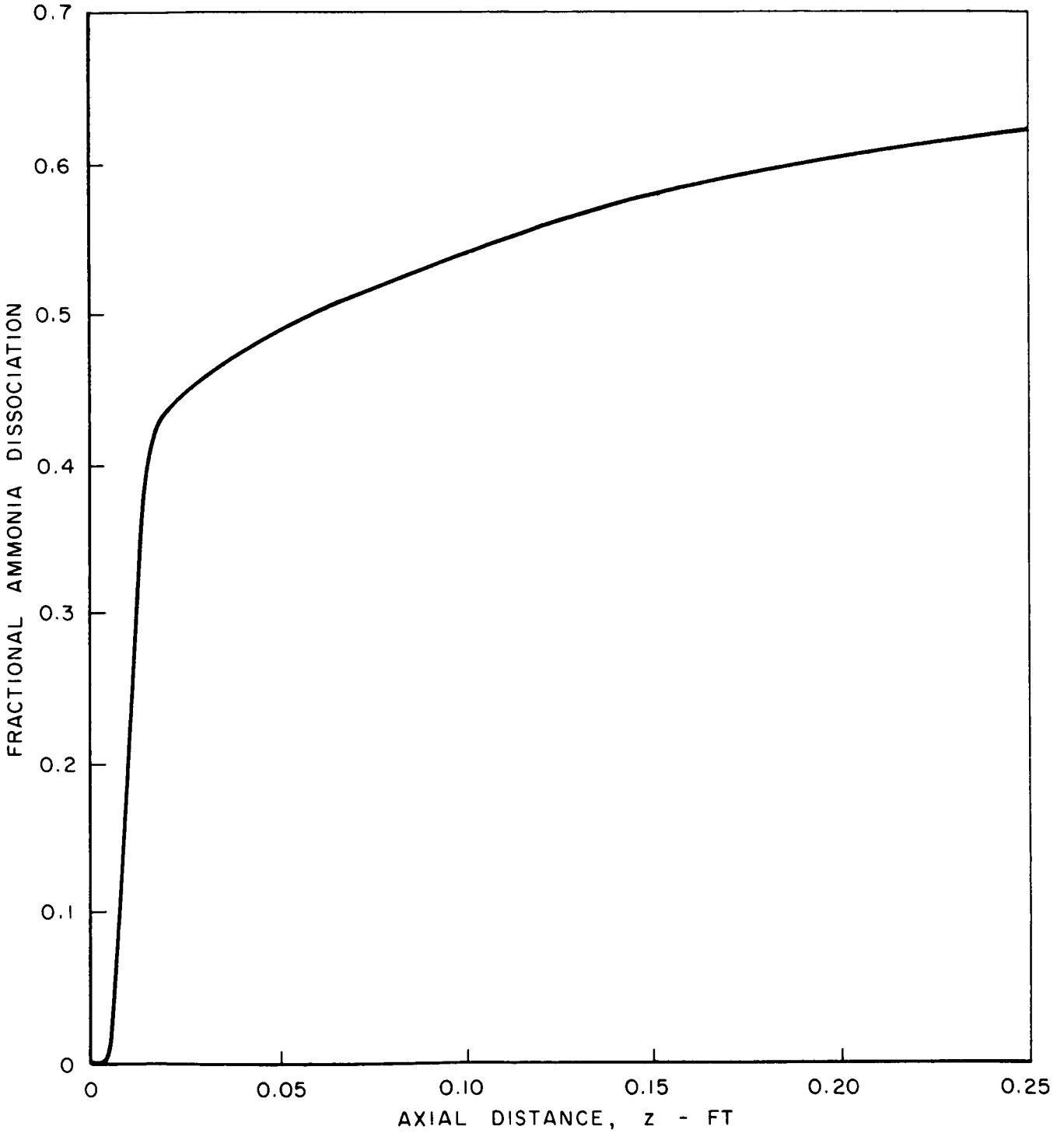

FIG. 20

STEADY-STATE AXIAL TEMPERATURE PROFILES FOR VARIOUS CHAMBER PRESSURES

G = 3.0 LB/FT^2 - SEC
STANDARD BED CONFIGURATION (SEE TEXT)

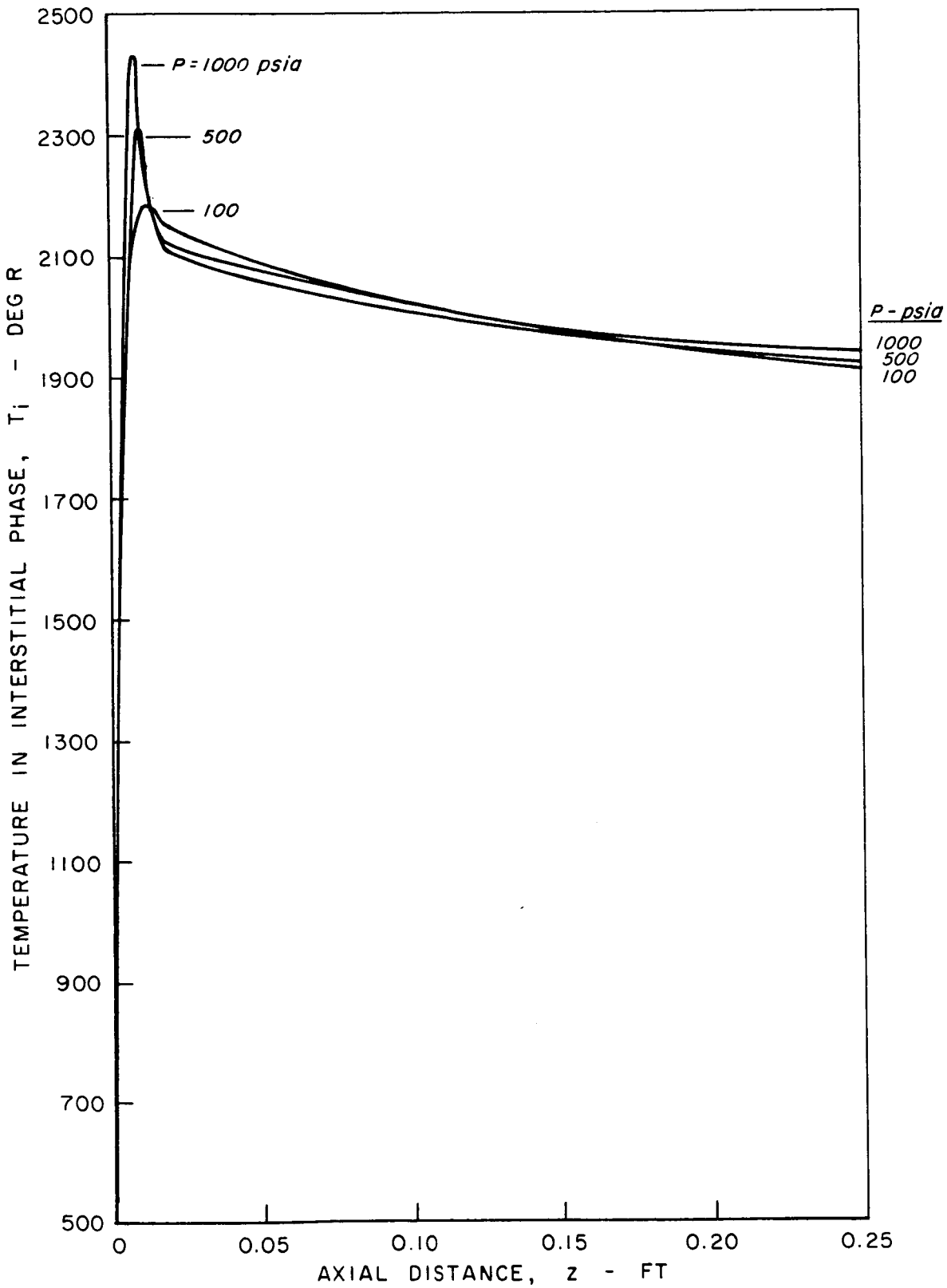

FIG. 21

STEADY-STATE AXIAL TEMPERATURE PROFILES FOR VARIOUS MASS FLOW RATES

P = 100 PSIA

STANDARD BED CONFIGURATION (SEE TEXT)

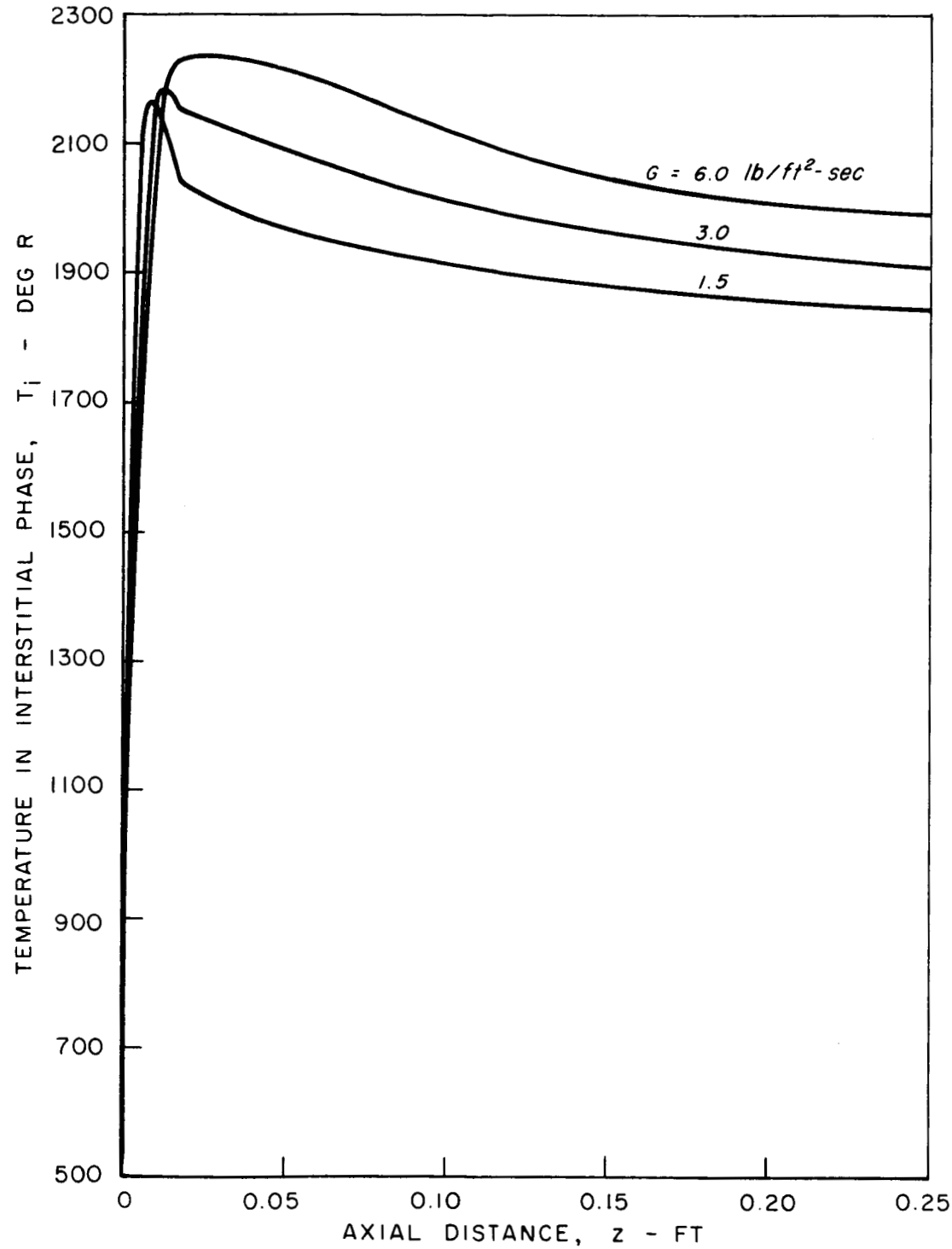

FIG. 22

STEADY-STATE AXIAL TEMPERATURE PROFILES FOR VARIOUS CATALYTIC BED CONFIGURATIONS

P = 100 PSIA

G = 3.0 LB/FT^2-SEC

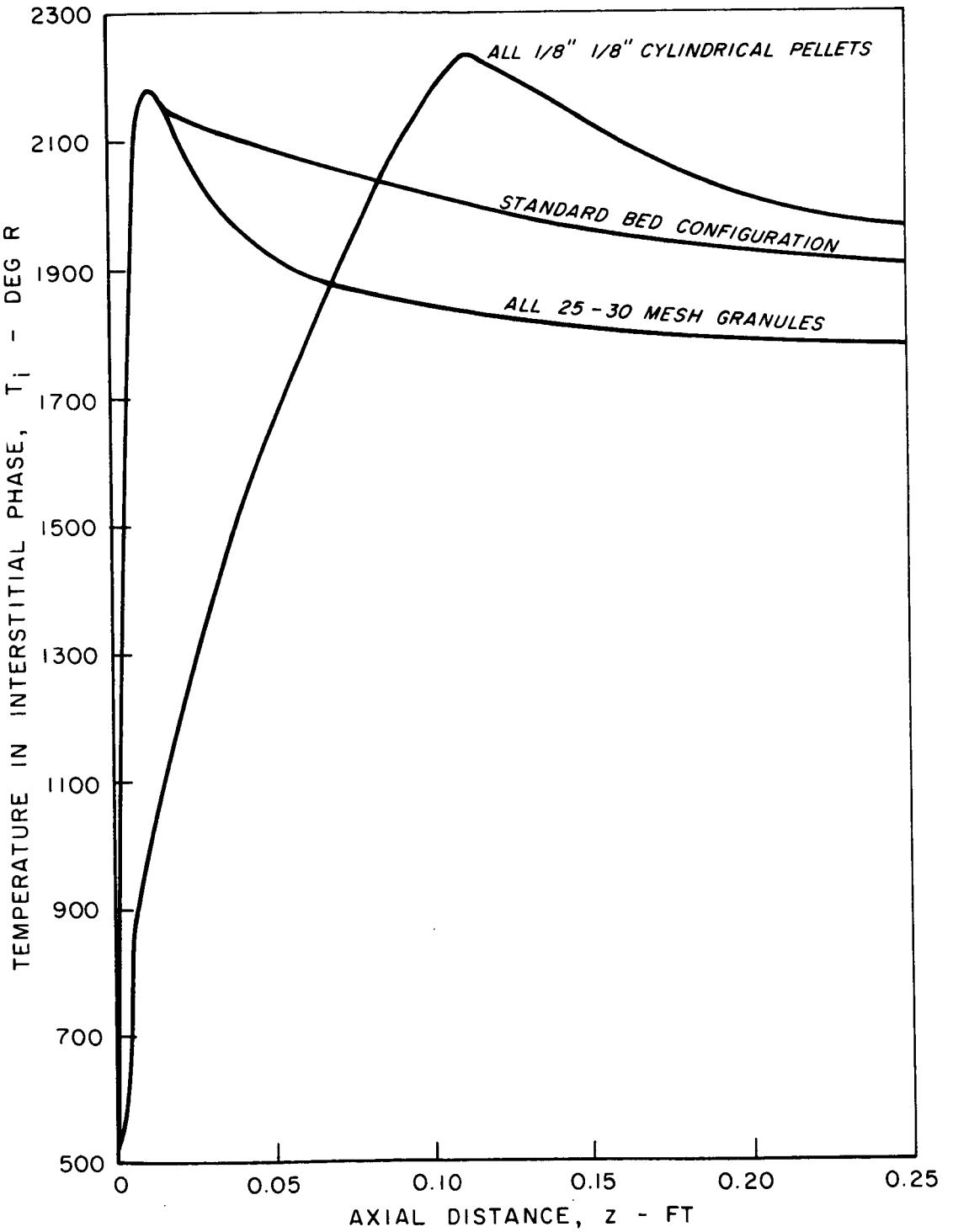

STEADY-STATE AXIAL TEMPERATURE PROFILES FOR VARIOUS HYDRAZINE AXIAL INJECTION PROFILES

P = 100 PSIA
BED CONFIGURATION: ALL 25-30 MESH GRANULES

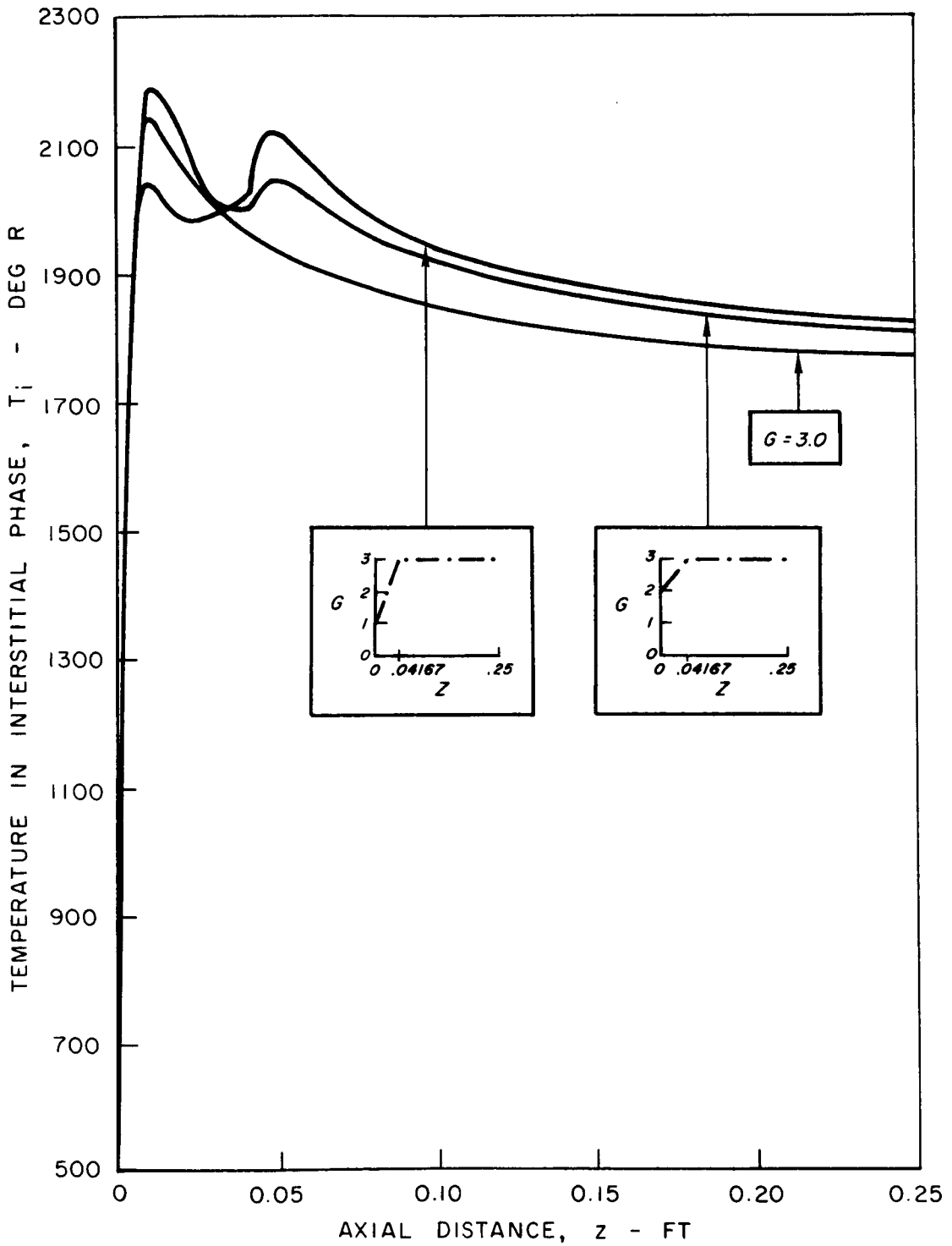

COMPARISON OF STEADY-STATE AXIAL TEMPERATURE PROFILES COMPUTED FROM STEADY-STATE AND TRANSIENT MODELS

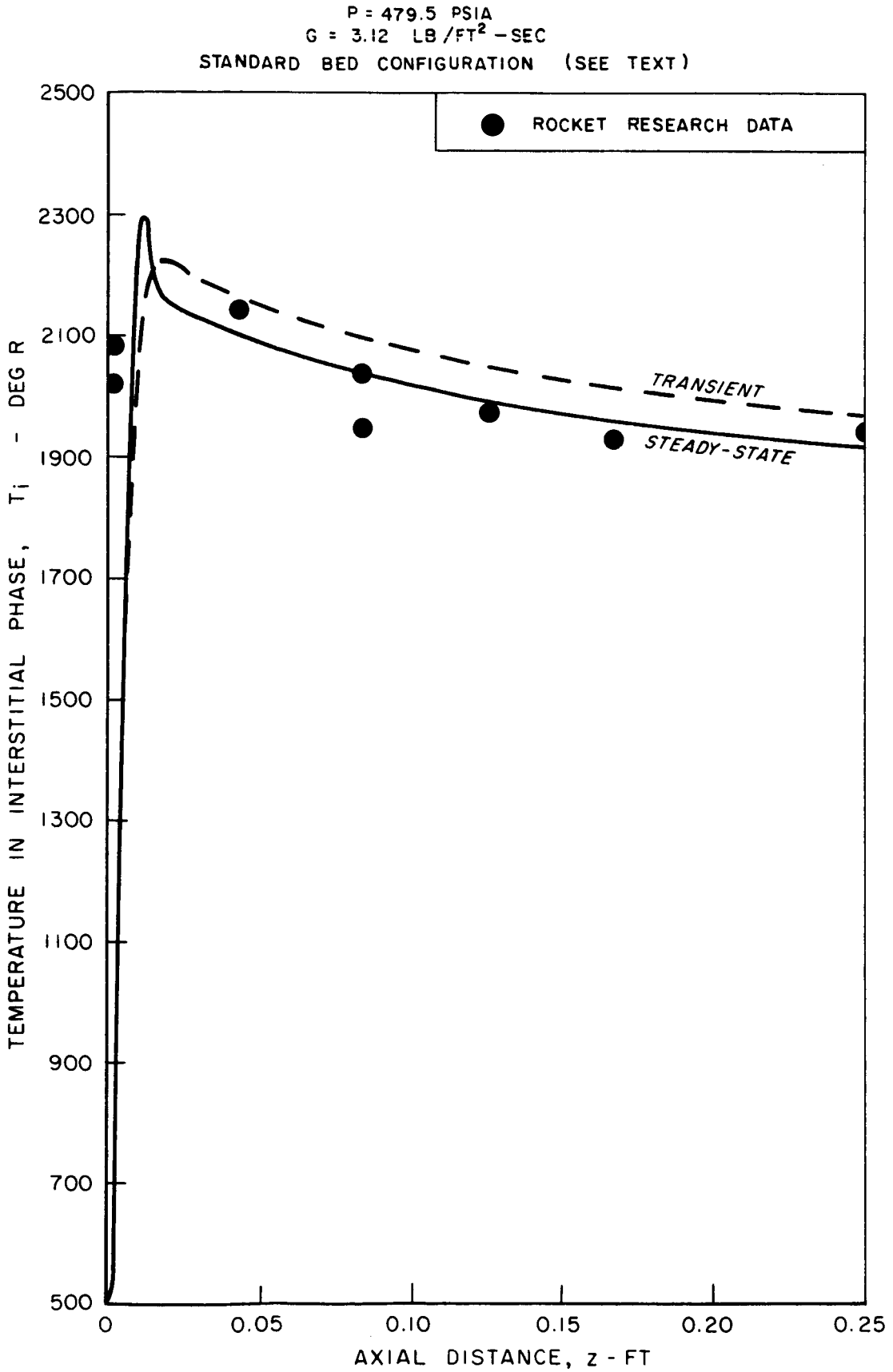

FIG. 25

COMPARISON OF STEADY-STATE AXIAL PROFILES OF MOLE-FRACTION OF AMMONIA COMPUTED FROM STEADY-STATE AND TRANSIENT MODELS

P = 479.5 PSIA
G = 3.12 LB/FT^2 - SEC
STANDARD BED CONFIGURATION (SEE TEXT)

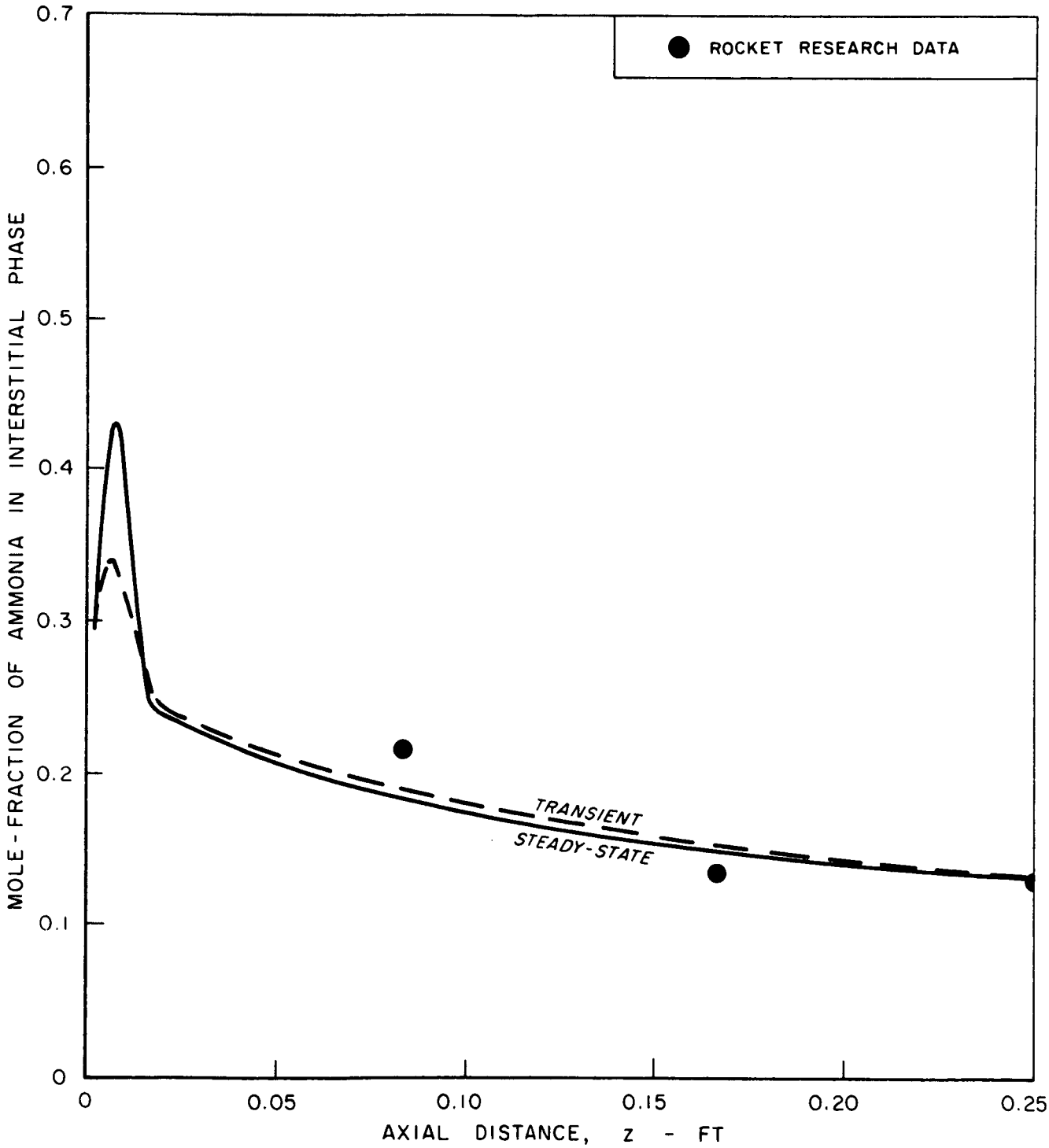

FIG. 26

TRANSIENT AXIAL TEMPERATURE PROFILES

P (FEED PRESSURE) = 479.5 PSIA
G = 3.12 LB/FT^2 - SEC
STANDARD BED CONFIGURATION (SEE TEXT)

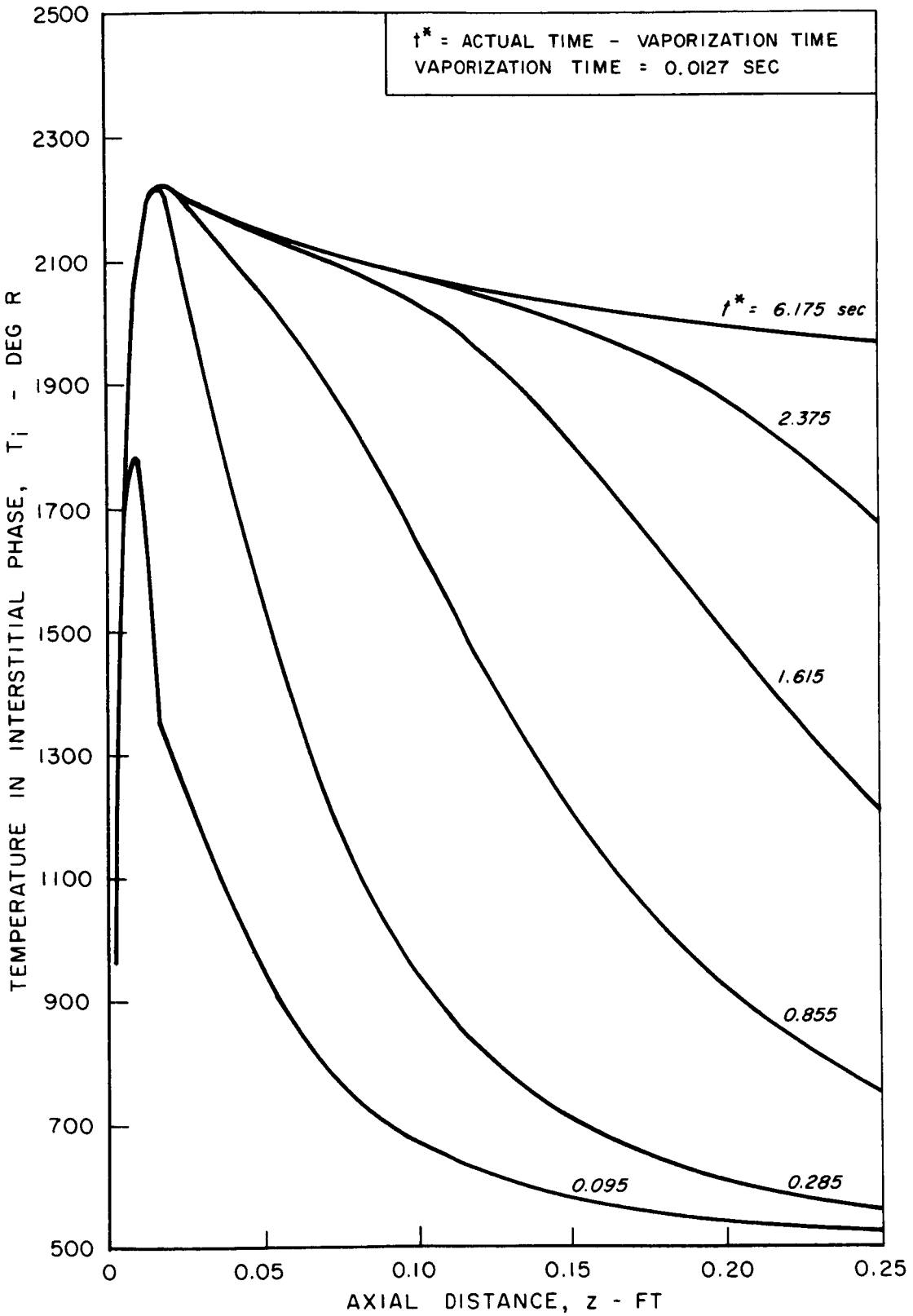

F910461-12

FIG. 27

VARIATION OF TEMPERATURE WITH TIME AT SEVERAL AXIAL POSITIONS

P (FEED PRESSURE) = 479.5 PSIA G = 3.12 LB/FT^2-SEC STANDARD BED CONFIGURATION (SEE TEXT)

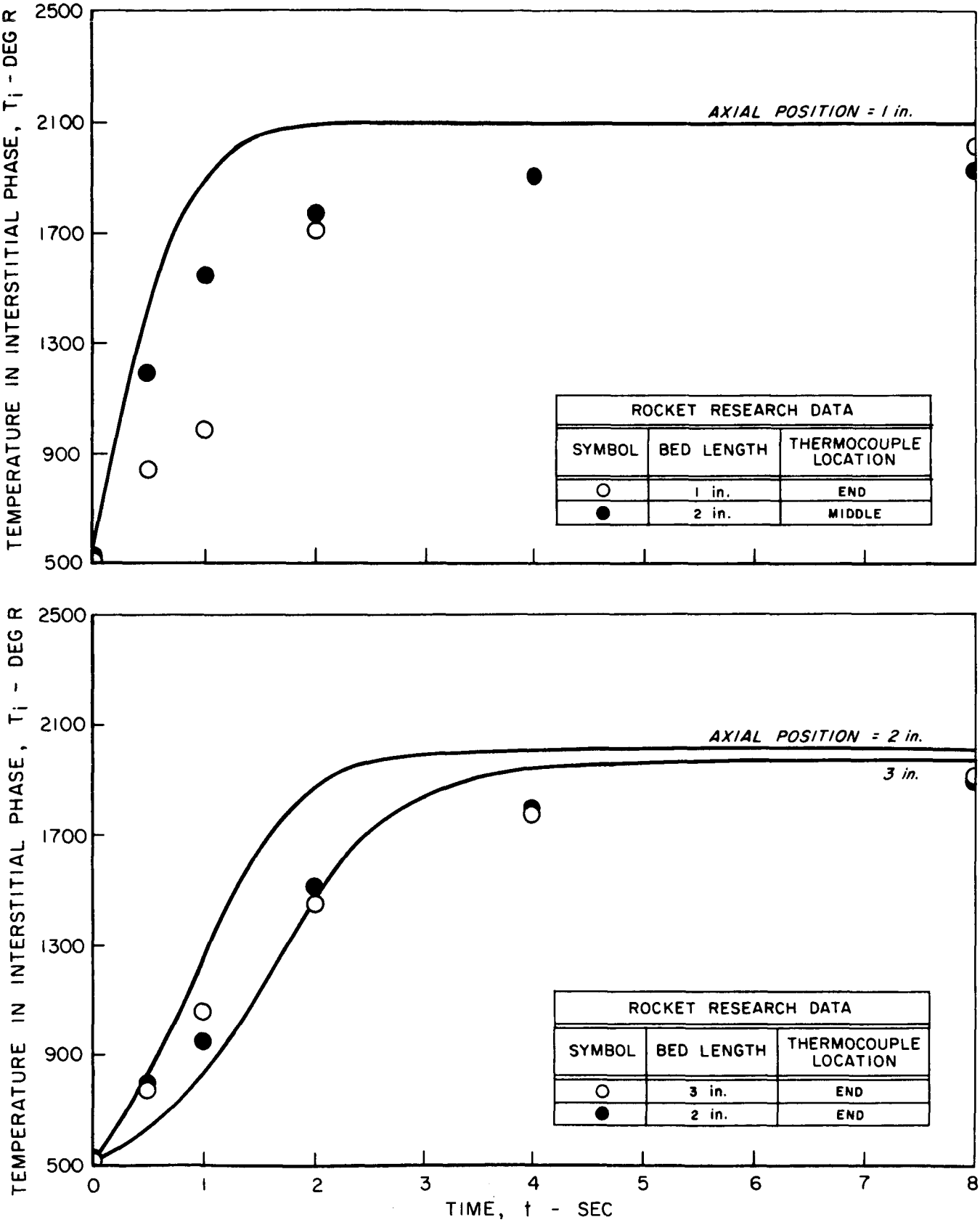

FIG. 28

TRANSIENT AXIAL PROFILES OF MOLE-FRACTION OF HYDRAZINE

P (FEED PRESSURE) = 479.5 PSIA
G = 3.12 LB/FT^2 - SEC
STANDARD BED CONFIGURATION (SEE TEXT)

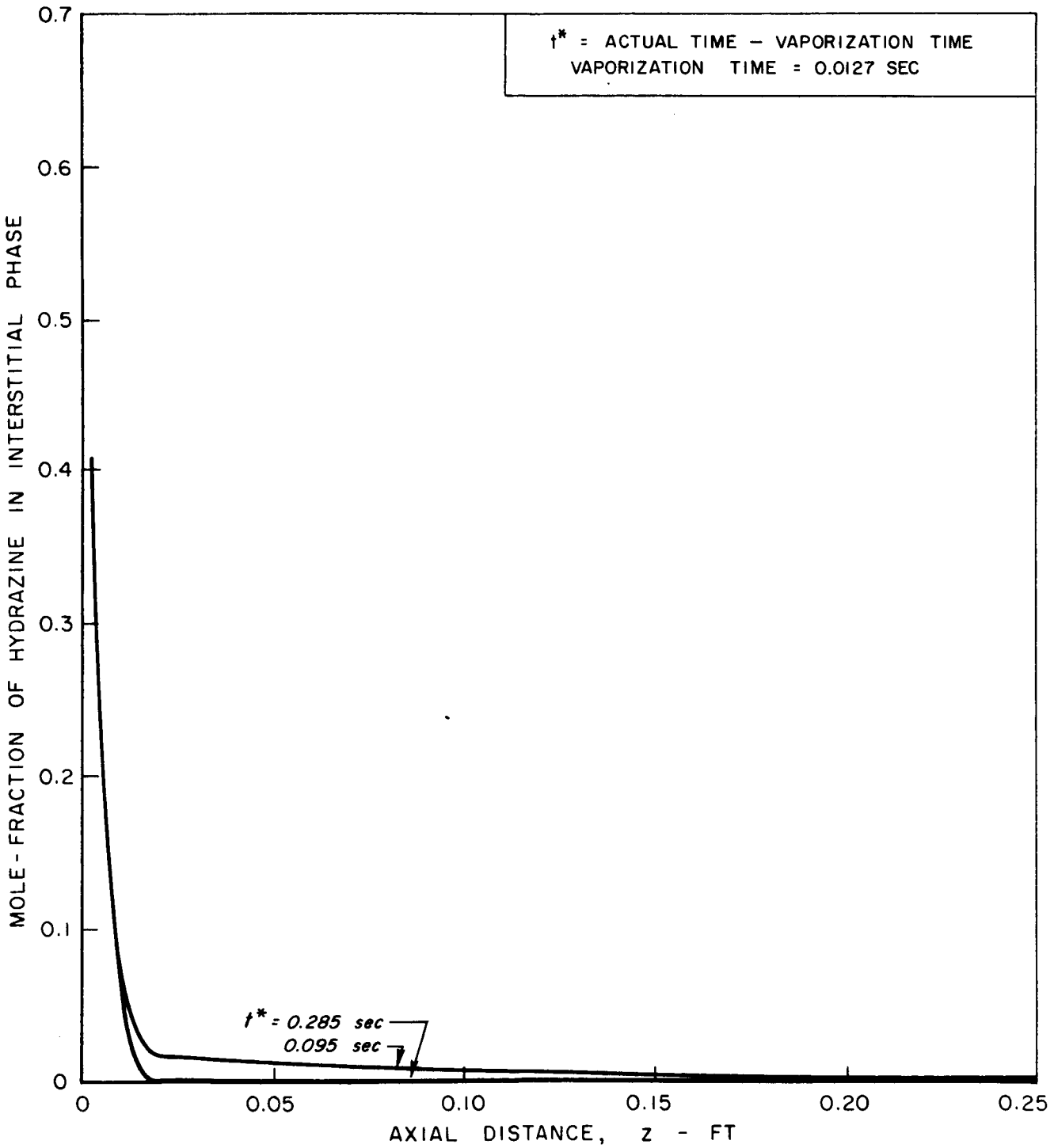

FIG. 29

TRANSIENT AXIAL PROFILES OF MOLE-FRACTION OF AMMONIA

P(FEED PRESSURE) = 479.5 PSIA
G = 3.12 LB/FT^2-SEC
STANDARD BED CONFIGURATION (SEE TEXT)

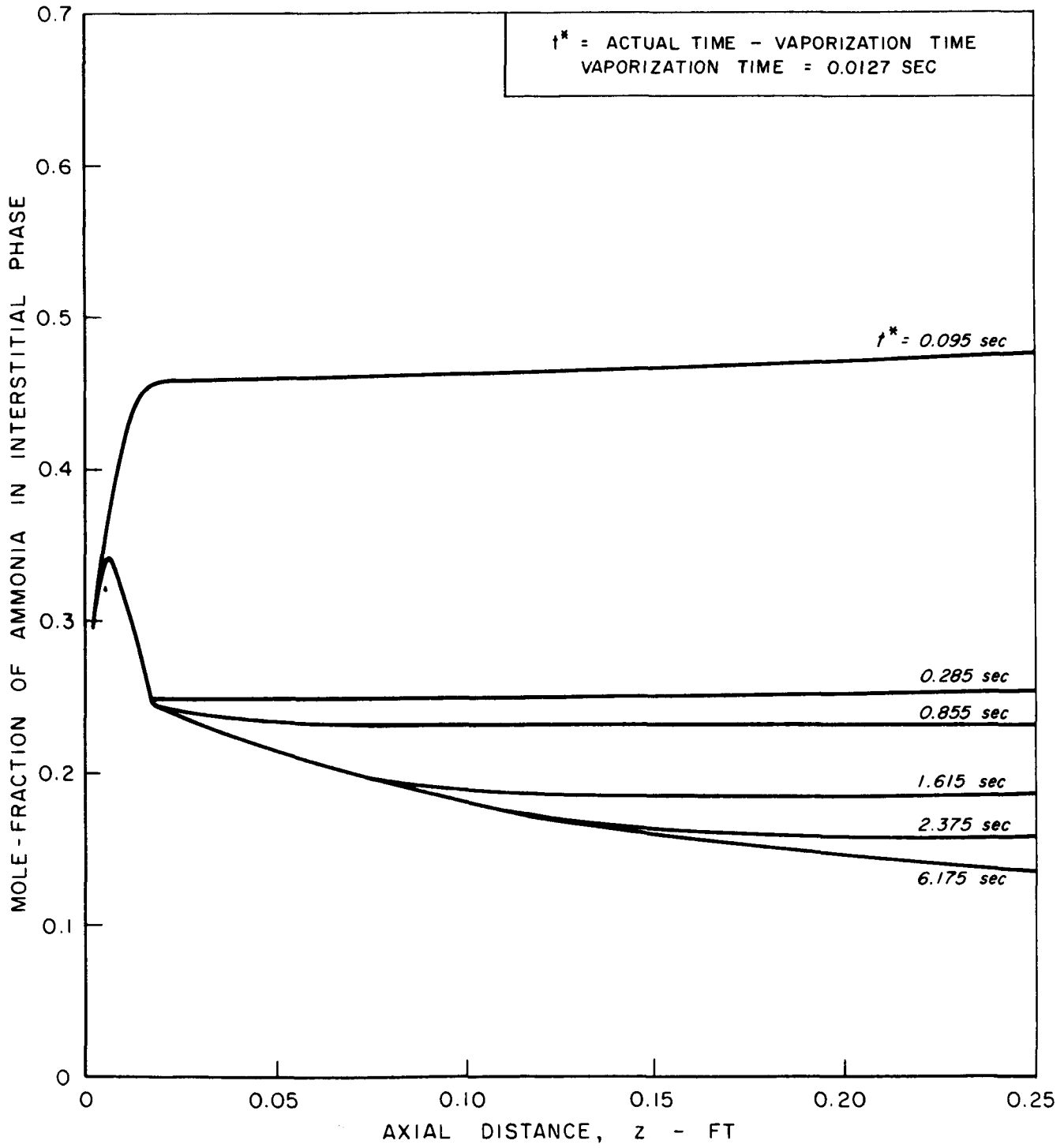

FIG. 30

TRANSIENT AXIAL PROFILES OF MOLE-FRACTION OF NITROGEN

P (FEED PRESSURE) = 479.5 PSIA
G = 3.12 LB/FT^2 - SEC
STANDARD BED CONFIGURATION (SEE TEXT)

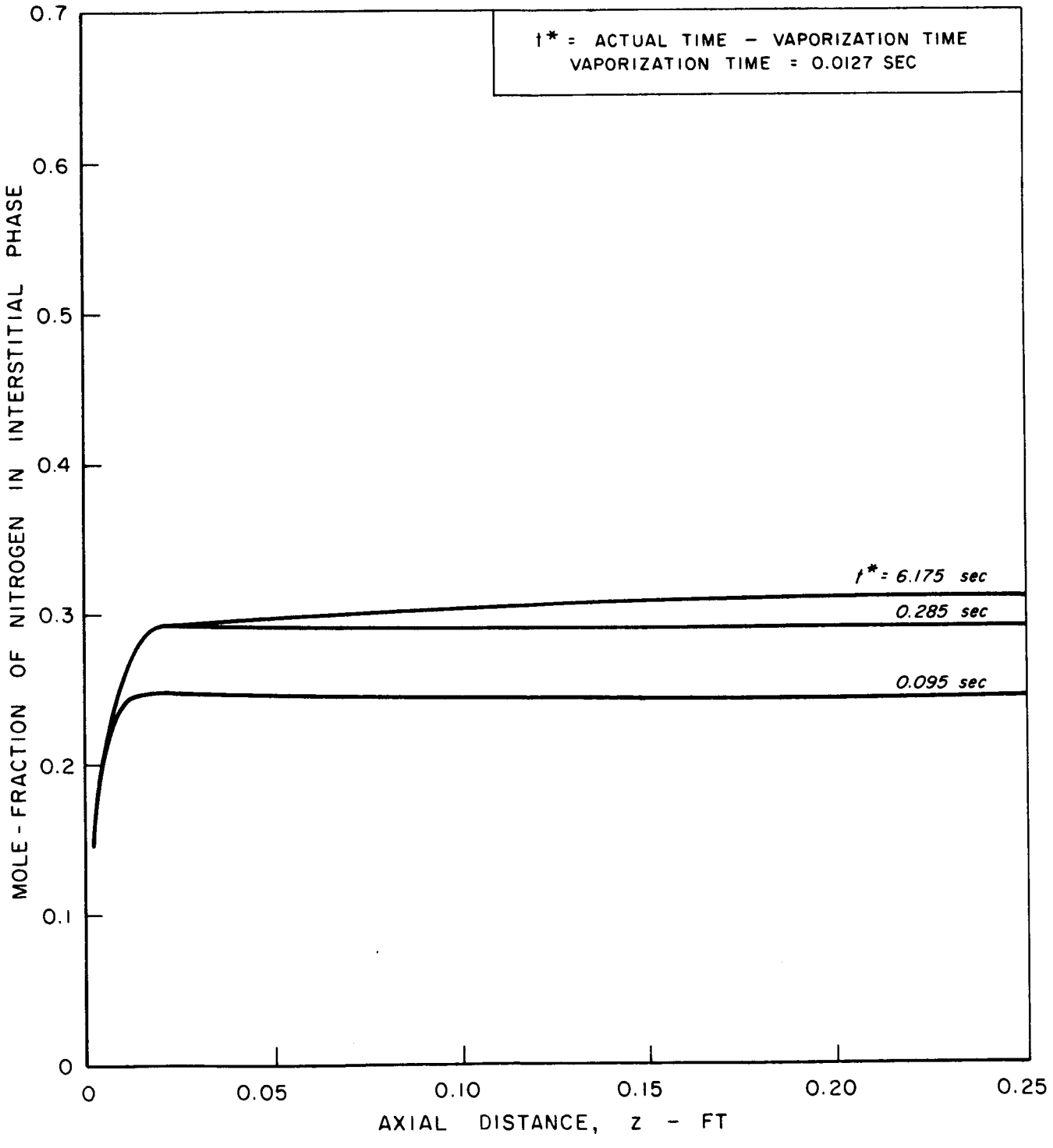

FIG. 31

TRANSIENT AXIAL PROFILES OF MOLE-FRACTION OF HYDROGEN

P (FEED PRESSURE) = 479.5 PSIA
G = 3.12 LB/FT^2 - SEC
STANDARD BED CONFIGURATION (SEE TEXT)

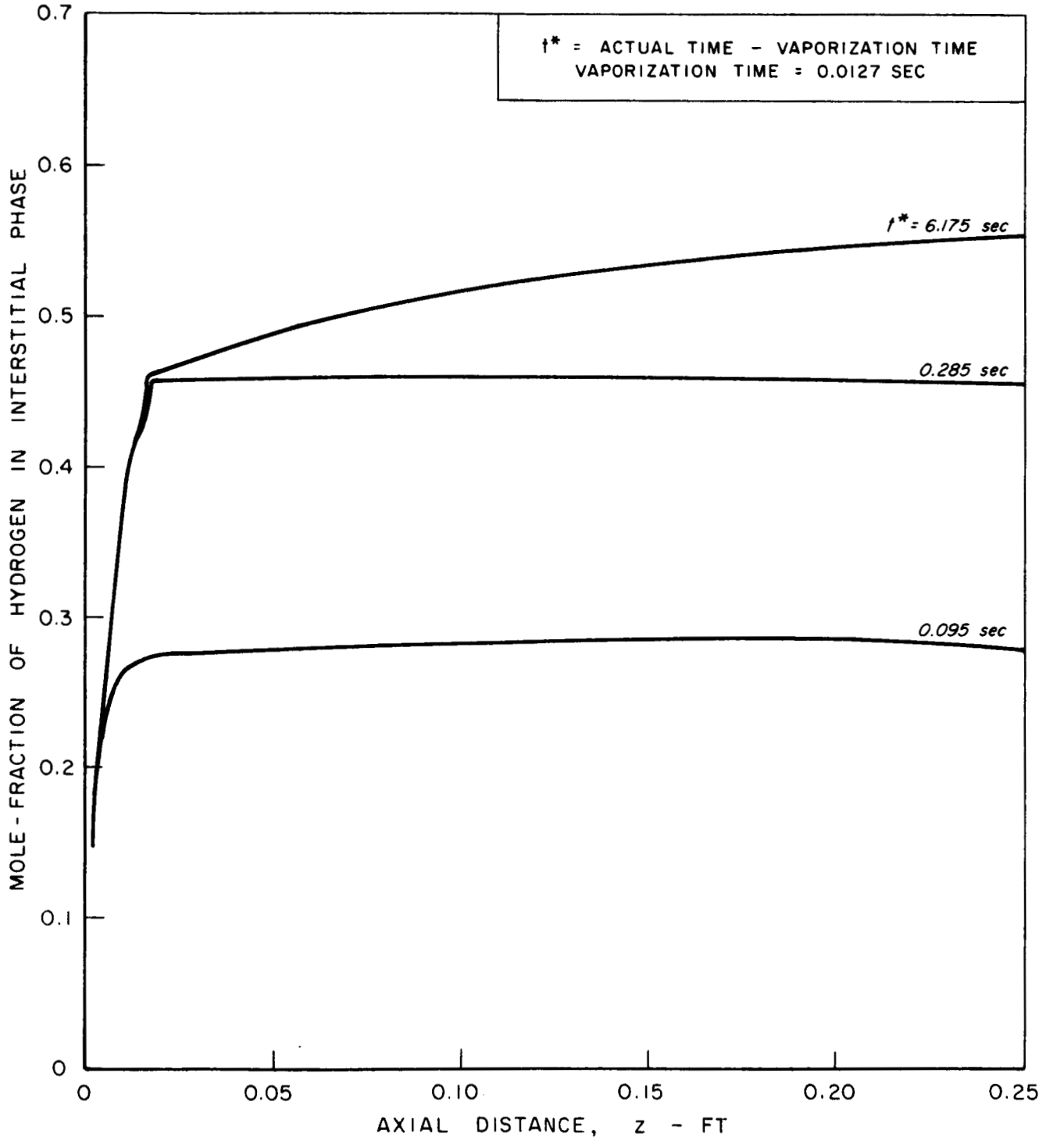

FIG. 32

VARIATION OF CHAMBER EXIT PRESSURE WITH TIME

P (FEED PRESSURE) = 479.5 PSIA
G = 3.12 LB/FT^2 - SEC
STANDARD BED CONFIGURATION (SEE TEXT)

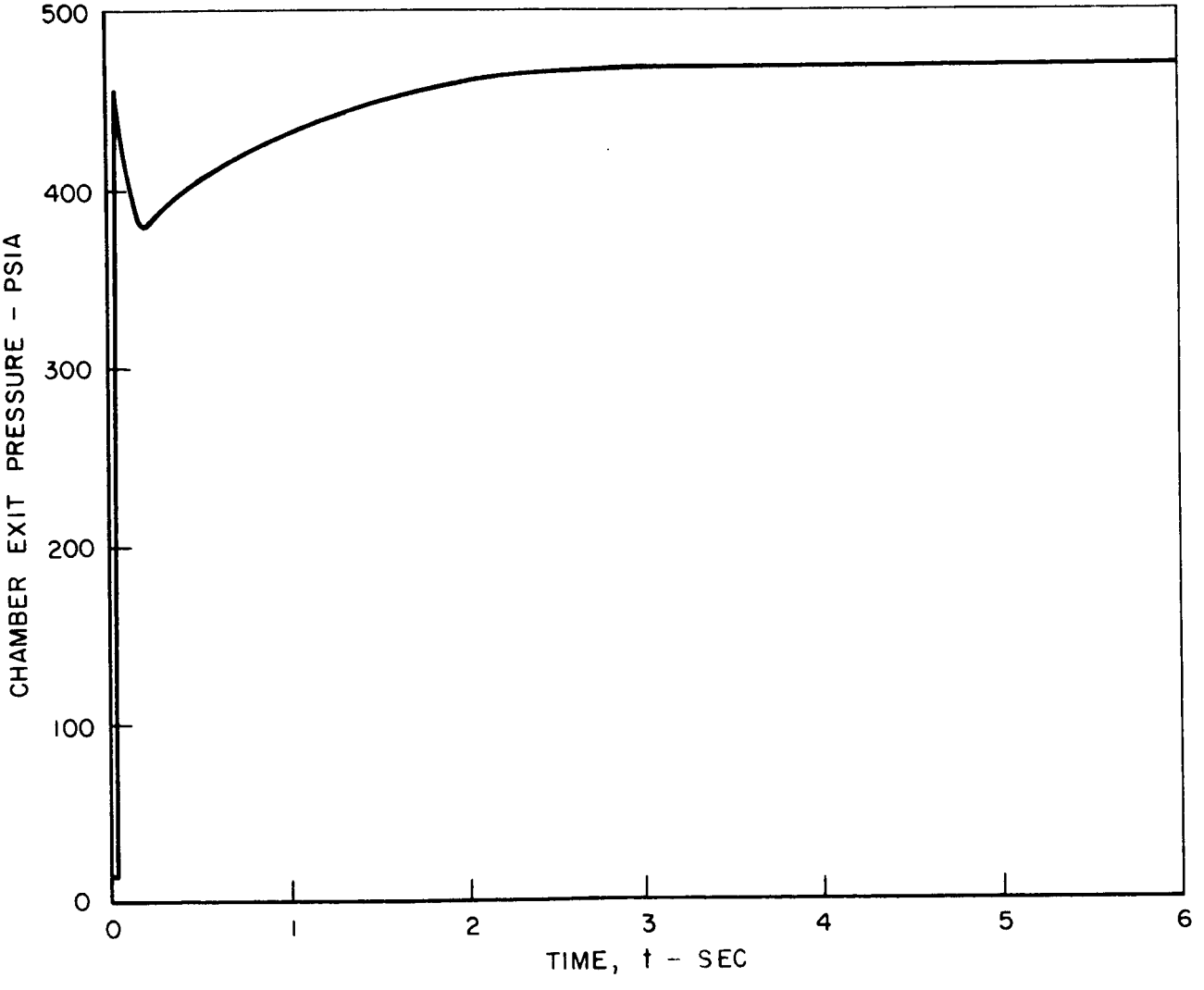

FIG. 33

TRANSIENT AXIAL TEMPERATURE PROFILES

P (FEED PRESSURE) = 1042 PSIA
G = 2.43 LB/FT^2 - SEC
STANDARD BED CONFIGURATION (SEE TEXT)

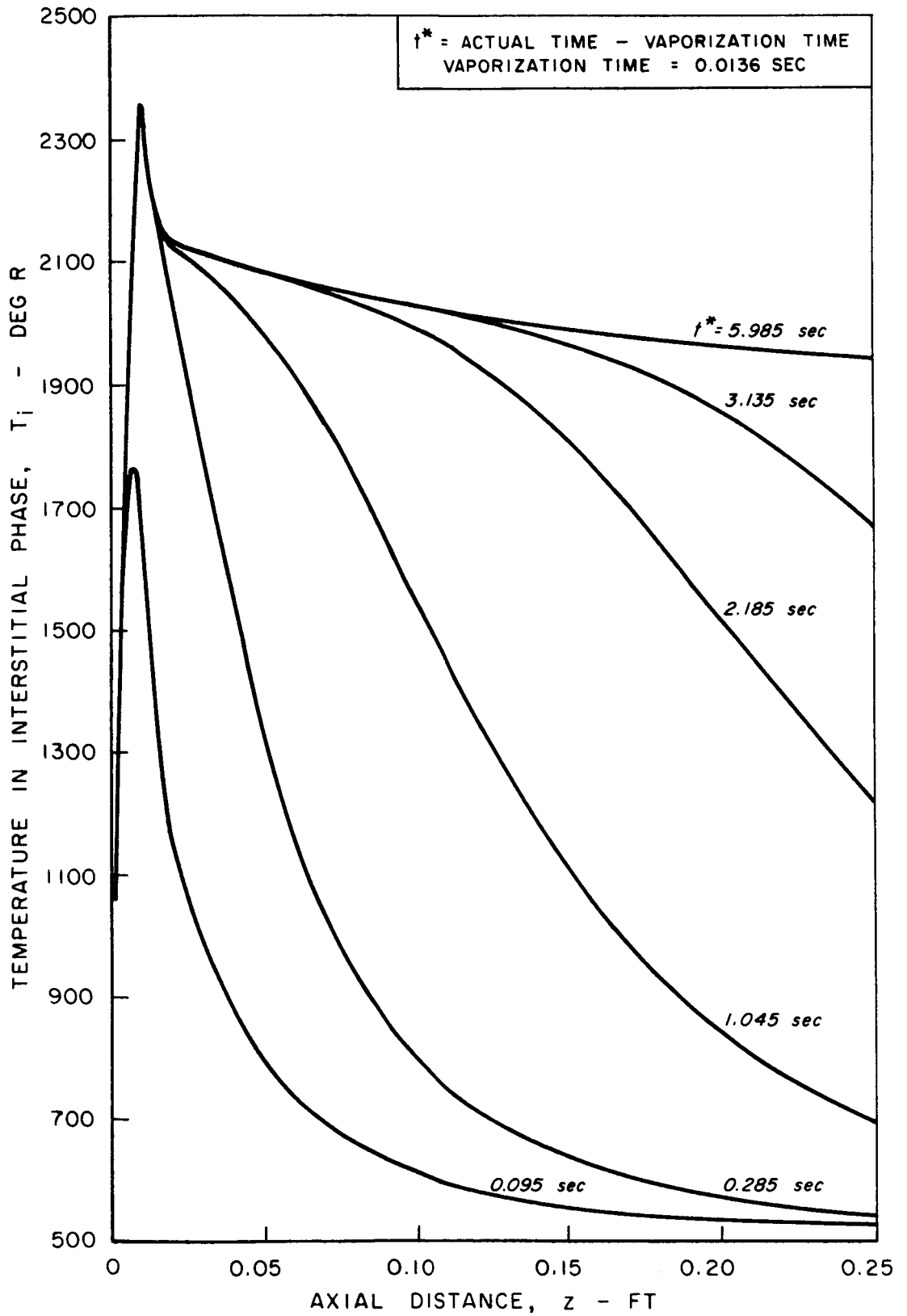

FIG. 34

VARIATION OF TEMPERATURE WITH TIME AT SEVERAL AXIAL POSITIONS

P(FEED PRESSURE) = 1042 PSIA G = 2.43 LB/FT^2 - SEC STANDARD BED CONFIGURATION (SEE TEXT)

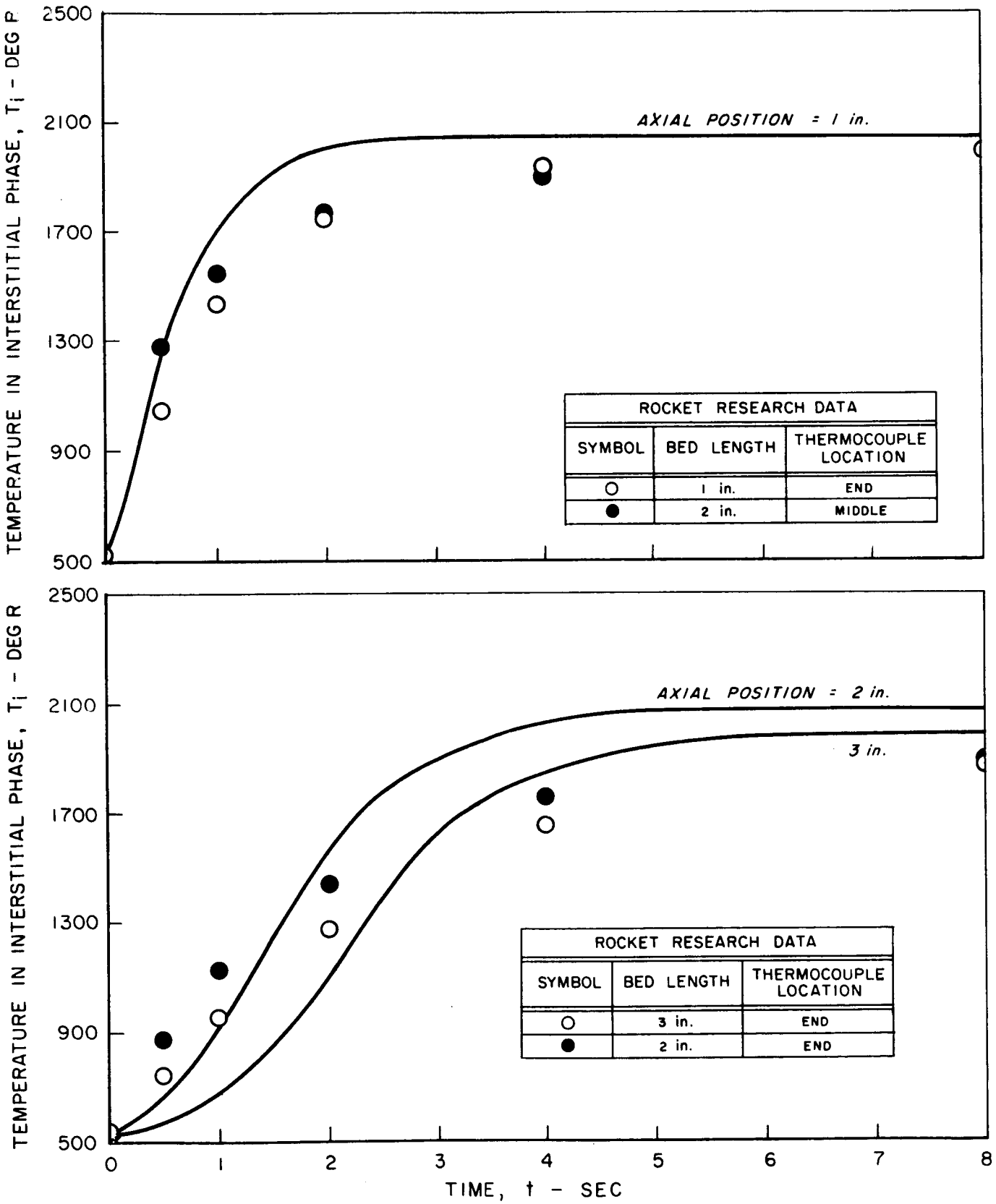

VARIATION OF CHAMBER EXIT PRESSURE WITH TIME

P (FEED PRESSURE) = 1042 PSIA
G = 2.43 LB/FT^2 - SEC
STANDARD BED CONFIGURATION (SEE TEXT)

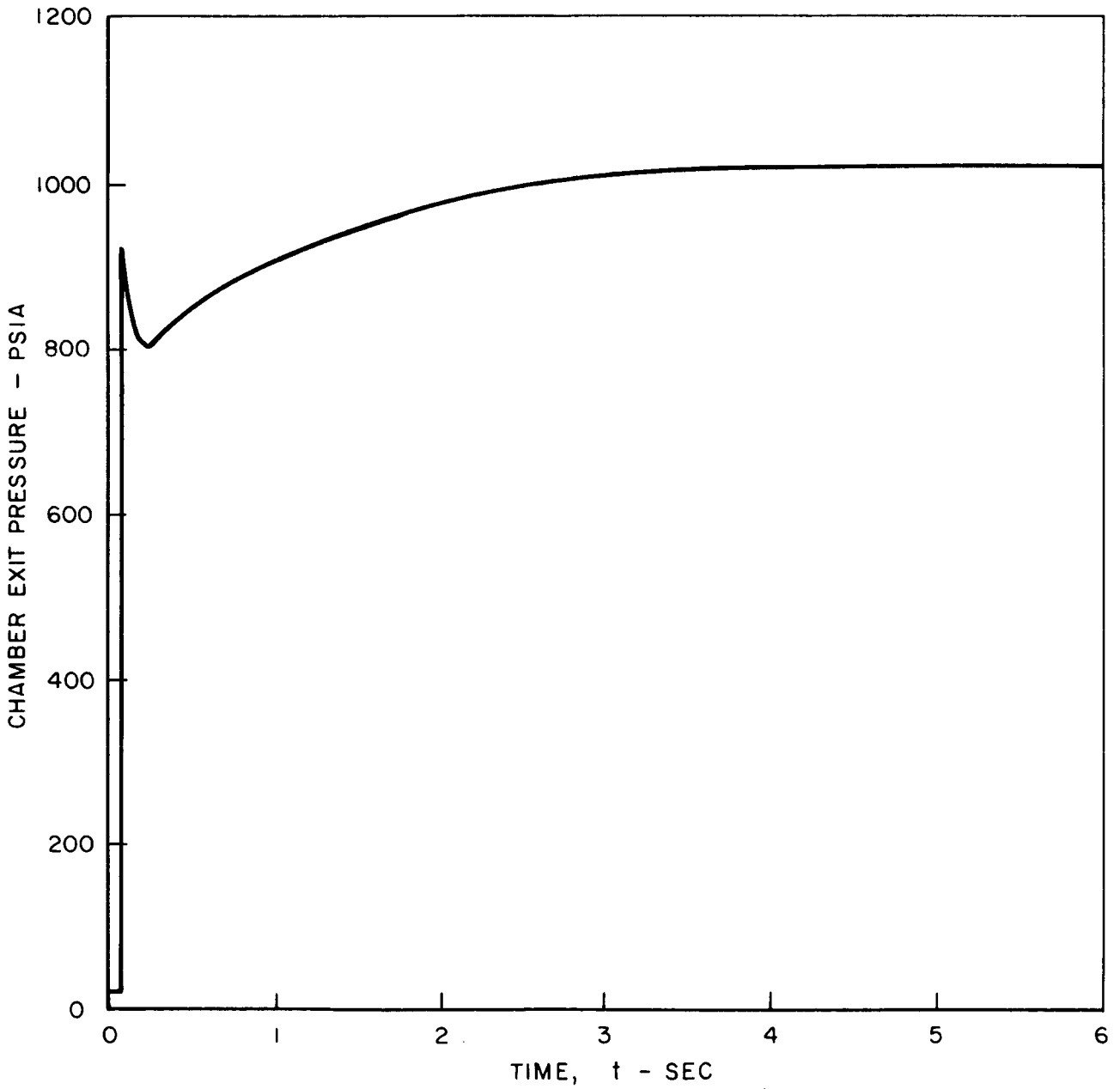

FIG. 36

TRANSIENT AXIAL TEMPERATURE PROFILES

P (FEED PRESSURE) = 974 PSIA
G = 6.29 LB/FT^2- SEC
STANDARD BED CONFIGURATION (SEE TEXT)

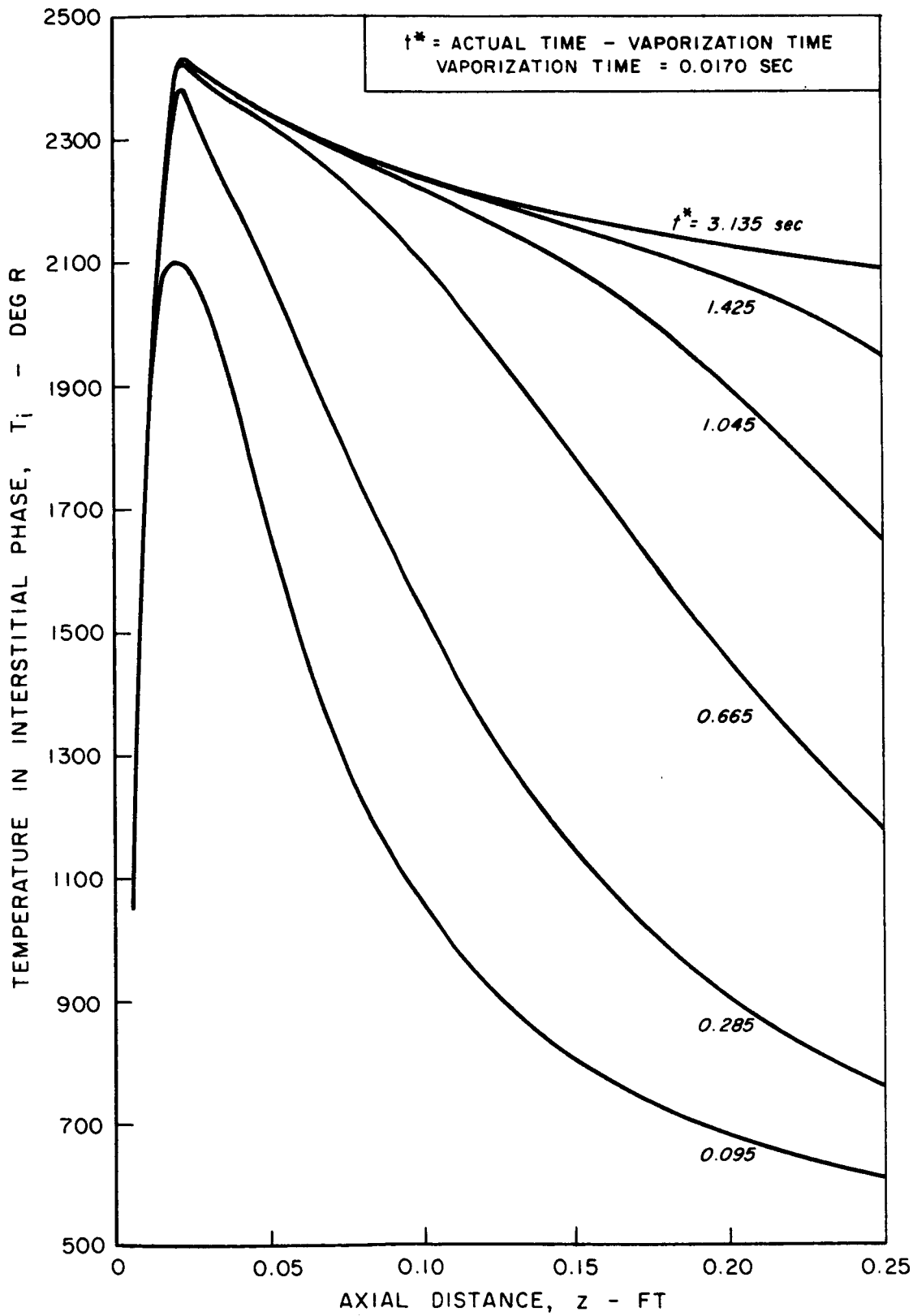

VARIATION OF TEMPERATURE WITH TIME AT SEVERAL AXIAL POSITIONS

P(FEED PRESSURE) = 974 PSIA G = 6.29 LB/FT^2-SEC STANDARD BED CONFIGURATION (SEE TEXT)

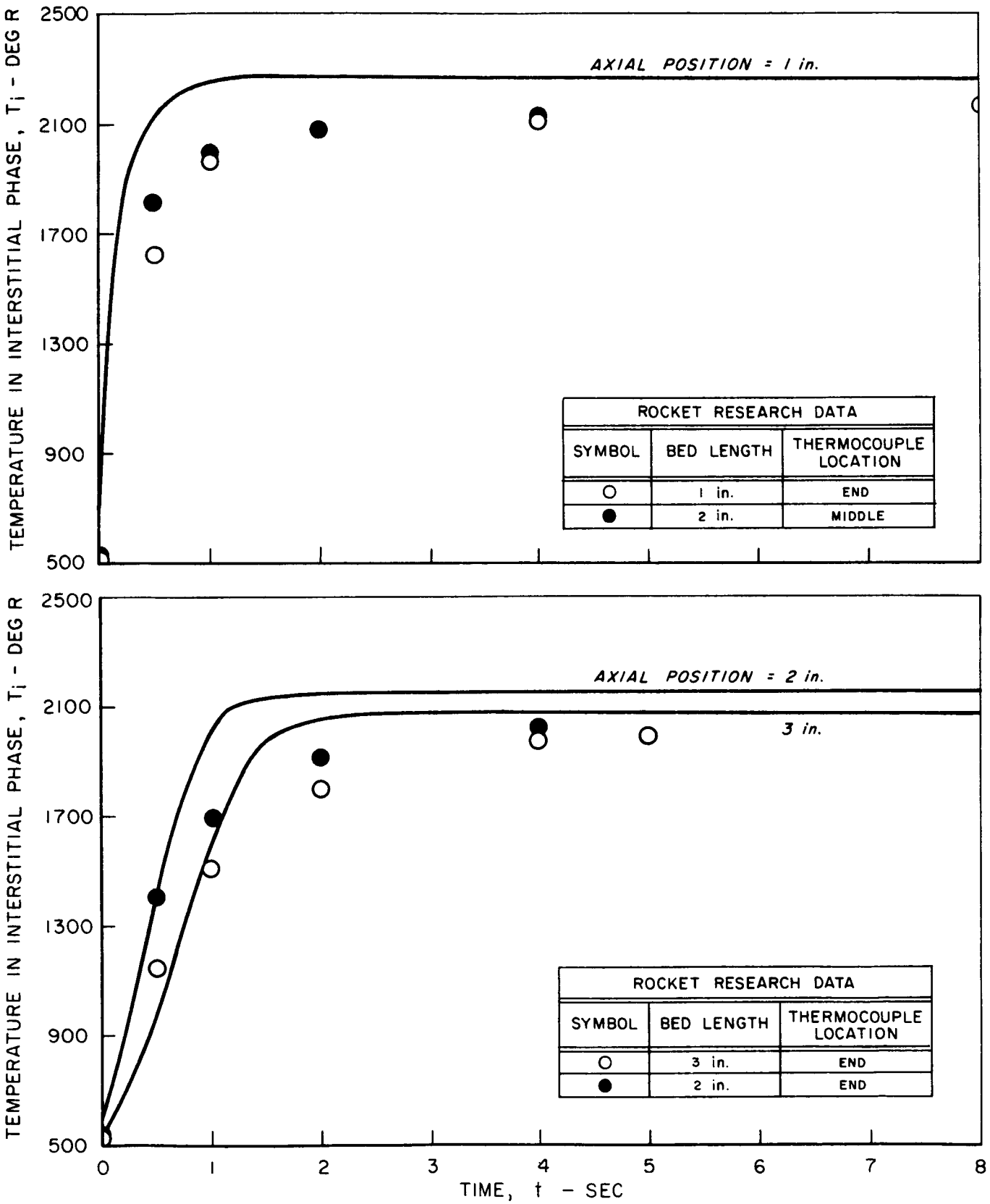

FIG. 38

VARIATION OF CHAMBER EXIT PRESSURE WITH TIME

P (FEED PRESSURE) = 974 PSIA
G = 6.29 LB/FT^2 - SEC
STANDARD BED CONFIGURATION (SEE TEXT)

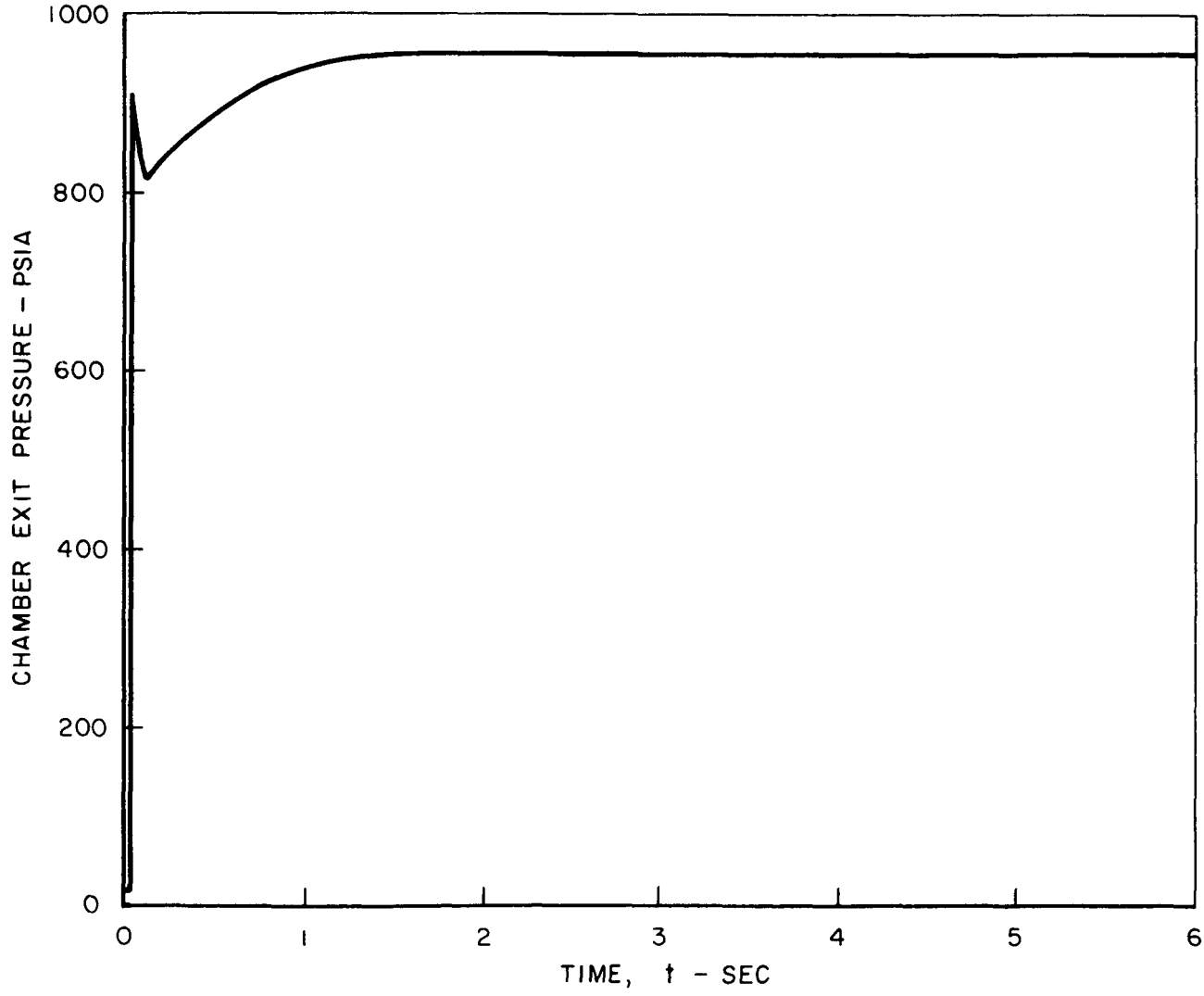

TRANSIENT AXIAL TEMPERATURE PROFILES

P (FEED PRESSURE) = 217.9 PSIA
G = 1.52 LB/FT^2 - SEC
STANDARD BED CONFIGURATION (SEE TEXT)

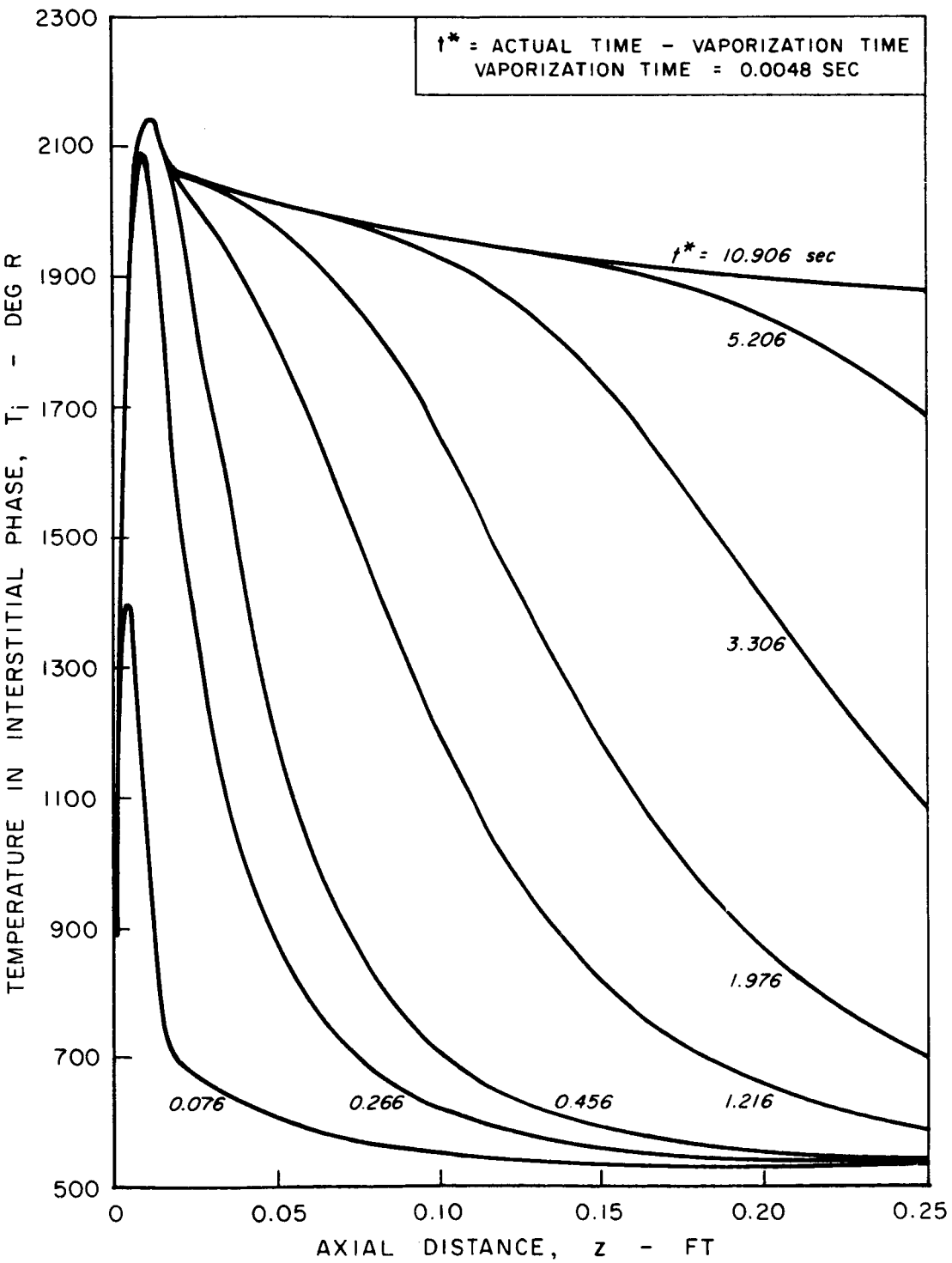

FIG. 40

VARIATION OF TEMPERATURE WITH TIME AT SEVERAL AXIAL POSITIONS

P (FEED PRESSURE) = 217.9 PSIA G = 1.52 LB/FT^2 - SEC STANDARD BED CONFIGURATION (SEE TEXT)

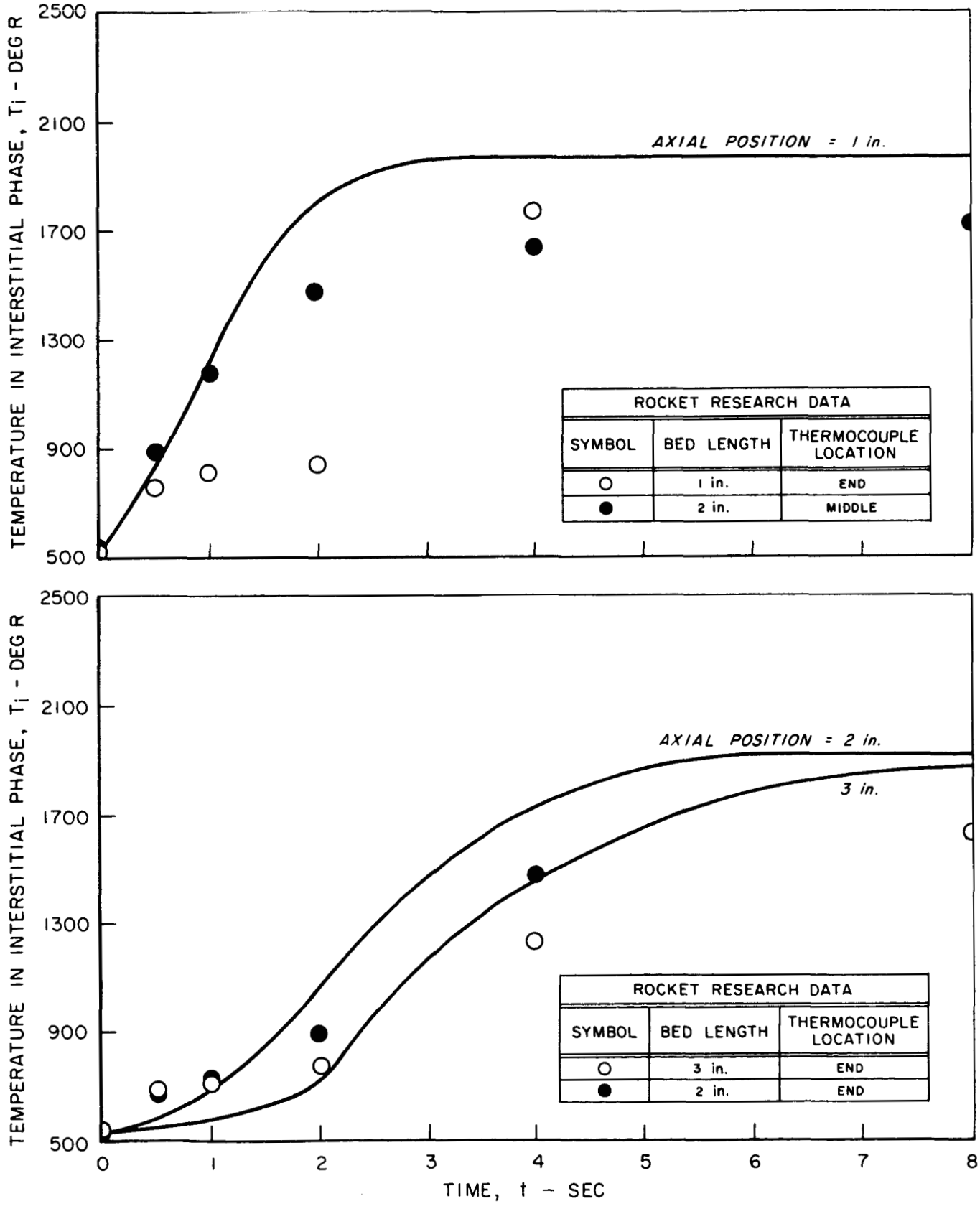

VARIATION OF CHAMBER EXIT PRESSURE WITH TIME

P (FEED PRESSURE) = 217.9 PSIA
G = 1.52 LB/FT^2 - SEC
STANDARD BED CONFIGURATION (SEE TEXT)

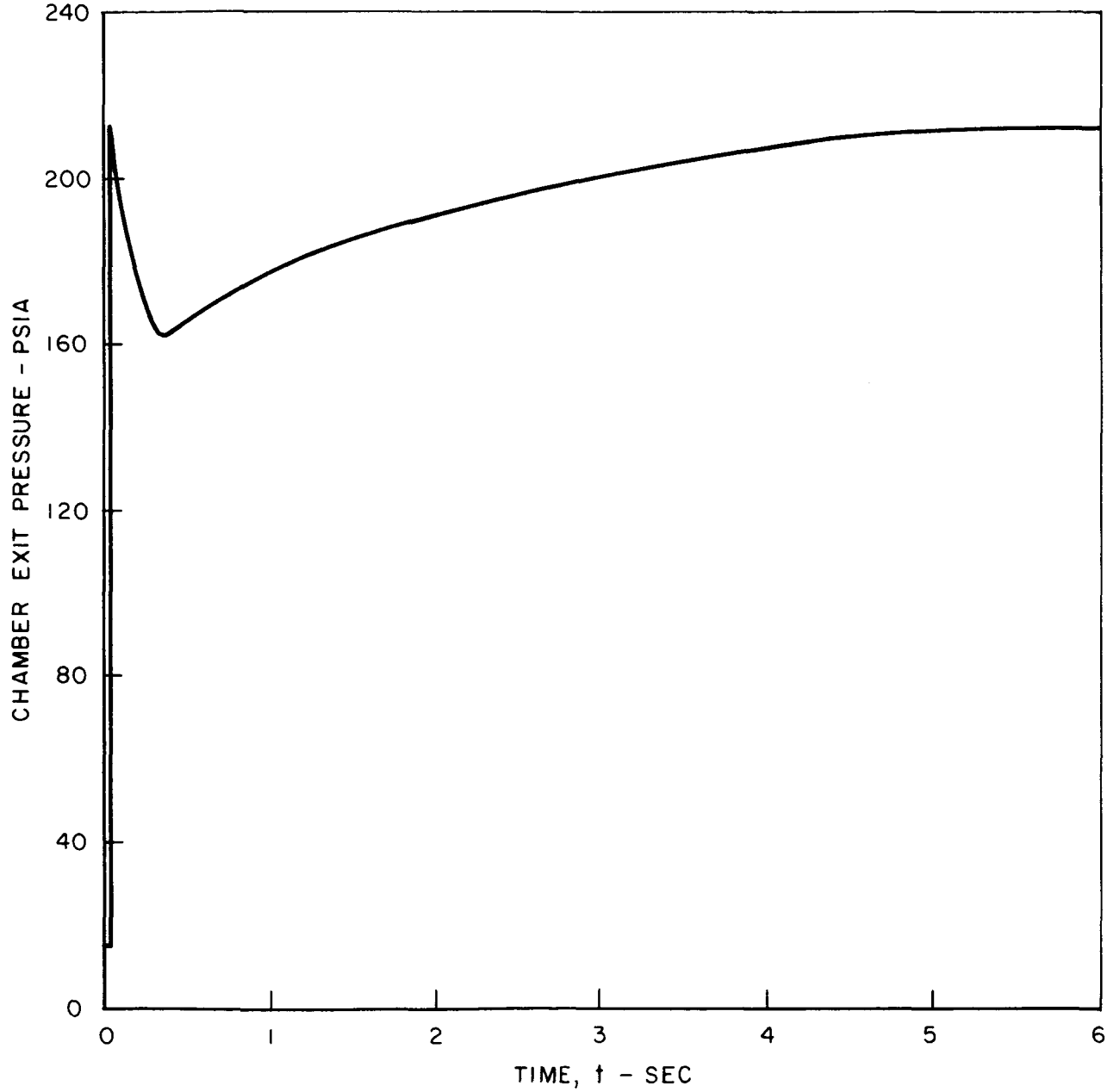

FIG. 42

TRANSIENT AXIAL TEMPERATURE PROFILES

P(FEED PRESSURE) = 111.4 PSIA
G = 1.51 LB/FT^2 - SEC
STANDARD BED CONFIGURATION (SEE TEXT)

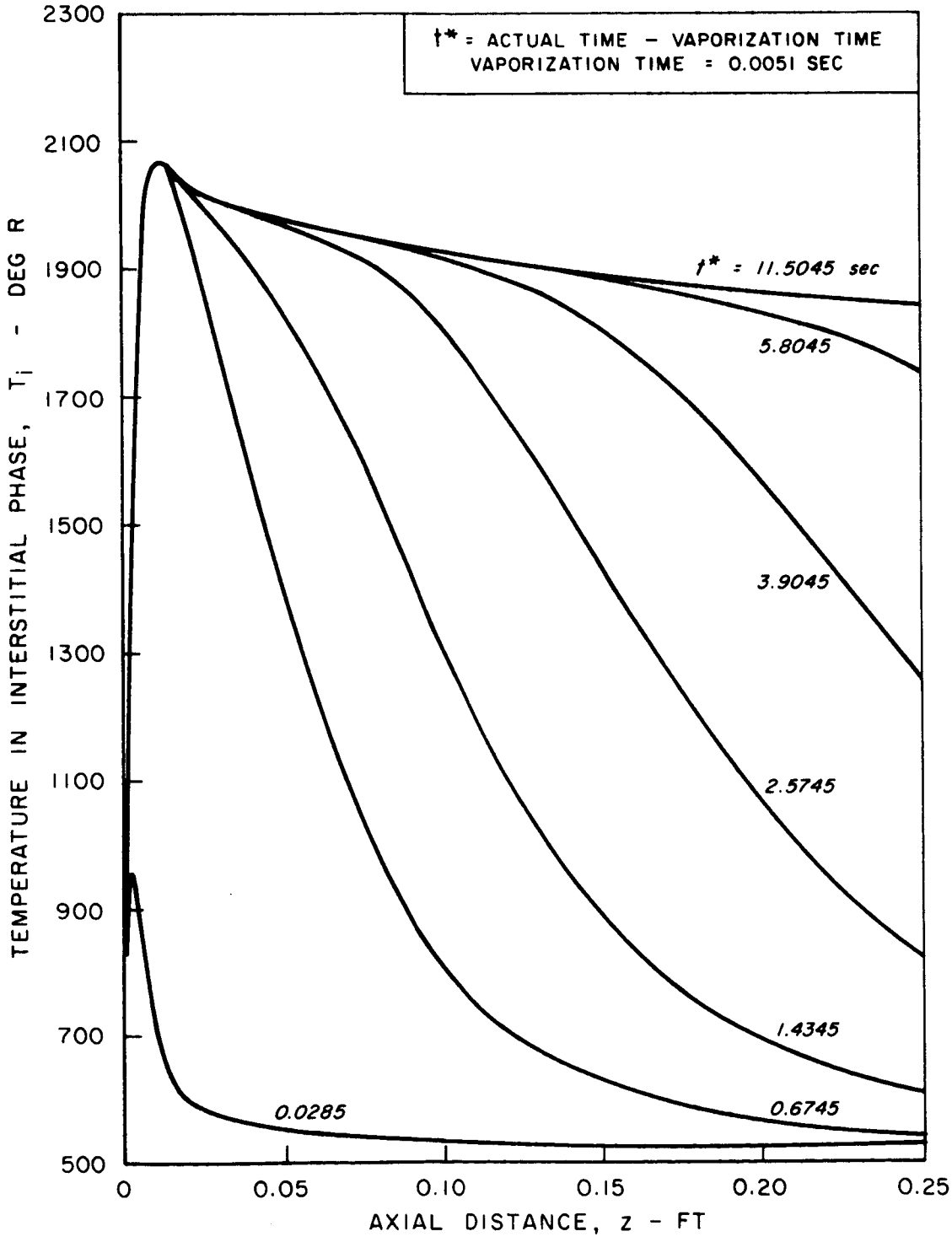

FIG. 43

VARIATION OF TEMPERATURE WITH TIME AT SEVERAL AXIAL POSITIONS

P(FEED PRESSURE) = 111.4 PSIA G = 1.51 LB/FT^2 - SEC STANDARD BED CONFIGURATION (SEE TEXT)

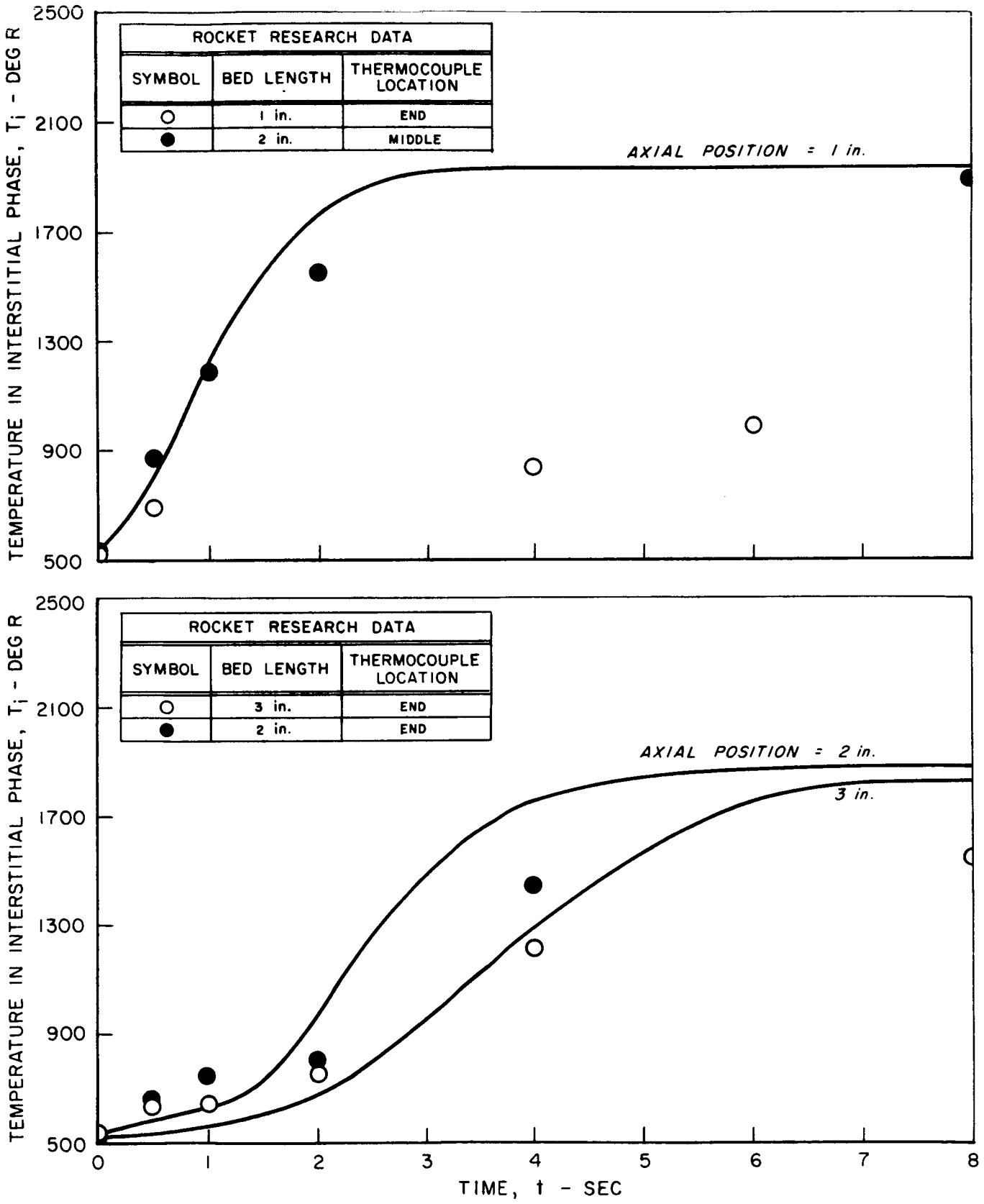

FIG. 44

VARIATION OF CHAMBER EXIT PRESSURE WITH TIME

P (FEED PRESSURE) = 111.4 PSIA
G = 1.51 LB/FT^2 - SEC
STANDARD BED CONFIGURATION (SEE TEXT)

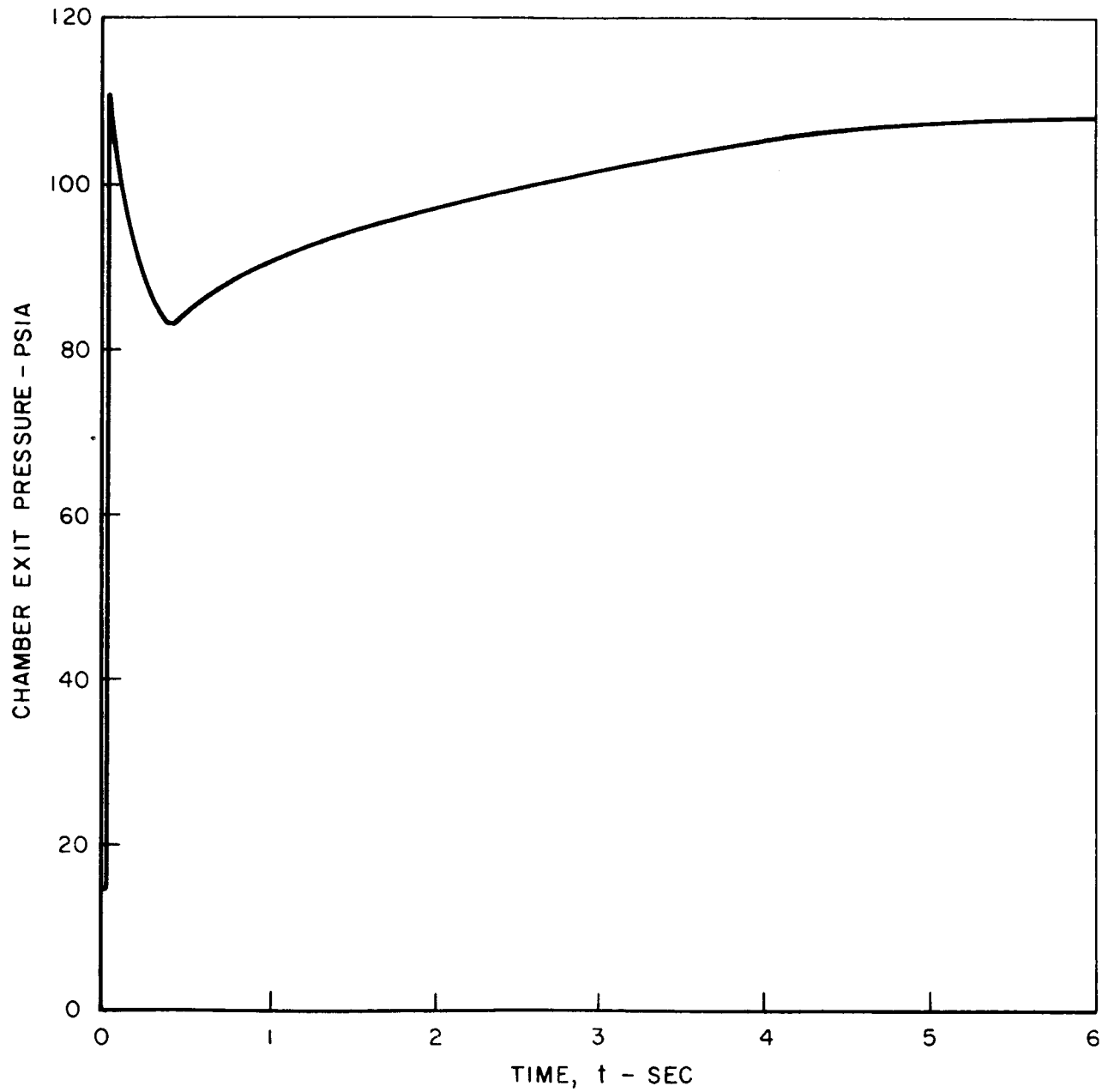

VARIATION OF EXIT GAS TEMPERATURE WITH TIME FOR VARIOUS FEED PRESSURES

G = 3.0 LB/FT^2 - SEC
STANDARD BED CONFIGURATION (SEE TEXT)

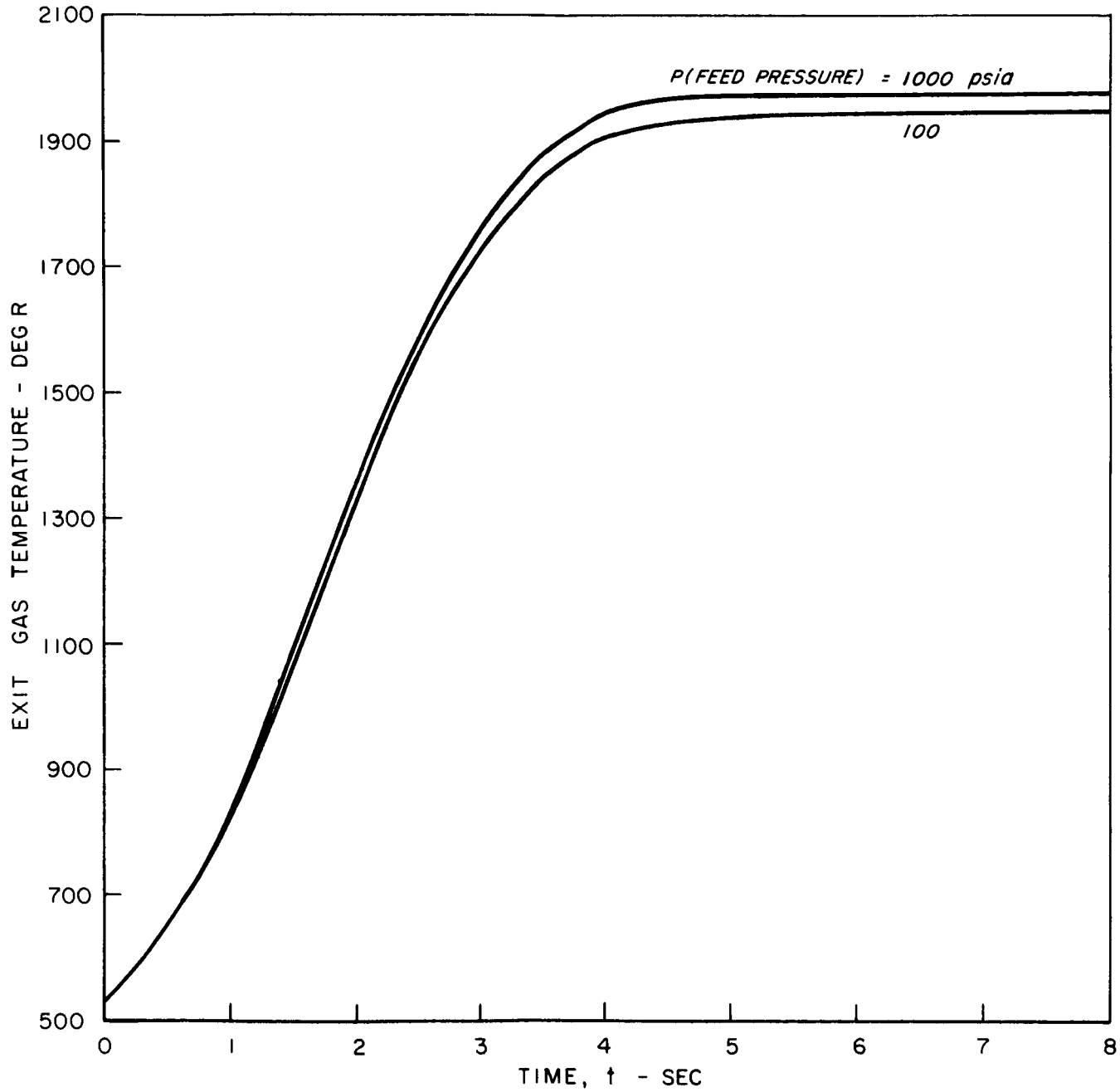

FIG. 46

VARIATION OF EXIT GAS TEMPERATURE WITH TIME FOR VARIOUS MASS FLOW RATES

P(FEED PRESSURE) = 100 PSIA

STANDARD BED CONFIGURATION (SEE TEXT)

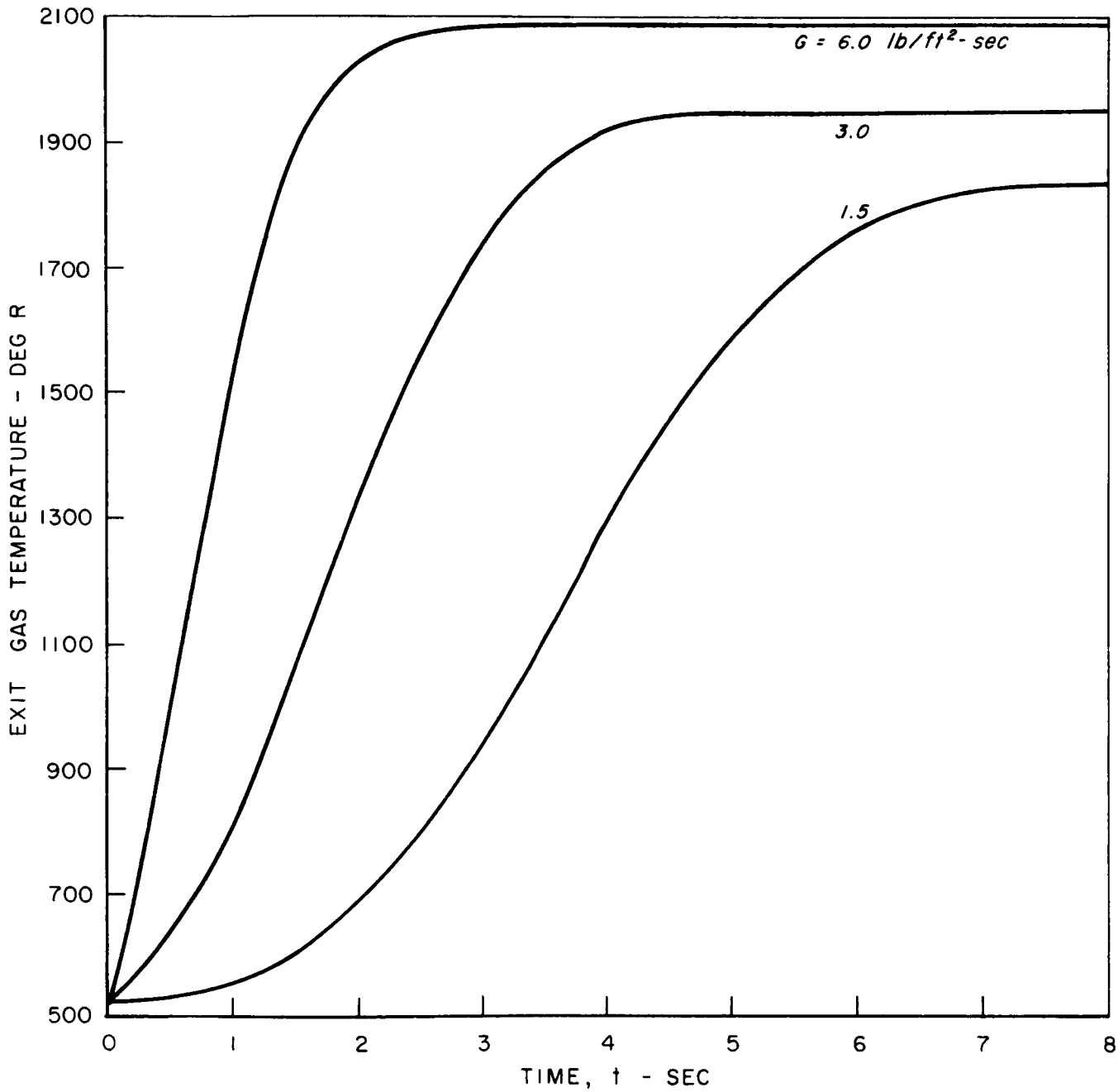

FIG. 47

VARIATION OF EXIT GAS TEMPERATURE WITH TIME FOR VARIOUS CATALYTIC BED CONFIGURATIONS

P (FEED PRESSURE) = 100 PSIA

G = 3.0 LB/FT^2 - SEC

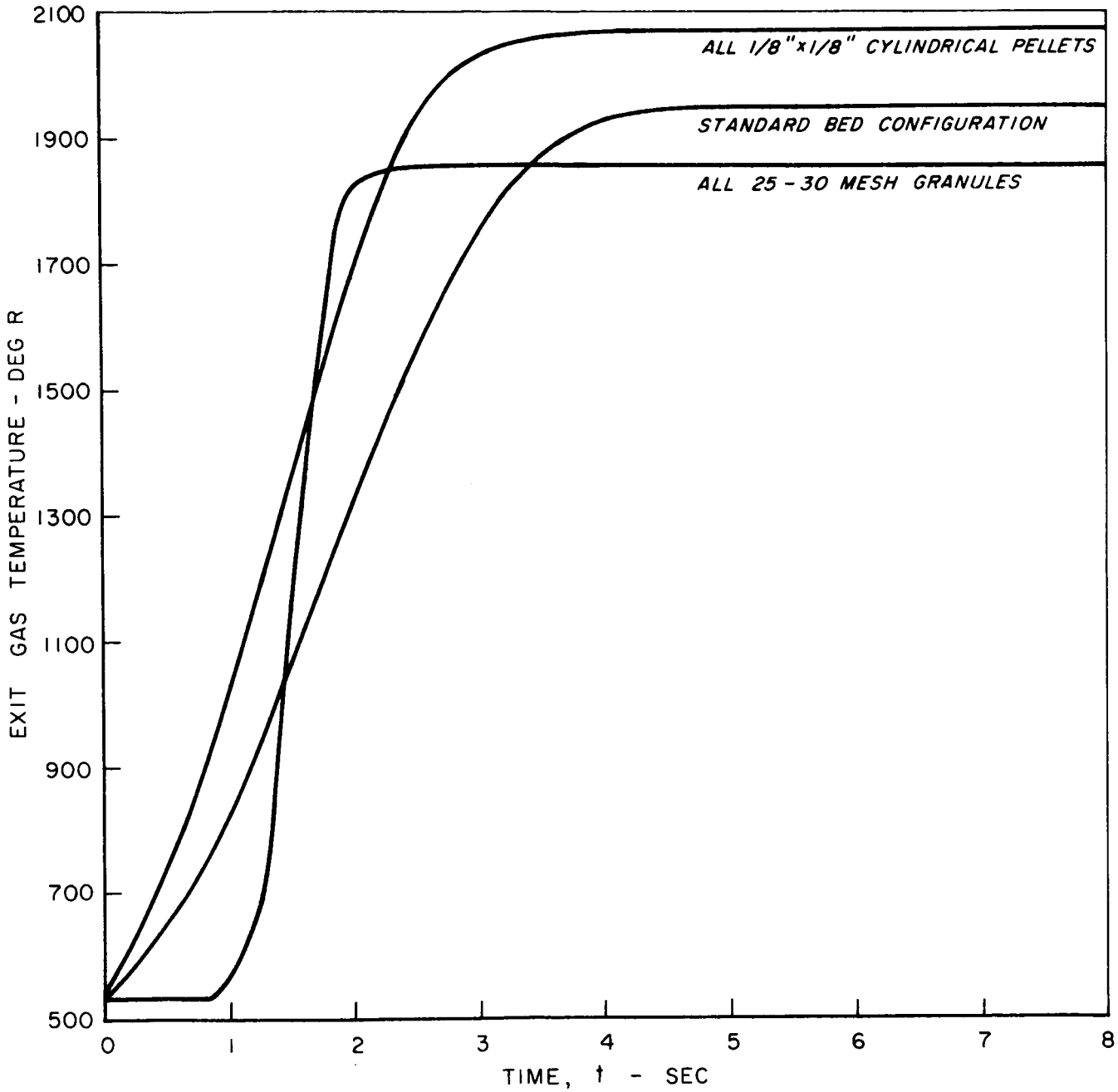

VARIATION OF EXIT GAS TEMPERATURE WITH TIME FOR VARIOUS HYDRAZINE AXIAL INJECTION PROFILES

P (FEED PRESSURE) = 100 PSIA

BED CONFIGURATION: ALL 25 - 30 MESH GRANULES

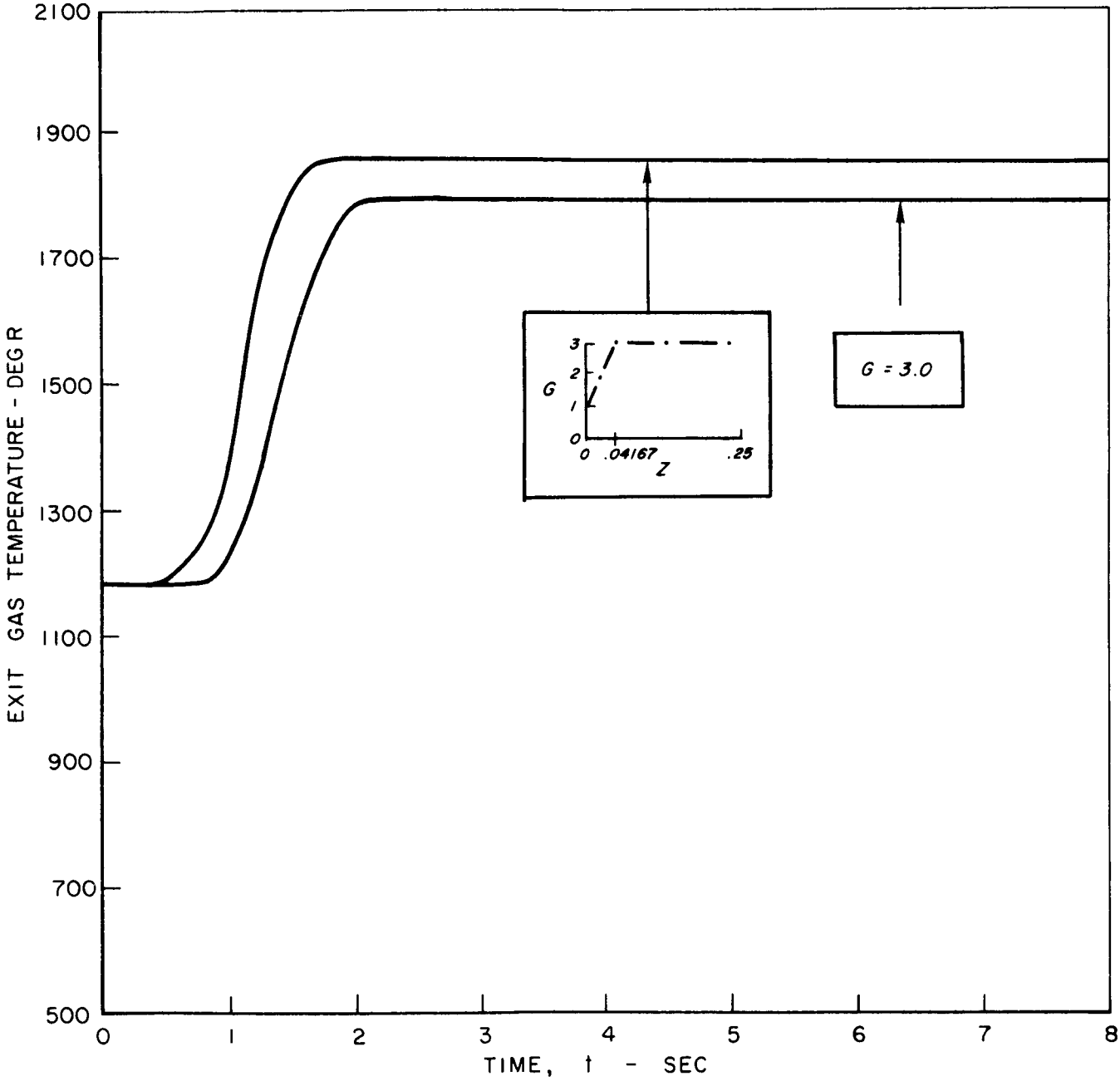

FIG. 49

VARIATION OF EXIT GAS TEMPERATURE WITH TIME FOR VARIOUS INITIAL BED TEMPERATURES

P(FEED PRESSURE) = 100 PSIA
G = 3.0 LB/FT^2 - SEC
STANDARD BED CONFIGURATION (SEE TEXT)

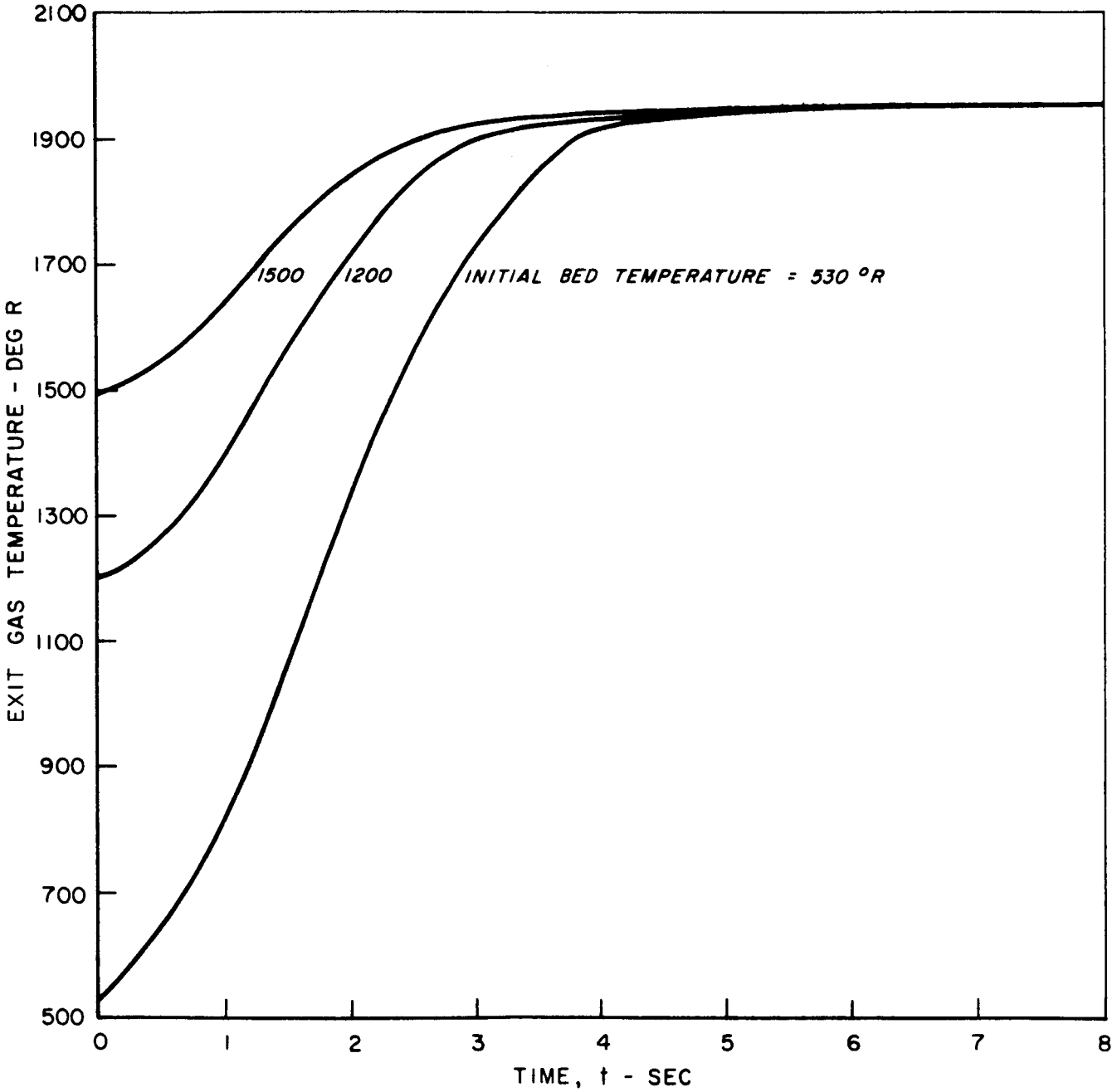

APPENDIX II

DISTRIBUTION LIST FOR FIRST ANNUAL PROGRESS REPORT
F910461-12

Addressee	Copies
National Aeronautics & Space Administration Washington, D. C. 20546 Attn: Chief, Liq. Prop. Res. & Tech., RPL	1
National Aeronautics & Space Administration Washington, D. C. 20546 Attn: Chief, Liq. Prop. Exp. Systems, RPX	10
National Aeronautics & Space Administration Washington, D. C. 20546 Attn: Dir., Launch Vehicles & Prop., SV	1
National Aeronautics & Space Administration Washington, D. C. 20546 Attn: Dir., Advanced Manned Missions, MT	1
NASA Ames Research Center Moffett Field, California 24035 Attn: Dir., Mission Analysis Division	1
Air Force Rocket Propulsion Laboratory Research and Technology Division Air Force System Command Edwards, California 93523 Attn: Mr. K. Rimer	1
Air Force Rocket Propulsion Laboratory Research and Technology Division Air Force System Command Edwards, California 93523 Attn: Capt. Noyce/32725	1
U. S. Naval Ordnance Test Station China Lake, California 93553 Attn: Mr. Duane Williams	1
U. S. Naval Ordnance Test Station China Lake, California 93553 Attn: Mr. James Dake	1
U. S. Naval Ordnance Test Station China Lake, California 93553 Attn: Mr. David Oliver	1
Jet Propulsion Laboratory 4800 Oak Grove Drive Pasadena, California 91103 Attn: Mr. Theodore W. Price	10
NASA Pasadena Office 4800 Oak Grove Drive Pasadena, California 91103 Attn: Contracting Officer	1
NASA Pasadena Office 4800 Oak Grove Drive Pasadena, California 91103 Attn: Office of Tech. Information & Patent Matters	1
Scientific & Technical Information Facility P. O. Box 5700 Bethesda, Maryland 20014 Attn: NASA Rep., Code CRT	2

Addressee	Copies
NASA Lewis Research Center 21000 Brookpark Road Cleveland, Ohio 44135 Attn: Mr. Paul Herr	3
NASA Lewis Research Center 21000 Brookpark Road Cleveland, Ohio 44135 Attn: Mr. I. A. Johnsen	1
Marshall Space Flight Center Huntsville, Alabama 35812 Attn: Mr. Kieth Coates	1
Department of Chemical Engineering University of British Columbia Vancouver 8, Canada Attn: Dr. J. Lielmezs	1
NASA Ames Research Center Moffett Field, California 94035 Attn: Technical Librarian	2
NASA Ames Research Center Moffett Field, California 94035 Attn: Mr. Harold Hornby Mission Analysis Division	Ltr. Only
NASA Ames Research Center Moffett Field, California 94035 Attn: Mr. Clarence A. Syvertson	Ltr. Only
NASA Goddard Space Flight Center Greenbelt, Maryland 20771 Attn: Technical Librarian	2
NASA Goddard Space Flight Center Greenbelt, Maryland 20771 Attn: Mr. Merland L. Moseson, Code 620	Ltr. Only
NASA Goddard Space Flight Center Greenbelt, Maryland 20771 Attn: Mr. D. Grant	Ltr. Only
Jet Propulsion Laboratory California Institute of Technology 4800 Oak Grove Drive Pasadena, California 91103 Attn: Technical Librarian	2
Jet Propulsion Laboratory California Institute of Technology 4800 Oak Grove Drive Pasadena, California 91103 Attn: Mr. Henry Burlage, Jr. Propulsion Div., 38	Ltr. Only
NASA Langley Research Center Langley Station Hampton, Virginia 23365 Attn: Technical Librarian	2

Addressee	Copies
NASA Langley Research Center Langley Station Hampton, Virginia 23365 Attn: Dr. Floyd L. Thompson, Dir.	Ltr. Only
NASA Langley Research Center Langley Station Hampton, Virginia 23365 Attn: Mr. R. Hook	Ltr. Only
NASA Lewis Research Center 21000 Brookpark Road Cleveland, Ohio 44135 Attn: Technical Librarian	2
NASA Lewis Research Center 21000 Brookpark Road Cleveland, Ohio 44135 Attn: Dr. Abe Silverstein, Dir.	Ltr. Only
NASA Lewis Research Center 21000 Brookpark Road Cleveland, Ohio 44135 Attn: Mr. Steve Cohen	Ltr. Only
NASA Marshall Space Flight Center Huntsville, Alabama 35812 Attn: Technical Librarian	2
NASA Marshall Space Flight Center Huntsville, Alabama 35812 Attn: Mr. Hans G. Paul, Code R-P+VED	Ltr. Only
NASA Marshall Space Flight Center Huntsville, Alabama 35812 Attn: Mr. Werner Voss, R-P&VE-PM	Ltr. Only
NASA Manned Spacecraft Center Houston, Texas 77001 Attn: Technical Librarian	2
NASA Manned Spacecraft Center Houston, Texas 77001 Attn: Dr. Robert R. Gilruth, Dir.	Ltr. Only
NASA Manned Spacecraft Center Houston, Texas 77001 Attn: Mr. H. Pohl	Ltr. Only
NASA Western Support Office 150 Pico Boulevard Santa Monica, California 90406 Attn: Technical Librarian	2
NASA Western Support Office 150 Pico Boulevard Santa Monica, California 90406 Attn: Mr. Robert W. Kamm, Dir.	Ltr. Only
NASA John F. Kennedy Space Center Cocoa Beach, Florida 32931 Attn: Technical Librarian	2
NASA John F. Kennedy Space Center Cocoa Beach, Florida 32931 Attn: Dr. Kurt H. Debus	Ltr. Only
NASA Test Facility Propulsion Engineering Office White Sands, New Mexico Attn: Technical Librarian	1
NASA Test Facility Propulsion Engineering Office White Sands, New Mexico Attn: Mr. I. D. Smith, Staff Chemist	Ltr. Only
Aeronautical Systems Division Air Force Systems Command Wright-Patterson Air Force Base Dayton, Ohio 45433 Attn: Technical Librarian	1
Aeronautical Systems Division Air Force Systems Command Wright-Patterson Air Force Base Dayton, Ohio 45433 Attn: Mr. D. L. Schmidt, Code ASRCNC-2	Ltr. Only
Air Force Missile Development Center Holloman Air Force Base, New Mexico 88330 Attn: Technical Librarian	1
Air Force Missile Development Center Holloman Air Force Base, New Mexico 88330 Attn: Maj. R. E. Bracken, Code MDGRT	Ltr. Only
Air Force Missile Test Center Patrick Air Force Base, Florida Attn: Technical Librarian	1
Air Force Missile Test Center Patrick Air Force Base, Florida Attn: Mr. L. J. Ullian	Ltr. Only
Air Force Systems Division Air Force Unit Post Office Los Angeles 45, California 90045 Attn: Technical Librarian	1
Air Force Systems Division Air Force Unit Post Office Los Angeles 45, California 90045 Attn: Col. Clark, Tech. Data Center	Ltr. Only
Technical Library AFFTC (FTBPP-2) Edwards AFB, California 93523 Attn: Technical Librarian	2
Technical Library AFFTC (FTBPP-2) Edwards AFB, California 93523 Attn: Mr. Myrtle C. Jones	Ltr. Only
Arnold Engineering Development Center Arnold Air Force Station Tullahoma, Tennessee 37388 Attn: Technical Librarian	1
Arnold Engineering Development Center Arnold Air Force Station Tullahoma, Tennessee 37388 Attn: Dr. H. K. Doetsch	Ltr. Only
Bureau of Naval Weapons Department of the Navy Washington, D. C. 20546 Attn: Technical Librarian	1
Bureau of Naval Weapons Department of the Navy Washington, D. C. 20546 Attn: Mr. J. Kay, RTMS-41	Ltr. Only

Addressee	Copies
Defense Documentation Center Headquarters Cameron Station, Building 5 5010 Duke Street Alexandria, Virginia 22314 Attn: Technical Librarian	1
Defense Documentation Center Headquarters Cameron Station, Building 5 5010 Duke Street Alexandria, Virginia 22314 Attn: TISIA	Ltr. Only
Headquarters, U. S. Air Force Washington 25, D. C. 20546 Attn: Technical Librarian	1
Headquarters, U. S. Air Force Washington 25, D. C. 20546 Attn: Col. C. K. Stambaugh, AFRST	Ltr. Only
Picatinny Arsenal Dover, New Jersey 07801 Attn: Technical Librarian	1
Picatinny Arsenal Dover, New Jersey 07801 Attn: Mr. I. Forsten, Chief Liquid Propulsion Lab., SMUPA-DL	Ltr. Only
Air Force Rocket Propulsion Laboratory Research and Technology Division Air Force Systems Command Edwards, California 93523 Attn: Technical Librarian	1
Air Force Rocket Propulsion Laboratory Research and Technology Division Air Force Systems Command Edwards, California 93523 Attn: Mr. H. Main, RPRR	Ltr. Only
Air Force Rocket Propulsion Laboratory Research and Technology Division Air Force Systems Command Edwards, California 93523 Attn: 1st Lt. D. Shantz	Ltr. Only
U. S. Atomic Energy Commission Technical Information Services Box 62 Oak Ridge, Tennessee 37830 Attn: Technical Librarian	1
U. S. Atomic Energy Commission Technical Information Services Box 62 Oak Ridge, Tennessee 37830 Attn: Mr. A. P. Huber Oak Ridge Gaseous Diffusion Plant (ORGDP) P. O. Box P	Ltr. Only
U. S. Army Missile Command Redstone Arsenal, Alabama 35809 Attn: Technical Librarian	1
U. S. Army Missile Command Redstone Arsenal, Alabama 35809 Attn: Dr. Walter Wharton	Ltr. Only
U. S. Naval Ordnance Test Station China Lake, California 93557 Attn: Technical Librarian	1
U. S. Naval Ordnance Test Station China Lake, California 93557 Attn: Code 4562 Chief, Missile Propulsion Division	Ltr. Only
Chemical Propulsion CPIA Information Agency Applied Physics Laboratory 8621 Georgia Avenue Silver Spring, Maryland 20910 Attn: Technical Librarian	1
Chemical Propulsion CPIA Information Agency Applied Physics Laboratory 8621 Georgia Avenue Silver Spring, Maryland 20910 Attn: Mr. P. Martin	Ltr. Only
Aerojet-General Corporation P. O. Box 296 Azusa, California 91703 Attn: Technical Librarian	1
Aerojet-General Corporation P. O. Box 296 Azusa, California 91703 Attn: Mr. L. F. Kohrs	Ltr. Only
Aerojet-General Corporation P. O. Box 1947 Technical Library, Bldg. 2015, Dept. 2410 Sacramento, California 95809 Attn: Technical Librarian	1
Aerojet-General Corporation P. O. Box 1947 Technical Library, Bldg. 2015, Dept. 2410 Sacramento, California 95809 Attn: Mr. R. Stiff	Ltr. Only
Aeronutronic Division Philco Corporation Ford Road Newport Beach, California 92663 Attn: Technical Librarian	1
Aeronutronic Division Philco Corporation Ford Road Newport Beach, California 92663 Attn: Mr. N. Stern	Ltr. Only
Aerospace Corporation 2400 East El Segundo Boulevard P. O. Box 95085 Los Angeles, California 90045 Attn: Technical Librarian	1
Aerospace Corporation 2400 East El Segundo Boulevard P. O. Box 95085 Los Angeles, California 90045 Attn: Mr. M. J. Russi	Ltr. Only
Aerospace Corporation 2400 East El Segundo Boulevard P. O. Box 95085 Los Angeles, California 90045 Attn: Mr. H. Greer, Propulsion Dept.	Ltr. Only
Arthur D. Little, Incorporated 20 Acorn Park Cambridge, Massachusetts 02140 Attn: Technical Librarian	1

Addressee	Copies
Arthur D. Little, Incorporated 20 Acorn Park Cambridge, Massachusetts 02140 Attn: Mr. E. Karl Bastress	Ltr. Only
Astropower Laboratory Douglas Aircraft Company 2121 Paularino Newport Beach, California 92663 Attn: Technical Librarian	1
Astropower Laboratory Douglas Aircraft Company 2121 Paularino Newport Beach, California 92663 Attn: Dr. George Moc, Dir. Research	Ltr. Only
Astrosystems International, Incorporated 1275 Bloomfield Avenue Fairfield, New Jersey 07007 Attn: Technical Librarian	1
Astrosystems International, Incorporated 1275 Bloomfield Avenue Fairfield, New Jersey 07007 Attn: Mr. A. Mendenhall	Ltr. Only
Atlantic Research Corporation Edsall Road and Shirley Highway Alexandria, Virginia 22314 Attn: Technical Librarian	1
Atlantic Research Corporation Edsall Road and Shirley Highway Alexandria, Virginia 22314 Attn: Mr. A. Scurlock	Ltr. Only
Beech Aircraft Corporation Boulder Division Box 631 Boulder, Colorado 80302 Attn: Technical Librarian	1
Beech Aircraft Corporation Boulder Division Box 631 Boulder, Colorado 80302 Attn: Mr. J. H. Rodgers	Ltr. Only
Bell Aerosystems Company P. O. Box 1 Buffalo, New York 14240 Attn: Technical Librarian	1
Bell Aerosystems Company P. O. Box 1 Buffalo, New York 14240 Attn: Mr. N. Safeer	Ltr. Only
Bell Aerosystems Company P. O. Box 1 Buffalo, New York 14240 Attn: Mr. N. R. Roth	Ltr. Only
Bell Aerosystems Company P. O. Box 1 Buffalo, New York 14240 Attn: Mr. J. Flanagan	Ltr. Only
Bendix Systems Division Bendix Corporation 3300 Plymouth Road Ann Arbor, Michigan 48105 Attn: Technical Librarian	1
Bendix Systems Division Bendix Corporation 3300 Plymouth Road Ann Arbor, Michigan 48105 Attn: Mr. John M. Brueger	Ltr. Only
Boeing Company P. O. Box 3707 Seattle, Washington 98124 Attn: Technical Librarian	1
Boeing Company P. O. Box 3707 Seattle, Washington 98124 Attn: Mr. J. D. Alexander	Ltr. Only
Missile Division Chrysler Corporation P. O. Box 2628 Detroit, Michigan 48231 Attn: Technical Librarian	1
Missile Division Chrysler Corporation P. O. Box 2628 Detroit, Michigan 48231 Attn: Mr. John Gates	Ltr. Only
Wright Aeronautical Division Curtiss-Wright Corporation Wood-Ridge, New Jersey 07075 Attn: Technical Librarian	1
Wright Aeronautical Division Curtiss-Wright Corporation Wood-Ridge, New Jersey 07075 Attn: Mr. G. Kelley	Ltr. Only
Missile and Space Systems Division Douglas Aircraft Company, Incorporated 3000 Ocean Park Boulevard Santa Monica, California 90406 Attn: Technical Librarian	1
Missile and Space Systems Division Douglas Aircraft Company, Incorporated 3000 Ocean Park Boulevard Santa Monica, California 90406 Attn: Mr. R. W. Hallet, Chief Engineer Advanced Space Tech.	Ltr. Only
Missile and Space Systems Division Douglas Aircraft Company, Incorporated 3000 Ocean Park Boulevard Santa Monica, California 90406 Attn: Mr. A. Pisciotta, Jr.	Ltr. Only
Aircraft Missiles Division Fairchild Hiller Corporation Hagerstown, Maryland 21740 Attn: Technical Librarian	1
Aircraft Missiles Division Fairchild Hiller Corporation Hagerstown, Maryland 21740 Attn: Mr. J. S. Kerr	Ltr. Only
General Dynamics Convair Division 5001 Kearny Villa Road P. O. Box 1628 San Diego, California 92112 Attn: Technical Librarian	1

Addressee	Copies
General Dynamics Convair Division 5001 Kearny Villa Road P. O. Box 1628 San Diego, California 92112 Attn: Mr. E. R. Peterson V.P., Research and Eng.	Ltr. Only
General Dynamics Convair Division 5001 Kearny Villa Road P. O. Box 1628 San Diego, California 92112 Attn: Mr. Frank Dore	Ltr. Only
Missile and Space Systems Center General Electric Company Valley Forge Space Technology Center P. O. Box 8555 Philadelphia, Pennsylvania Attn: Technical Librarian	1
Missile and Space Systems Center General Electric Company Valley Forge Space Technology Center P. O. Box 8555 Philadelphia, Pennsylvania Attn: Mr. F. Mezger	Ltr. Only
Missile and Space Systems Center General Electric Company Valley Forge Space Technology Center P. O. Box 8555 Philadelphia, Pennsylvania Attn: Mr. R. E. Emmer	Ltr. Only
Missile and Space Systems Center General Electric Company Valley Forge Space Technology Center P. O. Box 8555 Philadelphia, Pennsylvania Attn: Mr. B. H. Caldwell	Ltr. Only
Advanced Engine & Technology Department General Electric Company Cincinnati, Ohio 45215 Attn: Technical Librarian	1
Advanced Engine & Technology Department General Electric Company Cincinnati, Ohio 45215 Attn: Mr. D. Suichu	Ltr. Only
Grumman Aircraft Engineering Corporation Bethpage, Long Island, New York 11714 Attn: Technical Librarian	1
Grumman Aircraft Engineering Corporation Bethpage, Long Island, New York 11714 Attn: Mr. Joseph Gavin	Ltr. Only
Hughes Aircraft Company Aerospace Group Centinela and Teale Streets Culver City, California Attn: Technical Librarian	1
Hughes Aircraft Company Aerospace Group Centinela and Teale Streets Culver City, California Attn: Mr. E. H. Meier, V.P. & Div. Mgr. Research and Dev. Div.	Ltr. Only
Walter Kidde & Company, Incorporated 675 Main Street Belleville, New Jersey 07109 Attn: Technical Librarian	1
Walter Kidde & Company, Incorporated 675 Main Street Belleville, New Jersey 07109 Attn: Mr. K. A. Traynelis	Ltr. Only
Ling-Temco-Vought Corporation Astronautics P. O. Box 5907 Dallas, Texas 75222 Attn: Technical Librarian	1
Ling-Temco-Vought Corporation Astronautics P. O. Box 5907 Dallas, Texas 75222 Attn: Mr. Garland Whisenhunt	Ltr. Only
Lockheed Missiles and Space Company Attn: Technical Information Center P. O. Box 504 Sunnyvale, California 94088 Attn: Technical Librarian	1
Lockheed Missiles and Space Company Attn: Technical Information Center P. O. Box 504 Sunnyvale, California 94088 Attn: Mr. Y. C. Lee	Ltr. Only
Lockheed Propulsion Company P. O. Box 111 Redlands, California 92374 Attn: Technical Librarian	1
Lockheed Propulsion Company P. O. Box 111 Redlands, California 92374 Attn: Mr. H. L. Thackwell	Ltr. Only
Lockheed Propulsion Company P. O. Box 111 Redlands, California 92374 Attn: Mr. J. E. Fitzgerald	Ltr. Only
The Marquardt Corporation 16555 Saticoy Street Van Nuys, California 91409 Attn: Technical Librarian	1
The Marquardt Corporation 16555 Saticoy Street Van Nuys, California 91409 Attn: Mr. Warren P. Boardman, Jr.	Ltr. Only
The Marquardt Corporation 16555 Saticoy Street Van Nuys, California 91409 Attn: Mr. S. Minton	Ltr. Only
The Marquardt Corporation 16555 Saticoy Street Van Nuys, California 91409 Attn: Mr. J. Hardgrove	Ltr. Only
Baltimore Division Martin Marietta Corporation Baltimore, Maryland 21203 Attn: Technical Librarian	1
Baltimore Division Martin Marietta Corporation Baltimore, Maryland 21203 Attn: Mr. John Calathes (3214)	Ltr. Only

Addressee	Copies
Denver Division Martin Marietta Corporation P. O. Box 179 Denver, Colorado 80201 Attn: Technical Librarian	1
Denver Division Martin Marietta Corporation P. O. Box 179 Denver, Colorado 80201 Attn: Mr. J. D. Goodlette (A-241)	Ltr. Only
Denver Division Martin Marietta Corporation P. O. Box 179 Denver, Colorado 80201 Attn: Mr. A. J. Kullas	Ltr. Only
Orland Division Martin Marietta Corporation Box 5837 Orlando, Florida Attn: Technical Librarian	1
Orland Division Martin Marietta Corporation Box 5837 Orlando, Florida Attn: Mr. J. Ferm	Ltr. Only
McDonnell Aircraft Corporation P. O. Box 516 Municipal Airport St. Louis, Missouri 63166 Attn: Technical Librarian	1
McDonnell Aircraft Corporation P. O. Box 516 Municipal Airport St. Louis, Missouri 63166 Attn: Mr. R. A. Herzmark	Ltr. Only
McDonnell Aircraft Corporation P. O. Box 516 Municipal Airport St. Louis, Missouri 63166 Attn: Mr. R. E. Martens	Ltr. Only
Rocket Research Corporation 520 South Portland Street Seattle, Washington 98108 Attn: Technical Librarian	1
Rocket Research Corporation 520 South Portland Street Seattle, Washington 98108 Attn: Mr. Foy McCullough, Jr.	Ltr. Only
Rocket Research Corporation 520 South Portland Street Seattle, Washington 98108 Attn: Mr. Bruce Schmitz	Ltr. Only
Rocket Research Corporation 520 South Portland Street Seattle, Washington 98108 Attn: Dr. Duane Williams	Ltr. Only
Space & Information Systems Division North American Aviation, Incorporated 12214 Lakewood Boulevard Downey, California 90241 Attn: Technical Librarian	1
Space & Information Systems Division North American Aviation, Incorporated 12214 Lakewood Boulevard Downey, California 90241 Attn: Mr. H. Storms	Ltr. Only
Rocketdyne (Library 586-306) North American Aviation, Incorporated 6633 Canoga Avenue Canoga Park, California 91304 Attn: Technical Librarian	1
Rocketdyne (Library 586-306) North American Aviation, Incorporated 6633 Canoga Avenue Canoga Park, California 91304 Attn: Mr. E. B. Monteath	Ltr. Only
Rocketdyne (Library 586-306) North American Aviation, Incorporated 6633 Canoga Avenue Canoga Park, California 91304 Attn: Mr. E. V. Zettle	Ltr. Only
Rocketdyne (Library 586-306) North American Aviation, Incorporated 6633 Canoga Avenue Canoga Park, California 91304 Attn: Mr. N. Rodewald	Ltr. Only
Northrop Space Laboratories 3401 West Broadway Hawthorne, California 90250 Attn: Technical Librarian	1
Northrop Space Laboratories 3401 West Broadway Hawthorne, California 90250 Attn: Dr. William Howard	Ltr. Only
Astro-Electronics Division Radio Corporation of America Princeton, New Jersey 08540 Attn: Technical Librarian	1
Astro-Electronics Division Radio-Corporation of America Princeton, New Jersey 08540 Attn: Mr. S. Fairweather	Ltr. Only
Reaction Motors Division Thiokol Chemical Corporation Denville, New Jersey 07832 Attn: Technical Librarian	1
Reaction Motors Division Thiokol Chemical Corporation Denville, New Jersey 07832 Attn: Mr. Arthur Sherman	Ltr. Only
Reaction Motors Division Thiokol Chemical Corporation Denville, New Jersey 07832 Attn: Mr. Robert Gere	Ltr. Only
Republic Aviation Corporation Farmingdale, Long Island, New York Attn: Technical Librarian	1
Republic Aviation Corporation Farmingdale, Long Island, New York Attn: Dr. William O'Donnell	Ltr. Only

Addressee	Copies
Space General Corporation 9200 East Flair Avenue El Monte, California 91734 Attn: Technical Librarian	1
Space General Corporation 9200 East Flair Avenue El Monte, California 91734 Attn: Mr. C. E. Roth	Ltr. Only
Stanford Research Institute 333 Ravenswood Avenue Menlo Park, California 94025 Attn: Technical Librarian	1
Stanford Research Institute 333 Ravenswood Avenue Menlo Park, California 94025 Attn: Mr. Lionel Dickinson	Ltr. Only
TRW Systems One Space Park Redondo Beach, California 90278 Attn: Technical Librarian	1
TRW Systems One Space Park Redondo Beach, California 90278 Attn: Mr. D. Lee	Ltr. Only
TRW Systems One Space Park Redondo Beach, California 90278 Attn: Mr. V. Moseley	Ltr. Only
Tapco Division TRW, Incorporated 23555 Euclid Avenue Cleveland, Ohio 44117 Attn: Technical Librarian	1
Tapco Division TRW, Incorporated 23555 Euclid Avenue Cleveland, Ohio 44117 Attn: Mr. P. T. Angell	Ltr. Only
Thiokol Chemical Corporation Huntsville Division Huntsville, Alabama 35807 Attn: Technical Librarian	1
Thiokol Chemical Corporation Huntsville Division Huntsville, Alabama 35807 Attn: Mr. John Goodloe	Ltr. Only
United Technology Center 587 Methilda Avenue P. O. Box 358 Sunnyvale, California 94088 Attn: Technical Librarian	1
United Technology Center 587 Methilda Avenue P. O. Box 358 Sunnyvale, California 94088 Attn: Mr. B. Adelman	Ltr. Only

Addressee	Copies
Florida Research & Development Center Pratt & Whitney Aircraft United Aircraft Corporation P. O. Box 2691 West Palm Beach, Florida 33402 Attn: Technical Librarian	1
Florida Research & Development Center Pratt & Whitney Aircraft United Aircraft Corporation P. O. Box 2691 West Palm Beach, Florida 33402 Attn: Mr. R. J. Coar	Ltr. Only
Vickers Incorporated Box 302 Troy, Michigan Attn: Technical Librarian	1
Sunstrand Aviation 2421 11th Street Rockford, Illinois 61101 Attn: Technical Librarian	1
Sunstrand Aviation 2421 11th Street Rockford, Illinois 61101 Attn: Mr. R. W. Reynolds	Ltr. Only
Hamilton Standard Division United Aircraft Corporation Windsor Locks, Connecticut 06096 Attn: Technical Librarian	1
Hamilton Standard Division United Aircraft Corporation Windsor Locks, Connecticut 06096 Attn: Mr. R. Hatch	Ltr. Only
Technical Library Air Research Manufacturing Company 9851 Sepulveda Boulevard Los Angeles, California 90009 Attn: Technical Librarian	1
Technical Library Air Research Manufacturing Company 9851 Sepulveda Boulevard Los Angeles, California 90009 Attn: Mr. C. S. Coe	Ltr. Only
Technical Library Air Research Manufacturing Company 9851 Sepulveda Boulevard Los Angeles, California 90009 Attn: Mr. A. C. Standiffe	Ltr. Only
Technical Library Air Research Manufacturing Company 9851 Sepulveda Boulevard Los Angeles, California 90009 Attn: Dr. G. Sotter	Ltr. Only
Shell Development Company Emeryville, California Attn: Technical Librarian	1
Shell Development Company Emeryville, California Attn: Dr. H. Voge	Ltr. Only

Addressee	Copies	Addressee	Copies
Brooklyn Polytechnic Institute Department of Chemical Engineering 333 Jay Street Brooklyn, New York 11201 Attn: Technical Librarian	1		
Brooklyn Polytechnic Institute Department of Chemical Engineering 333 Jay Street Brooklyn, New York 11201 Attn: Prof. I. Miller	Ltr. Only		